FACULTY OF BIOSCIENCE ENGINEERING

A SURVEY OF MICROPLASTIC POLLUTION IN BELGIAN SOILS

A STUDY TO GAIN MORE INSIGHT IN THE OCCURENCE OF MICROPLASTICS IN BELGIAN SOILS, WITH A SPECIAL FOCUS ON PERI-URBAN AND REMOTE AREAS

Lies Vanthournout

Student ID: 01705945

Promotor: Prof. dr. ir. Stefaan De Neve

Co-promotor: Prof. dr. Andre Skirtach

Tutor: Nick Krekelbergh

A dissertation submitted to Ghent University in partial fulfilment of the requirements for the degree of master in Bioscience Engineering.

Academic year: 2022 - 2023

GHENT UNIVERSITY

Ghent, June 9, 2023

The promotor and co-promotor,

Prof. dr. ir. Stefaan De Neve,
Prof. dr. ir. Andre Skirtach

The author,

Lies Vanthournout

PREFACE

It is with great joy and a touch of relief that I can proudly present this master thesis. It's been a challenging year combining two master programs, but luckily I was able to achieve a result I can be satisfied with thanks to the support of various people.

First of all, I would like to thank both of my promotors. Professor Stefaan De Neve, for steering me in the right direction and providing me with helpful feedback and suggestions on how to proceed. Professor Andre Skirtach, for sharing his knowledge and expertise on the use of spectroscopic techniques. I would also like to thank my tutor, Nick Krekelbergh, for accompanying me during the soil sampling and for making me feel comfortable during the first weeks of the year and the entire period after that.

In addition, I would also like to thank some friends and family. My sister, Iris, for proofreading my thesis, and my parents for always supporting me. My boyfriend, Senne, for helping each time my Latex-code got stuck, teaching me how to edit figures in Inkscape and for always listening when I needed a moment to complain. Thank you, Nele and Laura, for making my last year in Ghent a year to never forget. A final and small thank you to my colleagues at Frituur 't Specialleken, for taking over my shifts when things got to busy for me.

CONTENTS

LIST OF ABBREVIATIONS

ABS	Acrylonitrile butadiene styrene
BR	Butadiene rubber
CR	Polychloroprene
EDPM	Ethylene propylene diene monomer
EPR	Ethylene propylene rubber
FTIR	Fourier-transform infrared
HDPE	High-density polyethylene
MP	Microplastics
NR	Natural rubber
OM	Organic matter
PA	Polyamide
PC	Polycarbonate
PEG	Polyethylene glycol
PEO	Polyethylene oxide
PET	Polyethylene therephthalate
PDMS	Polydimethylsiloxane
PP	Polypropylene
PS	Polystyrene
PSU	Polysulfone
PTFE	Polytetrafluoroethylene
PU	Polyurethane
PVC	Polyvinyl chloride
SAA	Styrene allyl alcohol
SAN	Styrene acrylonitrile
SBR	Styrene butadiene rubber
SOM	Soil organic matter
SIS	Styrene isoprene styrene
TWP	Tire wear particles
WWTPs	Wastewater treatment plants
XPS	Extruded polystyrene

ABSTRACT

A survey of microplastics (MP) pollution in Belgian soils is presented. Soil samples are taken across various locations in Belgium, with a specific focus on non-suspected soils with a variety in land-use types. Extraction of MP from soil samples is performed followed by analysis using Fourier-transform infrared (FTIR) spectroscopy and Raman spectroscopy. It can be concluded that a clear and solid extraction procedure and a combination of different identification techniques are necessary to reliably identify MP. Only when identification is foolproof, the effect of land-use type and proximity to urban activities can be investigated.

Een onderzoek naar microplastics (MP) vervuiling in Belgische bodems wordt voorgesteld. Bodemstalen worden genomen op verschillende locaties in België, met een specifieke focus op niet-verdachte bodems met verschillende soorten landgebruik. Extractie van MP uit deze bodemstalen wordt uitgevoerd, gevolgd door analyse met behulp van Fourier-transformatie infraroodspectroscopie (FTIR) en Ramanspectroscopie. Er kan worden geconcludeerd dat een duidelijke en solide extractieprocedure en een combinatie van verschillende identificatietechnieken noodzakelijk zijn om MP betrouwbaar te kunnen identificeren. Pas wanneer de identificatie waterdicht is, kan het effect van het type landgebruik en de nabijheid van urbane activiteiten worden onderzocht.

INTRODUCTION

World production of plastic is, although stabilized in Europe, still increasing worldwide. With an annual production of more than 9 billion tons and an annual production increasing rate of 8,7%, one may wonder where all these plastics end up (He et al., 2018). Plastic pollution in the ocean is a well-known phenomenon that is widely studied and that receives a lot of attention from the public (Gionfra, 2018). Initially, the scientific and public attention mainly focused on larger plastic debris, but during the last decades increasing attention was given to the occurrence of microplastics (MP) in oceans, and nowadays also the soil (Duis & Coors, 2016). MP can be extracted easily from the aquatic environment, they tend to accumulate along the shoreline and filter feeders living in the aquatic environment who are susceptible to the ingestion of MP are well-studied. MP in soils are often less visible and more difficult to quantify due to the heterogeneous nature of soils and the high variability in soil properties and composition. This is why research on MP in marine ecosystems is ahead on research for terrestrial ecosystems and soils (Rillig, 2012). However, more than 80% of the plastics found in marine environments have been produced, consumed, and disposed of on land. It is estimated that plastic pollution in soils is 4 to 23 times larger than in the oceans (Gionfra, 2018). By 2050, research indicates that 12 billion tons of plastic waste will accumulate in landfills or the environment if actions on waste management and plastic production are not taken (Gionfra, 2018). The number of publications on MP in soils has risen exponentially during the last decade (He et al., 2018). The soil can be considered as a major sink for MP, and at the same time also as a source of MP contaminants to the aquatic environment. The lack of robust analytical methods for the isolation of MP from complex, organic-rich soil matrices represents a major challenge in acquiring more knowledge on the occurrence and distribution of MP in soils (Hurley & Nizzetto, 2018). No standard method for the extraction of MP from the soil exists up until now. However, the extraction of MP from soils is a crucial first step in studying the type and amount of MP. Gathering more data regarding the abundance and distribution of MP in soils is a prerequisite to eventually assess their potential impact on and risk caused to soil ecosystems in further research (Zhou et al., 2020).

Investigating ‘non-suspected’ soils, meaning soils who are not subjected to continuous accumulation of contaminants from either localized or diffuse sources, can lead to more knowledge on the occurrence and distribution of MP in the environment. Typical examples of these contaminants include persistent toxic substances, like trace metals and persistent organic pollutants. Soils far away from main sources of pollutants, such as industrial sites, busy traffic roads, and waste dumps from municipal activities, can be considered to be ‘non-suspected’. Since MP can be transported through ecosystems in a very diffuse manner,

for instance atmospheric deposition, a clear demarcation of what a (non-)suspected soil is, continues to be missing (Yu, Zhu, & Li, 2012).

The goal of this thesis is to examine the abundance of MP in Belgian soils, with a specific focus on peri-urban and remote areas. These remote areas can be considered as 'non-suspected' soils. Different types of land-use will be discussed, such as pastures, agricultural land and nature reserves. MP originate from anthropogenic activities, and so contamination levels tend to correlate with population density (K. Liu et al., 2019). Agricultural activities such as plastic mulching, the application of soil amendments and road run-off are considered to be major sources of MP contamination (Corradini, Casado, Leiva, Huerta-Lwanga, & Geissen, 2021; K. Liu et al., 2019). It is suspected that there will be a higher occurrence of MP in land-use types closer to the main sources of MP contamination mentioned above (K. Liu et al., 2019).

Soil samples will be taken according to a standardized sampling pattern on different locations across Belgium. The final objective is to extract and analyze MP from these samples. This research will try to answer following questions:

- Are there MP present in non-suspected soils?
- What kind of MP are present in non-suspected soils?
- Is there a possible influence of proximity to urban activities on the polymer type of MP found?
- Is there a possible influence of land-use type on the polymer type of MP found?

1.1 Overview of the thesis

This master's dissertation consists of four parts. First, a theoretical background is given, explaining the main concepts related to MP. A definition is given and the origin of MP as well as their further fate are outlined, followed by potential extraction methods for MP and methods for analysis. In a second part the outline of the study is described. The selected sampling locations and the sampling strategy are discussed, followed by the eventual extraction of the MP and analysis through Fourier Transform-Infrared (FTIR) spectroscopy and Raman spectroscopy. Finally the results will be discussed thoroughly and an answer will tried to be provided on the research questions defined above.

LITERATURE STUDY

2.1 Getting to know MP

It is important to get a good view of the definition and concept of MP. A few general characteristics are discussed as a first acquaintance with MP.

2.1.1 Size

MP are synthetic organic polymer particles with a size smaller than 5 mm. In most definitions, a lower limit for the size of MP is not defined. In regard of the definition of nanoscale (1-100 nm), the term MP could be reserved for plastic particles with a size between 100 nm and 5 mm (Duis & Coors, 2016). In this paper, the focus will primarily be on MP with a size between 2 mm and 1,2 μm. This range is chosen because of methodological reasons and to narrow down the research focus to cope with the short time period this master dissertation is written in.

2.1.2 Shape

MP come in various forms and shapes, depending on the source they are originating from. Between 4 and 7 different categories are used for the classification of MP according to shape or form. Fiber, fiber bundle, fragment, sphere (or bead), pellet, film and foam are distinguished. Fibers and fragments are often dominant in soils with sewage sludge application. Foam usually occurs on riverside or coastal soils (Zhou et al., 2020). Different shapes can often be linked to different sources of MP. Table 2.1 gives an overview of the different shapes, linked to their possible source(s) (Rochman et al., 2019). In Figure 2.1 an overview is given of a few different MP shapes.

Table 2.1: Plastic shapes and the corresponding source(s) they can originate from. Retrieved from Rochman et al. (2019).

Shape	Source
Fibers and fiber bundles	Clothing, carpets
Pellets	Industrial feedstock, containing raw materials required in further industrial processing
Spheres (beads)	Personal care products, industrial scrubbers
Foam	Expanded polystyrene (EPS) foam products, who are used as insulation or in food packaging materials

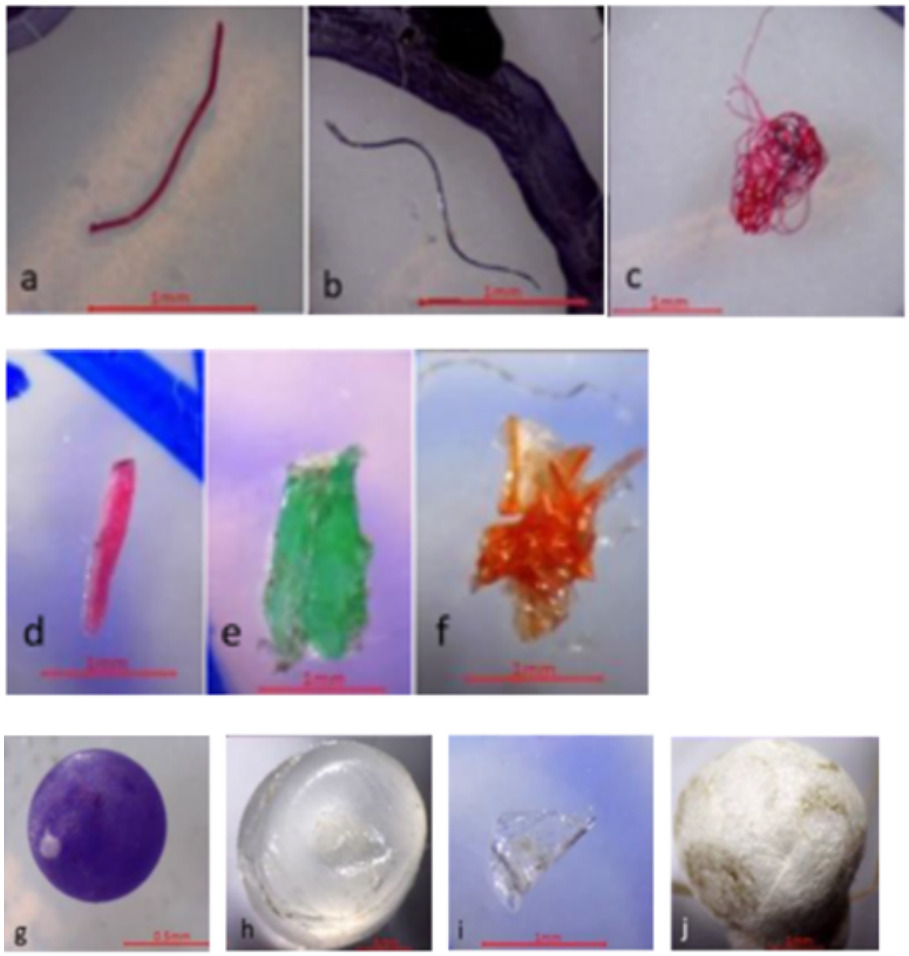

Figure 2.1: An overview of the different plastic shapes. Fibers (a, b), fiber bundle (c), fragments (d, e, f), spheres (g), pellets (h), films (i) and foams (j). Retrieved from Rochman et al. (2019).

2.1.3 Types of plastic polymers

Polypropylene (PP), polyethylene (PE), polyvinyl chloride (PVC), polyurethane (PU) and polyethylene terephthalate (PET) represent around 80% of the total manufacturer's polymer demand in Europe. These commodity plastics are produced in high volumes for purposes where exceptional material properties are not required (Kawecki, Scheeder, & Nowack, 2018). The most common MP polymers reported in soil samples are PP, PE, PET, polystyrene (PS), PVC, and polyamide (PA) or nylon. PE, PP and PET are often used in packaging materials, plastic mulching and textiles. Their wide applications range ensures a large presence of these plastic polymers in the soil, next to polymers linked to synthetic fibers (PA) and films from agricultural sources (PVC). Other less common polymers types include polymethyl methacrylate (PMMA), also referred to as acrylic, and synthetic rubbers (Perez et al., 2022).

2.1.4 Secondary and primary MP

MP found in the terrestrial or aquatic environment can be of two types: primary and secondary.

2.1.4.1 Primary MP

Primary MP are commonly defined as MP who are initially manufactured and released to the environment in a micro-size range (smaller than 5 mm). Personal care products, drilling fluids for oil and gas exploration, and industrial abrasives used for polishing, grinding, and other forms of surface preparation, are all considered to be important sources of primary MP (Duis & Coors, 2016).

2.1.4.2 Secondary MP

Secondary MP result from the fragmentation of larger plastic materials due to weathering and degradation. Plastic mulching, general littering and abrasion from car tires all contribute to the production of secondary MP (Duis & Coors, 2016).

In general, plastic materials are very resistant towards degradation. Plastic materials have been shown to survive for several decades, depending on the properties of the plastics as well as the surrounding environmental conditions. However, environmental weathering can still cause the breakdown of plastics, although at a very slow rate. Biotic and/or abiotic weathering processes cause changes in polymer properties. General processes of plastic degradation are illustrated in Figure 2.2 (K. Zhang et al., 2021). In soils however, degradation due to UV-radiation, thermal oxidation and physical abrasion happens rather slow. Biodegradation is a promising way to reduce MP pollution in the environment. In soils, waxworms and mealworms have been reported to efficively digest PE or PS plastics (Zhu, Zhu, Wang, & Gu, 2019).

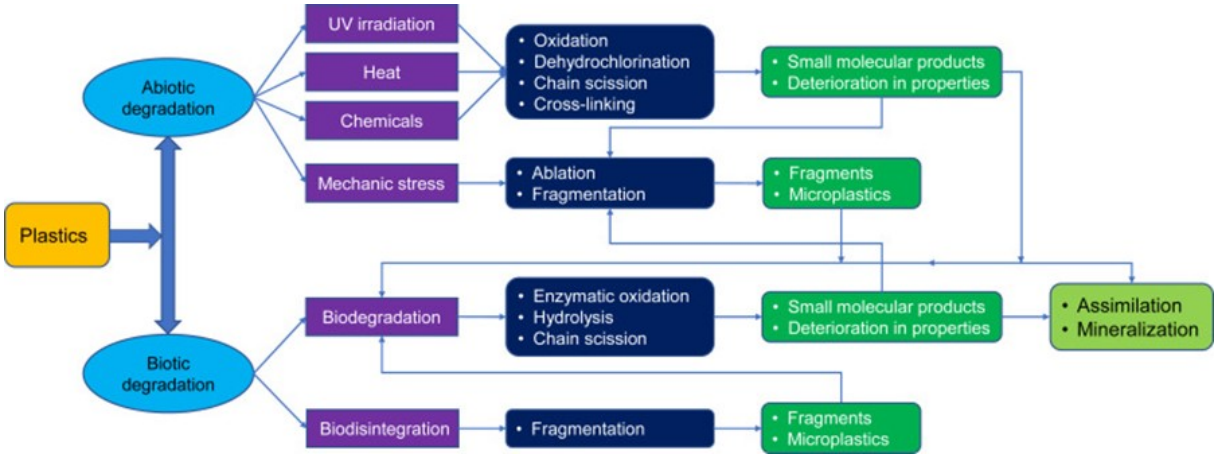

Figure 2.2: A schematic diagram showing the general processes involved in the degradation of plastics. Retrieved from K. Zhang et al. (2021).

- **Abiotic degradation of plastics**

Abiotic degradation of plastics refers to changes in physical or chemical properties that occur for plastics due to abiotic factors such as light, temperature, air, water, and mechanical

forces. Generally, abiotic degradation is expected to precede biodegradation due to the poor bioavailability of plastics, meaning that plastics are not easily broken down by biological processes due to their long chains of polymer molecules, which are very stable and resistant to degradation. In soils however, biotic degradation is expected to play a bigger role (K. Zhang et al., 2021).

- **Biotic degradation of plastics**

Biotic degradation of plastics refers to the deterioration of plastics caused by organisms. Organisms can degrade plastics either physically by biting, chewing and digestive fragmentation or biologically by biochemical processes. Microorganisms, including bacteria and fungi, and insects, can be responsible for biotic degradation of plastics in soils (K. Zhang et al., 2021). Figure 2.3 shows the biodegradation pathway of MP. Hydrolytic and oxidative degradation of plastics by various extracellular enzymes produced by soil organisms results in scission of the polymer chain, producing short-chain polymers and small molecular fragments (bio-fragmentation). The degradation products can be taken up by microorganisms when their molecular weight is small enough (assimilation). Small molecular degradation products can be assimilated and subjected to the intracellular metabolism of (micro)organisms. Eventually plastics can be mineralized into CO_2 and H_2O under aerobic conditions and into CH_4, CO_2, organic acids, H_2O, and NH_4 under anaerobic conditions due to both extracellular and intracellular processes (mineralization). These end products can be used for the formation of new microbial biomass (K. Zhang et al., 2021).

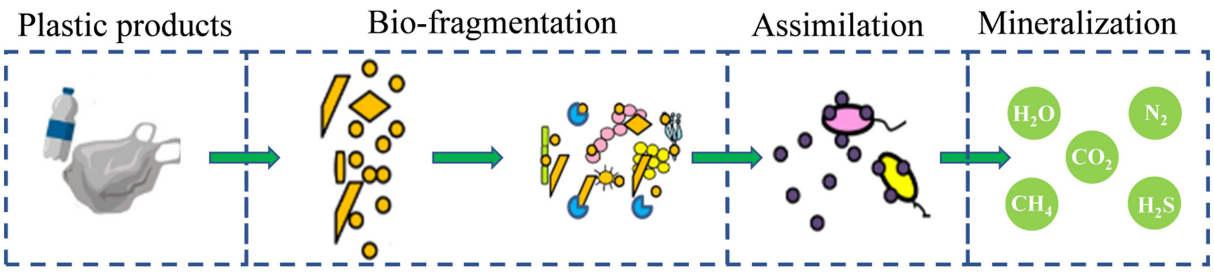

Figure 2.3: The biodegradation pathway of MP. Retrieved from Du et al. (2021).

Convential plastic materials have a low bioavailability and often only a very small fraction of the plastic polymers is exposed to potential degraders. In addition, macromolecule polymers can not be directly used by microorganisms, and extracellular enzymes are required to break down macromolecule polymers into small molecular products for cellular uptake and further metabolization (K. Zhang et al., 2021). Because of their strong potential for adaptability to different environmental conditions, microbials still succeed in decomposing different organic pollutants, including MP (K. Zhang et al., 2021).

2.2 Possible sources of MP

Various sources of MP contaminate the environment. The dominant sources of MP in soils include wastewater sludge and compost (soil amendments), organic fertilizers, and agricultural plastic mulch films (J. Huang et al., 2021). A selection of the most common sources will be discussed.

2.2.1 Soil amendments: compost and sewage sludge

Soil amendments are added to the soil to improve soil properties and soil nutrient content, causing higher yields. Current evidence suggest that soils receive plastic inputs by application of these amendments (Zubris & Richards, 2005).

- **Compost**

Compost is widely used as a fertilizer in agriculture. In 2008, 18 million tons of compost were produced in the EU. The normal annual recommended compost application for arable and (eroded) agricultural land lies around 10 tons per hectare (European Compost Network, 2022). Polymers such as PS and PU are sometimes added to compost to improve soil properties, they can boost water retention and inhibit methane production (Singh, Abdullah, Ma, & Sharma, 2023). Compost can integrate with natural soil and disperse MP components across a wide spatial area (Hurley & Nizzetto, 2018). Procedures such as sieving and sifting can help reduce the amount of plastics in fertilizers. However, MP are more challenging to remove because of their size (Weithmann et al., 2018). Consequently, compost, especially of municipal origin, must be considered as a serious entry path for plastics in soils (Gajst, 2016).

- **Sewage sludge**

The application of sewage sludge as a fertilizer is a common practice in agriculture. In Europe and North America, 50% of sewage sludge is processed and used for agricultural purposes (Nizzetto, Futter, & Langaas, 2016). Wastewater treatment plants (WWTPs) are capable of removing up to 90% of MP from the water and retain it in the sludge (Estahbanati & Fahrenfeld, 2016). During the primary (mechanical) treatment step in WWTPs, coarse suspended or floating solids are removed from the wastewater by screens or sieves. Sand and other heavy particles are retained in sand traps and floating material is removed in grease separators. Coarse screens are suitable for removing macroplastics from wastewater. As a result of their opening size, they will not be able to capture smaller MP. MP with a high density can be expected to sediment and, thus, to be captured in the sand trap or in the sludge (Duis & Coors, 2016). Concerns over the potential environmental and human health impacts from the use of sewage sludge, have led to the introduction of regulations. While

these regulations include limits on pollutants, MP contamination is hardly taken into account. In particular, the EU Directive (EU 86/278/EEC) on the protection of the environment sets limits on the concentration allowances for 7 heavy metals present in sewage sludge. MP concentrations are not mentioned (Gionfra, 2018). Therefore, although the application of sludge-based fertilizers contributes to nutrient and organic matter (OM) recycling on land, the potential consequences for sustainability and food security from the mass transfer of MP and associated harmful substances from sludge from WWTPs to farmland should also be considered (Zhou et al., 2020).

2.2.2 Plastic mulching

Plastic mulching is a widespread technique to receive greater harvest and improve crop quality by increasing soil temperature, protecting agricultural crops, suppressing weeds and enhancing water use efficiency (Duis & Coors, 2016). Nowadays, with an area of 4270 km^2, plastic mulching accounts for the largest proportion of covered agricultural surface in Europe. Although plastic mulching helps to increase yields, these thin plastic foils can embrittle and the fragments can end up in the soil (Scarascia-Mugnozza, Sica, & Russo, 2011). Plastic residues originating from plastic mulching directly affect soil properties. For instance, they cause a retardation of crop growth, they affect field operations and they can potentially harm wildlife by ingestion (Gionfra, 2018). Successive enrichment of plastic fragments in soil by plastic mulching can also be a possible endangerment for the environment because of the release of harmful pollutants, like phthalates (Steinmetz et al., 2016). Approximately 20 million hectares of farmland worldwide practices plastic mulching, with China accounting for the largest proportion (around 90%) (Y. Huang, Liu, Jia, Yan, & Wang, 2020). In the EU the market for plastic mulch is estimated to be 100 000 tons per year. However only 32% of plastic is collected at the end of use, with the rest is either landfilled, left in soils or burned. Less than one third of plastic mulch is currently considered as biodegradable (E. Liu, He, & Yan, 2014). The rate of degradation is a function of the structure of the plastic material and the environment. Environmental aspects in order for degradation to occur include the presence of microorganisms and the presence of oxygen, moisture and mineral nutrients. A plastic material is more biodegradable when it has a low molecular weight, high surface area, vulnerable polymer chain ends available for degradation and is relatively non-water resistant (J.-C. Huang, Shetty, & Wang, 1990).

2.2.3 Irrigation and flooding

Nowadays, an area of 270 million ha is irrigated worldwide, accounting for 18% of total agricultural land (Bruinsma, 2017). In many developing countries cleaned sewage water or groundwater is often used for irrigation. However, due to climate change, population growth and urbanization, water scarcity is increasing in many regions of the world. Hence, also the direct use of partially treated or even untreated wastewater for irrigation of agricultural fields is rising and may become the only water source for many farmers (WHO, 2006). Untreated

wastewater contains large amounts of MP, derived from the effluent of washing machines or care products like shampoos or peelings. The direct use of untreated wastewater for irrigation of agricultural fields presumably serves as a source of MP in soils, and results in plastic contaminants in farmland environments. MP were detected in household wastewater with concentrations from 1 000 up to 627 000 items per m^3 (He et al., 2018). In better developed countries like Israel, Australia or the United States of America (particularly in California and Florida) most wastewater is treated before use. The MP concentrations are smaller compared to the concentrations in untreated wastewater, nonetheless irrigation with treated water can also serve as a source for MP in soils (Mateo-Sagasta, Medlicott, Qadir, Raschid-Sally, & Drechsel, 2013).

Extreme meteorological events may lead to overbank flooding, erosion and deposition of river sediments to land. These events may influence the distribution of MP from aquatic environments to inland areas (Guasch et al., 2022). Overbank deposition likely enriches alluvial soils with micro(nano)plastic particles, because fluvial sediments have been shown to contain high concentrations of MP (Hurley & Nizzetto, 2018).

2.2.4 Littering and street runoff

Littering near roads and trails or illegal dumping of waste is an important input of plastic in soils. Up to now, there are no studies available that quantify the amount of plastic introduced into soil by littering or illegal dumping of waste. Large parts of litter can wash away from highways during storms, including non-biodegradable substances like plastic. Road runoff is a major transport route for urban pollutants and a significant contributor to a deteriorated water quality in receiving waters. Although most of these point sources (e.g. illegal dumping of waste) are restricted to the roadside/trail environment, larger plastic items can be washed or blown out and contaminate other ecosystems, like adjacent fields (Bläsing & Amelung, 2018).

2.2.5 Tire abrasion

Around 30% of MP that pollute rivers, lakes and oceans, consists of tire wear (Sommer et al., 2018). Tires are generally made up of a complex mixture of polymers, mostly styrene butadiene rubber (SBR), but also butadiene and natural rubber (BR, NR) (Hüffer, Wagner, Reemtsma, & Hofmann, 2019). With increasing automobile demand, tire consumption increases correspondingly. The global annual emission of particles from tires, also called tire wear particles (TWP), is estimated to be more than 3,3 Mton. Approximately two thirds of these particles end up in soils via runoff or atmospheric transport by air. A small part is retained by separate sewer systems in urban areas. Depending on the distance from the road, transport dynamics and the traffic frequency, concentrations of tire plastics can range from 0,1 to 117 g per kg soil (Leifheit, Kissener, Faltin, Ryo, & Rillig, 2021). It has been shown that the concentration of TWP decreases with the distance from the road to the sampling

site (Saito, 1989). The total amount of TWP lost per kilometre varies widely and depends on several parameters (Verschoor, 2015):

- Tire characteristics: size, tread depth, pressure, temperature, chemical composition.
- Vehicle characteristics: weight, distribution load, engine power.
- Road surface characteristics: road material, texture pattern, condition, wetness.
- Vehicle operation: speed, acceleration, brake frequency.

The total emission of TWP can also be calculated by multiplying vehicle kilometers traveled with emission factors (milligrams of TWP emission per kilometer) (Luo et al., 2021). It is assumed that fine particles originating from tire abrasion do not remain within the roadside environment but are transported into freshwater and marine ecosystems. As a consequence, tire abrasion has been identified as a serious source for MP in the marine environment (Bläsing & Amelung, 2018).

2.2.6 Atmospheric deposition

It seems reasonable to assume that plastic can be blown out from surfaces like poorly managed landfills or streets and transported by wind (Dris et al., 2015). Recent studies by Allen et al. (2019), Ambrosini et al. (2019), and Y. Zhang, Gao, Kang, and Sillanpää (2019) have illustrated that atmospheric MP particles can be transported to ocean surface air and remote areas, such as mountain catchments, glacial debris of an Alpine glacier and Tibetan glaciers. Atmospheric deposition is likely to play an important part as a source of MP in the non-suspected soils investigated in this research. The wind speed, direction, convection lift and turbulence are considered as important vectors who can affect MP transport, and which further influence the flux mechanism and source-sink dynamics of plastic pollution in both marine and terrestrial environments. It is not known to what extent atmospheric fallout contributes to aquatic and terrestrial contamination (Y. Zhang et al., 2020). In China, a study was conducted that estimated the concentrations of non-fibrous MP in atmospheric fallout to range from 175 to 313 particles/m^2/day in the city of Dongguan (Cai et al., 2017).

2.3 Further circulation in our environment

MP pollution appears ubiquitous in marine, freshwater, terrestrial and atmospheric environmental compartments. These environments are interlinked, with a diverse network of source-sink pathway connections that can influence the flux and retention of MP between these environmental matrices (Y. Zhang et al., 2020). Water currents, wind and tides are the main components of MP transport in the aquatic environment, which lead to a prolonged sinking process and migration in sea coastal zone and further inland movement of MP (Akdogan & Guven, 2019).

The translocation of MP in the soil is dependent of their size, because smaller MP are preferred for bioturbative transport (Bläsing & Amelung, 2018). Even if plastic is retained in soils, the sink function of soils for plastic items is overcome when erosion takes place. Water erosion is mainly influenced by land-use and cover and is highest on bare soil, followed by vineyards and other arable lands (Bläsing & Amelung, 2018). In Belgium, high erosion rates have been reported for the silty soils in the hilly landscape of the south of Flanders (Vandaele & Poesen, 1995). Wind erosion results in the atmospheric deposition of MP. Wind-eroded sediment and dust can result in environmental- and human exposure to MP far away from their original source (Rezaei, Riksen, Sirjani, Sameni, & Geissen, 2019).

2.3.1 (Bio)turbation

MP are transferred and transported by soil fauna, e.g., larvae, earthworms and vertebrates, either by attachment to the outside of these animals or by ingestion and excretion (Zhou et al., 2020). Migration of MP in soil by bioturbation suggests that plant processes (such as root growth and uprooting) and inputs from various animals (for example larvae, earthworms, vertebrates, etc.) can serve as preferential paths for MP movement. MP can be swallowed and subsequently excreted by earthworms, resulting in mainly horizontal transport. Vertical transport from shallow to deep soils is the result of the burrowing of anecic earthworms and mosquitoes. Mosquito larvae have been reported to readily eat MP, which can persist in a mosquito's guts during metamorphosis from the larval to adult stage. The ability of soil animals to transport and distribute MP in soil is significantly enhanced when there exists a predator-prey relationship. It can be speculated that intricate food webs in soil ecosystems, composed of diverse and complex species relationships, will contribute more to the migration of MP compared to single species (Guo et al., 2020).

Tillage activities, such as tilling and ridging, make it easy for MP to be carried into underlying soil layers. In addition, the harvest of tubers may facilitate the vertical migration of MP. Nevertheless, these external forces have little effect on the downward motion of MP since traditional farming practices only affect the topsoil (Zhou et al., 2020).

2.3.2 Leaching

Leaching, defined as the loss of mineral and organic solutes due to percolation in soil, has a strong role in facilitating the vertical movement of MP (Zhou et al., 2020). More specifically, the term "lessivage" is used, which is the downward transportation of clay particles suspended in water (Quénard, Samouëlian, Laroche, & Cornu, 2011). A necessary requirement for leaching is that the particle size is smaller than the diameter of the pore, otherwise particles will be hold back (Bläsing & Amelung, 2018). Soil texture determines the pore size and thus has an important influence on the migration of MP. The two most common MP shapes (spherical and granular) easily migrate into deeper soils, while other shapes (such as fibers and films) interact differently with soil aggregates and may inhibit MP migration in soil. Next to shape, other properties of MP can influence their mitigation potential, such as size and aggregation state. Heterogeneous aggregates and/or adhesion of MP to OM should be further investigated (Zhou et al., 2020). MP can be integrated into soil aggregations and can be incorporated into soil clumps to varying degrees, e.g. loosely in microbeads and fragments or more tightly in microfibers (Guo et al., 2020). The presence of MP in soils can lead to a decline of the structural integrity of the soil, resulting in desiccation cracking (Wan, Wu, Xue, & Hui, 2019). Soil water infiltration and soil cracks can be considered as important reasons for vertical transport of MP (Jin et al., 2022).

2.3.3 Erosion

Arable land susceptible to soil erosion is a potentially important source of MP entering aquatic ecosystems (Rehm, Zeyer, Schmidt, & Fiener, 2021). Studies found that basic properties such as density, shape, and size have a strong effect on the vertical transport of MP in porous media (Han, Zhao, Ao, Hu, & Wu, 2022). A study by Rehm et al. (2021) showed that coarse MP are more likely to be lost via soil erosion, while for fine MP vertical transport below the plough layer is more important. MP density influences the retention rate of MP in soils. Higher density equals a higher retention (Han et al., 2022).

MP fiber contamination can affect soil properties such as bulk density or capacitive indicators of soil physical quality, and influence the formation of stable aggregates. MP fibers have a soil particle binding effect that can reduce erodibility in a porous medium (Ingraffia et al., 2022).

2.4 Effects and consequences

2.4.1 Effects on soil ecosystems

As emerging persistent contaminants, MP can be taken up by soil biota (He et al., 2018). Their uptake depends on properties such as size, shape, density and colour (due to prey item resemblance) (Wright, Thompson, & Galloway, 2013). Much more is still left to be discovered regarding the potential toxicity of MP and the consequences of exposure towards soil organisms (Duis & Coors, 2016).

Biomagnification, known as the phenomena where increasing concentrations of a contaminant occur at a higher trophic level, is not yet known to be the case for MP (Duis & Coors, 2016). Most studies focus on MP in the aquatic ecosystem because water pollution by MP has been regarded as one of the most important and serious global concerns. Only a few studies have focused on plastic pollution derived from landfill sludge and agricultural plastic mulch in soil ecosystems. Most of the above mentioned research can be summarized as followed (Chae & An, 2018):

- MP may affect the survival and fitness of soil organisms and they (or their additives) can accumulate in soil organisms (Huerta Lwanga et al., 2016).
- MP can cause molecular changes in soil organisms, possibly indicating an immune response (Rodriguez-Seijo et al., 2017).
- MP can absorb other pollutants, who can desorb post ingestion with potential for toxicity and/or accumulation in the food chain (Hodson, Duffus-Hodson, Clark, Prendergast-Miller, & Thorpe, 2017).
- MP can be transported horizontally and vertically via soil organisms in the soil ecosystem (Chae & An, 2018).

MP may also function as a vector for organisms, transporting them over large distances. They can harbor unique communities of microorganisms, as has been found on aquatic MP. Their high surface area makes them ideal for housing microorganisms, including potentially pathogenic ones (Prata, 2018). Overall, the amount and progress of research on the (eco)toxicity of plastic wastes in the soil ecosystem is still very limited. Therefore, advancing research in this field is necessary to protect the soil environment from serious plastic pollution, which threatens food, groundwater and ecosystem safety (Chae & An, 2018).

2.4.2 Human exposure to MP

The presence of micro- and nanoplastics in the food chain creates a risk to human health. The average human consumes around 39 000 to 52 000 MP particles per year (depending on age and gender) (Yee et al., 2021). MP are difficult to remove from the respiratory

system because of their polymeric structure and sometimes fibrous shape. They can release hazardous substances from their surfaces, such as persistent organic pollutants and plasticizers. All of the above may cause MP to be a possible risk for human health (Prata, 2018).

There are three key routes for MP and nanoplastics to end up in the human body (Yee et al., 2021):

1. Ingestion. Due to their ubiquitous presence in both aquatic and terrestrial areas, it is highly probable that MP are present in many food products.
2. Inhalation. It is estimated that a person's lungs can be exposed to 26 to 130 airborne MP per day. Inhaled airborne MP originate from urban dust, and include synthetic textiles and rubber tyres
3. Skin contact. Micro- and nanoplastics can enter the skin through weakened or wounded skin, sweat glands and hair follicles.

Additionally, monomers and additives found in MP are known to be endocrine disruptors and have been identified in the human body and bodily fluids. Leachates, such as contaminants or monomers, seem to contribute to the scale of inflammation in the respiratory system caused by MP. However, the role of chemical and particle toxicity of MP for humans is not yet fully understood (Prata, 2018).

2.5 Extraction and identification of MP

Once plastic accumulates soils, it becomes part of a complex mixture of OM and mineral substituents. Due to interactions between OM and mineral parts, soil OM (SOM) may become very stable and persist for up to a few hundred years (Bläsing & Amelung, 2018). It is necessary to remove the sample matrix for the analysis of MP, preferably isolating the MP particles from the soil matrix and removing adhering materials. MP particles may be encased by soil aggregates, making them difficult to analyze (Möller, Löder, & Laforsch, 2020). The complex composition and heterogeneity of the soil make separating MP from the soil matrix challenging (Perez et al., 2022). An essential first step in the MP study of soils is to discover a technique for soil aggregate dispersion without running the danger of destroying or artificially fragmenting MP (Möller et al., 2020). Kaiser and Asefaw Berhe (2014) suggest sonification as a possible method for the dispersion of soil aggregates. Another possible method is through the use of a peptisation liquid (Thomas, Schütze, Heinze, & Steinmetz, 2020). An overview of the possible pathways that can be followed during the extraction procedure is given in the flowchart below.

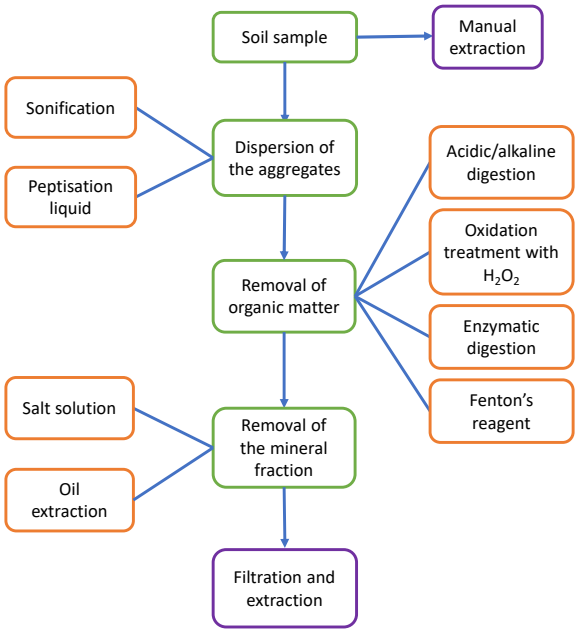

Figure 2.4: Flowchart of different pathways possible for the extraction of MP from soil samples.

2.5.1 Manual extraction

Sieving and manual sorting are basic techniques for isolating MP. A stereo microscope can be used to filter out material that is mineral or biological, such as particles with visible cell structures. Manual sorting and visual recognition do have some restrictions. They take a lot of time, are labor intensive, and they are highly prone to bias and misidentification. Therefore, it is extremely difficult to identify a polymer with sufficient accuracy. (Möller et al., 2020). The use of the hot needle test can confirm the distinction between natural and plastic particles by using the thermoplastic properties of the synthetic particles. Plastic particles will melt, while non-plastic material will burn into ashes (Perez et al., 2022).

2.5.2 Removal of the organic fraction

The density range of OM, 1,34 - 1,52 g/cm^3, overlaps with the density of many types of plastic and can therefore obscure the detection of MP and interfere with identification (Radford et al., 2021). OM within soils is one of the most difficult fractions to remove without destroying the MP particles (Möller et al., 2020). To effectively digest SOM without damaging the MP, the digestion method, reagent, temperature, concentration, and pH must be considered (Perez et al., 2022).

To eliminate the organic portion of the sample matrix, both acidic and alkaline digesting techniques are often applied (Möller et al., 2020). Alkaline digestion might cause discoloration or damage to the investigated MP, while certain acids may dissolve different types of polymers, including PS and PA (Al-Azzawi et al., 2020; Thomas et al., 2020). For instance, PA and PE fibers were shown to be destroyed by sodium hydroxide treatment. In general, strong acidic or alkaline solutions used to purify samples will cause uncontrollable bias in the sample's final MP composition (Möller et al., 2020). Table 2.2 gives an overview of different acidic and alkaline solutions that can be used for digestion of OM in soil samples.

Table 2.2: Acidic and alkaline digesting techniques to remove the organic fraction of the sample matrix (Hurley et al., 2018; Möller et al., 2020; Thomas et al., 2020).

Acidic digestion	Alkaline digestion
HCl, HNO_3, HNO_3:$HClO_4$ (4:1), H_2SO_4	NαOH, KOH

Oxidation treatment with hydrogen peroxide (30% H_2O_2) is also a commonly used technique in soil analysis to remove SOM. To reduce the reaction time, higher temperatures during oxidation can be handled. However, plastics are sensitive to degradation and melting at temperatures above 70 °C (Thomas et al., 2020). The oxidation treatment is best done at lower temperature, to destroy OM in the context of MP isolation from organic rich sediment matrices (Möller et al., 2020). The efficacy of this procedure is sometimes poorly, resulting in bleaching the OM rather than removing it. The degradation of some polymer types has also

been noted as a result of H_2O_2 oxidation. These include polyethylene (PE) and polypropylene (PP), which are among the most commonly produced plastics globally (Hurley et al., 2018).

Fenton reaction is a viable alternative to hydrogen peroxide, as oxidation occurs more rapidly than traditional H_2O_2-oxidation (Al-Azzawi et al., 2020). Some organic compounds, such as highly chlorinated aromatic compounds, are recalcitrant to H_2O_2 but can be removed easily using Fenton's reagent (Hurley et al., 2018). Fenton's reagent uses ferrous cations to catalyze the oxidation of organic components with H_2O_2 (Möller et al., 2020). Due to the intense exothermal reaction, it is important to take care not to surpass 70 °C while treating organic-rich samples with Fenton's reagent in order to prevent thermal deterioration of the MP (Möller et al., 2020). Furthermore, the pH of the reagent must be adjusted in the range from 3 to 5 to encourage the dissolution of the ferrous sulfate granules and optimize the degradation of OM (Hurley et al., 2018). Fenton's reagent has the ability to efficiently remove OM from soil samples. Because it is very inexpensive and quick, it has the potential to play a significant role in the examination of terrestrial samples for MP (Möller et al., 2020).

Enzymatic digestion can be an alternative to chemical digestion methods. Chemical methods can be effective, but they can also cause damage to some polymers. Enzymatic methods are known to be gentler, but are often laborious, expensive and time consuming (Courtene-Jones, Quinn, Murphy, Gary, & Narayanaswamy, 2017). So far the majority of reports on enzymatic digestion techniques have been tested on aquatic samples. Results from a series of enzymatic digestions combined with short treatments with H_2O_2 show promising results for the use on soil samples. Using several enzymes may lead to better digestion efficiency than, for instance, a single oxidation step using H_2O_2 since the utilized enzymes can target distinct chemical molecules (Möller et al., 2020).

2.5.3 Removal of the mineral fraction

For the separation of MP from sediment, density separation protocols are most commonly applied using high density salt solutions as extraction media (Möller et al., 2020). The average density of plastic is situated between 0,9 and 1,6 g/cm^3, with an exception for polytetrafluorethylene (PTFE) which has a density of 2,2 g/cm^3. The soil mineral fraction is known to have a higher density, resulting in the mineral fraction settling at the bottom and the plastic particles floating on top (Thomas et al., 2020). Solutions with different densities can be used to target specific MP. The extraction of low-density MP can be done using water or saturated sodium chloride. However, these inexpensive solvents are not suitable for the extraction of high-density MP. Other, more expensive, salt solutions, such as sodium iodide, zinc chloride, and calcium chloride, can be used in that case. Care should be taken when handling these salt solutions since they are more hazardous compared to water or sodium chloride solutions (Perez et al., 2022).

Another method for separating MP from the mineral fraction is oil extraction, as illustrated in Figure 2.5. Most plastics have lipohilic properties. When a soil sample containing MP is thoroughly mixed with water and canola or olive oil, the MP particles will convey into the oil layer when coming into contact with the oil. The procedure is simple, safe, cheap, and time efficient, but may require an additional step to remove organic substances from the sample (Möller et al., 2020).

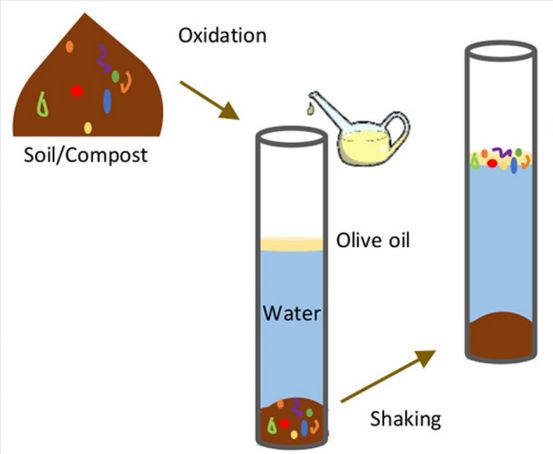

Figure 2.5: Extraction of MP using olive oil. Retrieved from Scopetani et al. (2020).

2.5.4 Identifying MP

Identification of MP is based on the physical and chemical characterisation of isolated particles after extraction of these particles from the soil matrix. At present, combinations of physical (e.g., microscopy) and chemical (e.g., spectroscopy) analyses are widely used (Shim, Hong, & Eo, 2017). The main advantages of chemical imaging can be summarized, when compared to other instrumental analysis methods (Xu, Thomas, Luo, & Gowen, 2019):

- Spectroscopic analysis in chemical imaging mode can acquire enriched information such as chemical composition, size and shape of the individual particle, and abundance of each polymer particle type within a sample.
- More efficient and labour-saving than other analytical methods.

The following table provides an overview of a few existing techniques for the identification and/or quantification of MP:

Table 2.3: Analytical techniques for identification and chemical composition detection of MP (Sorolla-Rosario et al., 2023; Tirkey & Upadhyay, 2021).

Technique	Features
SEM-EDS: Scanning electron microscopy	High resolution topography images of MP, information about MP surface and additives present on it
FTIR: Fourier transform-infrared spectroscopy	Chemical characterization for MP bigger than 20 μm, provides individual band patterns by specific infrared spectra for different plastic types
NIR: Near infrared spectroscopy	Non-destructive spectroscopic technique where no sample preparation is required and bulk samples can be easily examined, for MP bigger than 1 mm
Raman spectroscopy	Generates a 'fingerprint' of the chemical structure of MP bigger than 1 μm, which allows for the identification of particles in the sample
NMR: Nuclear magnetic resonance	Spectroscopic technique that provides quantitative and qualitative determination, can detect MP of any shape, size and polymer type
TED-GC/MS: Thermal extraction desorption-gas chromatography/ mass spectrometry	Combines spectroscopic analysis and pyrolysis for identification and quantification of MP

The two most common methods used for identification of MP are Fourier-transform infrared (FTIR) spectroscopy and Raman spectroscopy. These spectroscopic techniques require low sample amounts with minimal sample preparation and they are suitable for the discrimination between plastics and natural particles in marine and soil samples (Ivleva, Wiesheu, & Niessner, 2017). Despite some advantages of Raman spectroscopy (see 2.5.4.3), the identification of MP through the use of Raman spectroscopy is yet to attain the popularity of FTIR techniques (Araujo, Nolasco, Ribeiro, & Ribeiro-Claro, 2018). This is mainly because analyzing samples through Raman is more time-consuming compared to analyzing with FTIR (Xu et al., 2019).

2.5.4.1 Raman spectroscopy

Raman spectroscopy, a chemical analyzing technique, is recognized as a promising tool for MP analysis. It is based on the interaction of radiation with molecular vibrations. Molecular spectra have their origin in transitions between molecular energy levels. The pattern of such

energy levels is uniquely characteristic for a molecule. Often a knowledge of only salient features of this pattern is sufficient to identify a molecule (Staveley, 2016).

In Raman spectroscopy, a monochromatic beam of electromagnetic radiation (usually from a laser) is used to illuminate a sample (Bumbrah & Sharma, 2016). The laser light generating the electrical field induces a dipole moment for the molecules present in the sample, resulting in a scattering of the incoming radiation. This induced dipole moment can be split up into 3 components (Vandenabeele, 2013):

1. Elastic scattering of the electromagnetic radiation. The scattered light has the same frequency as the incoming radiation. This type of scattering is called Rayleigh scattering.
2. Inelastic scattering of the electromagnetic radiation. The scattered light has a higher energy compared to the incident beam. This type of scattering is called anti- Stokes scattering.
3. Inelastic scattering of the electromagnetic radiation. The scattered light has a lower energy compared to the incident beam. This type of scattering is called Stokes scattering.

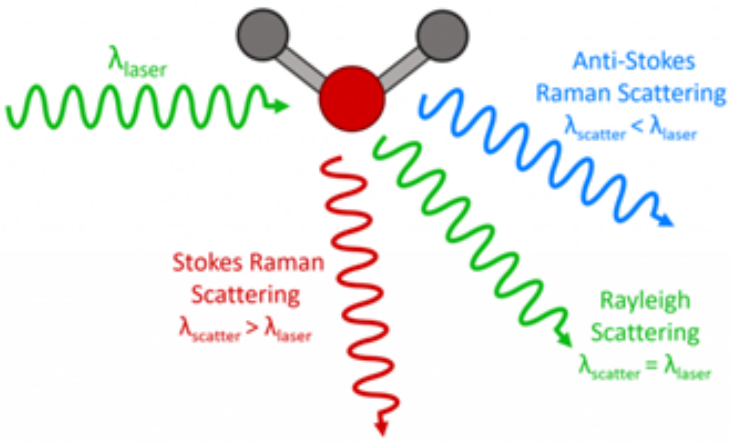

Figure 2.6: Three types of scattering processes that can occur when light interacts with a molecule. Retrieved from Edinburgh Instruments (2022).

The intensity of the scattered radiation is measured as a function of its wavelength. A Raman spectrum is usually plotted as a function of the wavenumber w (cm^{-1}), which is related to the difference in frequency between the scattered light and the incident electromagnetic radiation (Vandenabeele, 2013). Raman spectra thus arise due to inelastic collision between incident monochromatic radiation and molecules of sample. When the frequency of incident radiation is higher than frequency of scattered radiation, Stokes lines appear in Raman spectrum. But when the frequency of incident radiation is lower than frequency of scattered radiation, anti-Stokes lines appear in Raman spectrum (Bumbrah & Sharma, 2016).

2.5.4.2 FTIR

Infrared spectroscopy is a method in which the molecular vibrations of a sample are analyzed, resulting in characteristic features (so-called fingerprints) for the identification of chemical compounds. Although IR spectroscopy had been already introduced for the analysis of plastic in environmental samples in 1978, it was rapidly replaced with the use of FTIR spectroscopy. In contrast to the older more time-consuming mode, where the spectra are recorded through a stepwise shift of the wave-length, in FTIR spectroscopy, all wavelengths can be collected at the same time and then be processed by means of a Fourier transformation (Ivleva et al., 2017).

Functional groups can be linked to characteristic IR absorption bands, which correspond to the fundamental vibrations of the functional groups, as shown in Figure 2.7 (Berthomieu & Hienerwadel, 2009). A molecule that is irradiated with a continuous spectrum of infrared energy may absorb light quanta proportionally to the amount of infrared energy absorbed. The spectrum of the remaining radiation shows an absorption band at a frequency, v, of complex vibrational and rotational movements of molecules. Vibrations, which modulate the molecular dipole moment, are visible in the infrared. Complex molecules show numerous options of internal vibrations (Schmitt & Flemming, 1998). A fundamental vibration is infrared active (i.e., it absorbs the incident infrared light) if there is a change in the dipole moment of the molecule during the course of the vibration. Symmetric vibrations are usually not detected in infrared. In contrast, the asymmetric vibrations of all molecules are detected (Berthomieu & Hienerwadel, 2009). It has been internationally accepted that the position of absorption bands is expressed in wavenumbers (cm^{-1}), which is the reciprocal of the wavelength (Schmitt & Flemming, 1998). In FTIR spectroscopy, radiation is recorded simultaneously over all wavelengths. An interferogram is the result of the signal detection and contains all the information of the sample over all wavelengths. The sample-spectrum is then calculated from the interferogram by fast Fourier transform techniques with elaborated mathematical algorithms (Schmitt & Flemming, 1998).

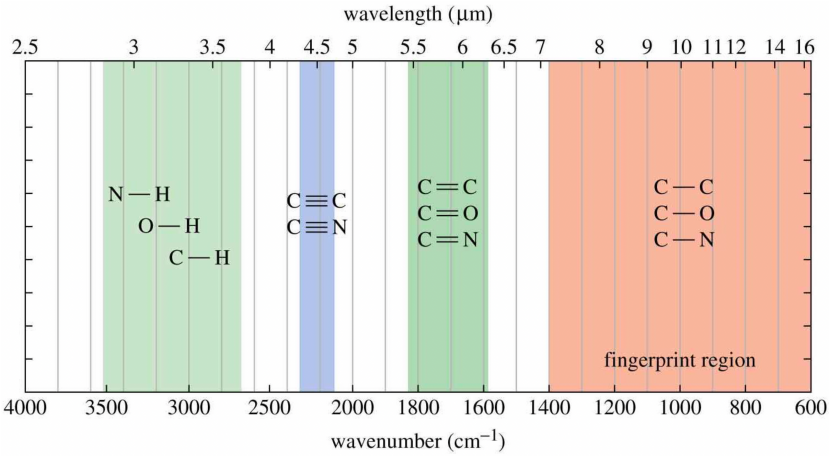

Figure 2.7: Common types of bonds, together with their stretching frequencies. Retrieved from Wade and Simek (2023).

The region of the IR spectrum containing most complex vibrations (600 to 1400 cm^{-1}) is commonly called the fingerprint region of the spectrum (Wade & Simek, 2023).

2.5.4.3 Comparing Raman to FTIR

Both Raman- and FTIR spectroscopy have their (dis)advantages. Raman spectroscopy shows a better spatial resolution, higher sensitivity to non-polar functional groups, lower water inference and narrower spectral bands. FTIR on the other hand is less prone to fluorescence interference and causes none to limited sampling heating, avoiding deformation of the MP (Araujo et al., 2018). Because of the difference in spatial resolution, Raman spectroscopy is able to assess MP samples smaller than 10 μm while infrared spectroscopy can only identify microparticles larger than 10 to 20 μm (Ivleva et al., 2017).

Both techniques, Raman and FTIR are considered to be complementary techniques because of the following fundamental rules (Nishikida & Coates, 2003):

- A vibration absorbs infrared energy when the molecular vibration induces a net change in dipole moment during the vibration. This is considered an active infrared vibration.
- When the molecular vibrations induces a net change in the bond polarizability during the vibration, the vibration is considered Raman active.

As a result, Raman spectroscopy is most sensitive to highly symmetric covalent bonds with little or no natural dipole moment (e.g. C-C, C-H) (Hodkiewicz & Scientific, 2010). FTIR is more sensitive to vibrations involving functional groups that have strong intermolecular interactions (e.g. C-O, O-H) (Smith, 2015).

MATERIALS AND METHODS

3.1 Sampling locations

The goal of this thesis is to investigate the presence of MP in 'non-suspected' soils. Existing literature does not yet provide an exact definition to describe non-suspected soils. An own interpretation will be given to the meaning of non-suspected soils, based on several land use types who are currently not considered to be the main focus for MP research, such as gardens, public parks, forests and agricultural land. These land use types are often overlooked compared to industrial sites or landfills, where MP pollution is expected to be ubiquitous (Nematollahi, Keshavarzi, Mohit, Moore, & Busquets, 2022). The sampling locations are chosen according to a gradient from (peri)-urban to rural and natural habitats. Natural habitats are expected to be less prone to MP contamination. As mentioned before in paragraph 2.2, anthropogenic inputs, including soil amendments, plastic mulching, irrigation, and littering, are the most important sources of MP. It is expected that locations closer to these types of activities/sources will be more prone to MP contamination, and thus to be more 'suspected'. Campus Coupure is located in the city center of Ghent, an urban environment, and Ardooie was selected because of it's proximity to the highway. Dourbes, the Bosland-site and the Kempense Heuvelrug are all located in remote areas of Wallonia and Flanders. Gentbrugse Meerse is situated in between these two extremes, a nature reserve just outside of the city center of Ghent.

Table 3.1 gives an overview of all sampling locations with information regarding their soil type according to the World Reference Base for Soil Resources (WRB) and the Belgian soil classification (Vlaamse Overheid, n.d.). Each sampling location is briefly described in the following section. The numbering on the images to indicate the different replications is continued to be used throughout this thesis.

Table 3.1: Soil types of the different sampling locations according to the World Reference Base for Soil Resources (WRB) and the Belgian classification (Vlaamse Overheid, n.d.). For Dourbes there is no WRB classification, since data was only available for Flanders.

Location	WRB classification	Belgian classification
Campus Coupure	Technosol (TC)	Artificial soil, built-up zone (OB)
Gentbrugse Meersen	Eutric Gleyic Cambisols (gl.eu), Eutric Retisols (Loamic) (eu)	Moderately wet sand loam soil (Ldp), moderately dry light sand loam soil with heavily mottled, fragmented texture B horizon (Pcc)
Ardooie	Eutric Gleyic Retisols (gl.eu)	Moderately wet sandloam soil with heavily mottled, fragmented texture B horizon (Ldc)
Dourbes	\	Soils on loose sediments with a coarse element content of more than 5%, dry soil, structure B horizont (Gbb)
Bosland-site	Albic Podzols (Arenic, Ruptic) (ab)	Very dry to moderately wet sandy soil with clear iron and/or humus B horizon (t-ZAg)
Kempense Heuvelrug	Dystric Protic Arenosols (pr.dy)	Dune soil (X)

3.1.1 Campus Coupure

Campus Coupure or the Faculty of Bio-science Engineering, Ghent University, is located in the city center of Ghent. Samples were taken in the garden in front of the faculty building. Three sampling plots were chosen parallel to the channel (connecting the Leie with the Brugse Vaart). Soil from Campus Coupure will be labeled as 'CP'.

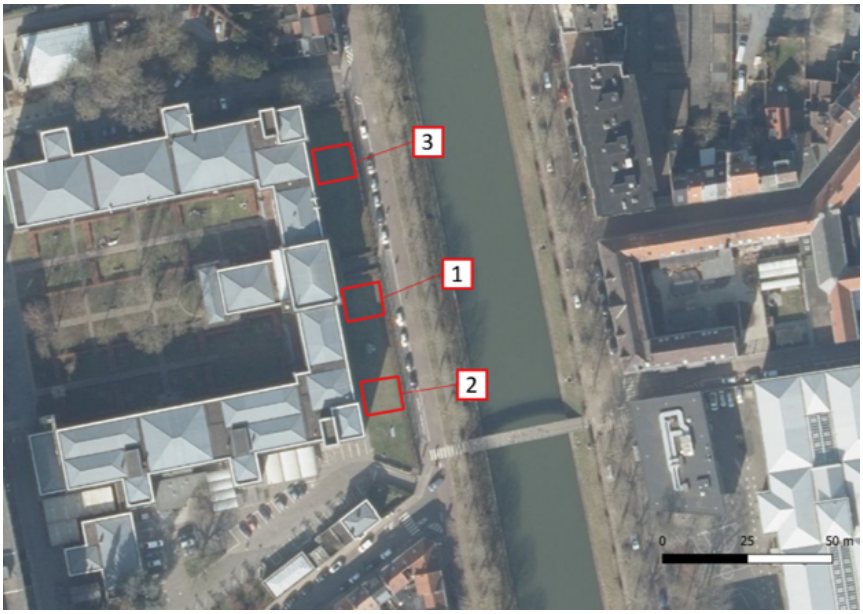

Figure 3.1: Sampling locations at Coupure, Ghent.

3.1.2 Gentbrugse Meersen

The region selected in Gentbrugse Meersen is used during summertime as a pasture field for cattle. It is used all year round by the public for leisure, dog walking, exercise, etc. Three sampling fields were selected randomly across the field in Gentbrugse Meersen. Soil from Gentbrugse Meersen will be labeled as 'GB'.

Figure 3.2: Sampling locations at Gentburgse Meersen, Ghent.

3.1.3 Agricultural field, Ardooie

Samples were taken on an agricultural field located next to the E403, a highway who passes through Ardooie. Archaeological excavations by BAAC Vlaanderen took place on this site

during the soil sampling. During these excavations, the top layer of soil was removed on a few square meters spread across the field. This caused limitations for soil sampling since samples could not be taken in area's were excavations took place.

Two locations were selected and on each location three plots were sampled. One of the locations was deliberately chosen in the immediate vicinity of the highway. The other one was located as far away as possible from the highway. Soil from Ardooie will be labeled '1AR' for the sampling location furthest from the highway and '2AR' for the sampling location closest to the highway.

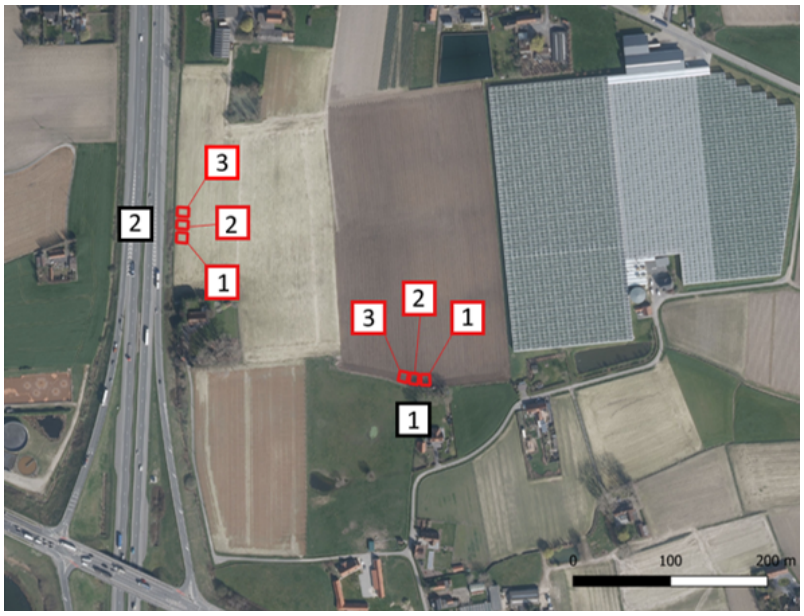

Figure 3.3: Sampling locations at agricultural field, Ardooie.

3.1.4 Geophysical center at Dourbes

The Geophysical center is located in a remote area in Dourbes, a small village near the French border. It is used to measure and study different geophysical phenomena, such as cosmic rays, the atmospheric electric field, meteorology, etc. The center was established in 1956, far from all electric and magnetic disturbances and is classified as a protected nature reserve (Koninklijk Meteorologisch Instituut, 2022). Three areas around the center were selected for taking soil samples. Soil from Dourbes will be labeled as 'D'.

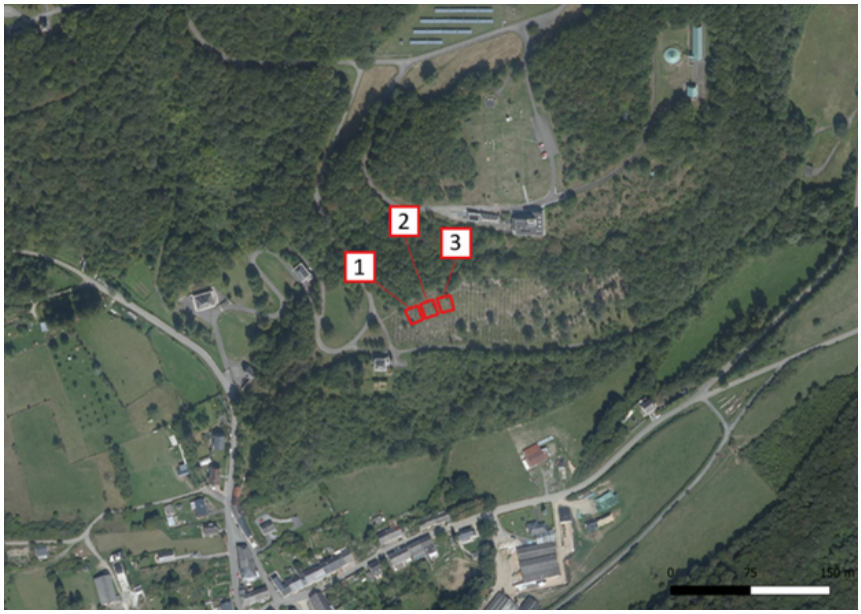

Figure 3.4: Sampling locations at the Geophysical center, Dourbes.

3.1.5 Bosland-site

The Bosland-site is located in Pelt, a municipality in the province of Limburg, Flanders. This recognized forest reserve, mainly consisting of pine trees, is managed by Boslab. Boslab is a community who connects science and nature through a variety of research and nature projects. All the areas managed by Boslab are called 'Bosland'. Three sampling fields were selected randomly across the forest. Soil from the Bosland-site will be labeled as 'P'.

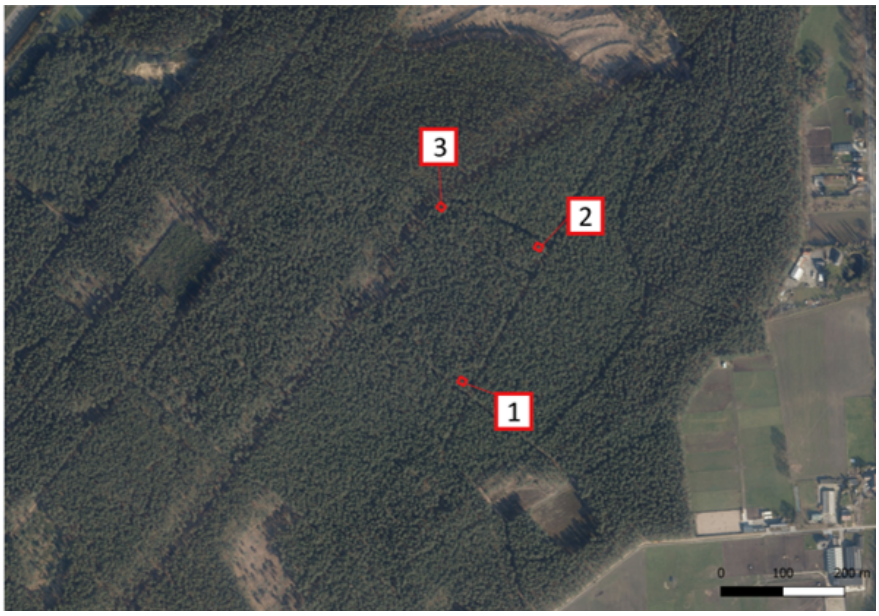

Figure 3.5: Sampling locations at Pelt.

3.1.6 Kempense heuvelrug

This nature-reserve, located between Herentals and Retie (two villages in Antwerp, Flanders), is governed by De Stichting Kempens Landschap. Three sampling areas were selected within the domain to extract soil samples from. Soil from the Kempense Heuvelrug will be labeled as 'KH'.

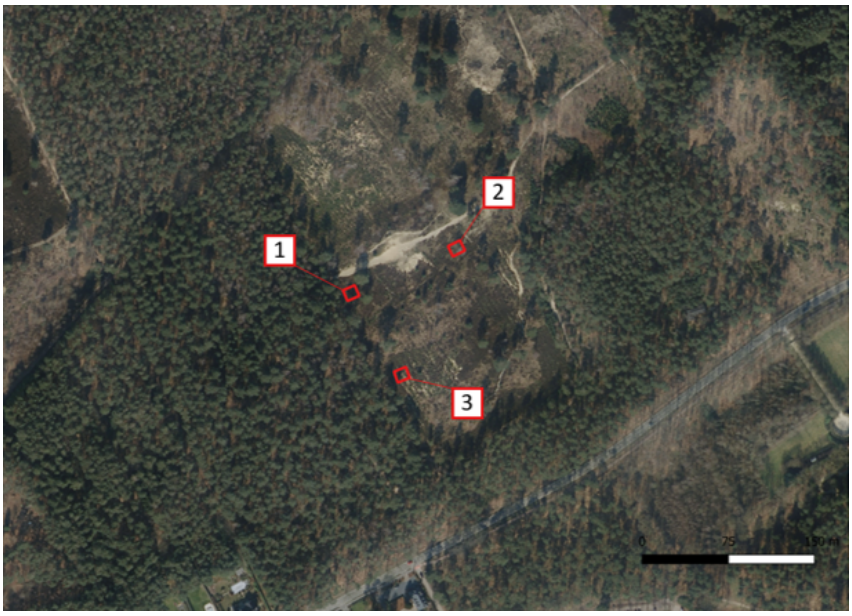

Figure 3.6: Sampling locations at Kempense Heuvelrug.

3.2 Soil sampling strategy

At each sampling location, three replications of the following sampling strategy were carried out.

A plot of 10 m (width) x 11 m (length) was demarcated. The plot was divided into 4 parts through five vertical lines along the width, each drawn at 2.5 m distance from each other. The samples were taken on the vertical lines, in an alternating pattern along the lines:

- 6 samples were taken starting at the outside of the plot and with a distance of 2 meters between the samples.
- 6 samples were taken at a distance of 1 meter from the outside of the plot and with a distance of 2 meters between the samples.

This resulted in a total of 30 augerings per plot. An auger with a diameter of 15 mm was used for taking the samples. Samples were collected to a depth of 20 cm. For one individual augering, the upper 0 – 5 cm (referred to as soil with label 'A') was removed and saved separately from the lower 5 – 20 cm (referred to as soil with label 'B'). After collecting a sample, the auger was wiped clean with kitchen paper to avoid contamination with MP between the samples. Finally, the cups containing all the samples from the upper 0 - 5 cm and the cups containing all the samples from the lower 5 - 20 cm were covered with aluminium foil to again contamination.

The three replications were carried out at similar places on the full sampling area. The area of interest for sampling was outlined in QGIS 3.26.2 for each location.

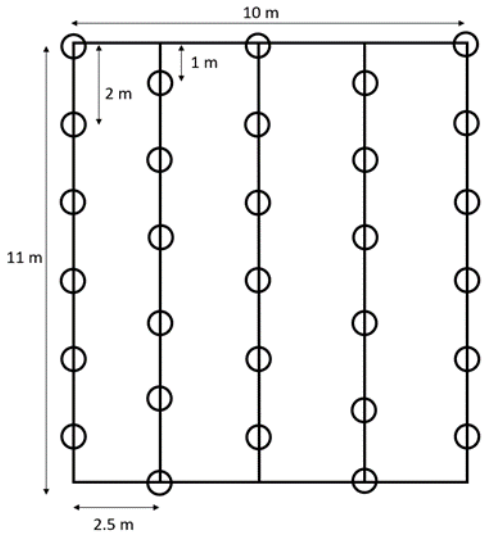

Figure 3.7: Soil sampling strategy followed at each location.

During the soil sampling procedure, contamination with plastic materials was avoided in the best way possible. Samples taken were stored in a wooden box in aluminium cups and

instantly covered with aluminium foil to avoid possible atmospheric MP contamination. It was important to avoid MP contamination during the sampling procedure and also during the extraction procedure that followed (section 3.4), since environmental samples were investigated. Extreme caution was needed during the preparation and handling of samples who contained unknown concentrations of MP, since a minor contamination with plastic can lead to the identification of this material in the samples, while the material did not originate from the samples.

3.3 Drying and sieving

The samples were placed in an oven at 40°C for at least 24 hours. This temperature was chosen, since temperatures above 40°C may affect the polymers' physical and structural properties by melting or degradation (Thomas et al., 2020). After drying, soil samples that belonged to the same location, the same depth and the same replication were bulked into one composite sample in a glass jar.

For example, in Dourbes there were 3 replications (1, 2 and 3). Each replication contained soil from the top layer (0-5 cm) labeled as A, and soil from the bottom layer (5-20 cm) labeled as B. This resulted in a total of six different final soil samples from Dourbes (D1A, D1B, D2A, D2B, D3A, D3B).

The composite soil samples were crushed with a mortar with pestle and sieved at 2 mm with a stainless steel sieve. Grinding of soil samples can increase particle fragmentation and can induce melting by frictional heat (Thomas et al., 2020). Crushing with mortar and pestle was done as gently as possible in this context.

3.4 Extraction procedure

During the whole extraction procedure, contamination with plastic material was avoided by only using glass lab material, covering the samples with aluminium foil between steps, and by placing the samples inside the fume hood when covering was not possible (e.g. in the hot water tub).

3.4.1 Dispersion of the aggregates

As MP may be incorporated into soil aggregates and thus not be easily separable from other soil constituents, additional preparative steps are required to promote the disintegration of soil aggregates and dispersion of grains (Thomas et al., 2020). To avoid further deformation and degradation of MP by grinding, the remaining soil aggregates, after crushing the soil with pestle and mortar, can be removed by using a dispersion agent (Thomas et al., 2020). A dispersion agent can be defined as a substance that can be used to reduce the aggregation of solid or liquid particles. In this case, sodium hexamethaphosphate is used to disperse the soil particles and preventing them from agglomeration (Chilingar, 1952).

To prepare the sodium hexamethaphosphate solution 23,66 g of $Nα_2CO_3$ and 142,80 g of $Nα_6[(PO_3)]_6$ were dissolved in water and diluted to a volume of 10,0 L in a 10,0 L volumetric flask. 50 ml of this solution was added to 10,00 g dried and sieved soil and swirled on a shaker plate for 15 minutes. This was repeated for all soil samples from each location, each replication and each depth.

3.4.2 First attempt for the removal of OM: Fenton's reagent

The density range of OM, 1,34 - 1,52 g/cm^3, overlaps with the density of many types of plastic and can therefore obscure the detection of MP and interfere with identification (Radford et al., 2021). Removal can be done using Fenton's reagent, a solution of $FeSO_4$ and H_2O_2, diluted with water. Because of its ease in operation, the simple system and the possibility to work in a wide range of temperatures, using Fenton's reagent seemed a logical choice for the removal of OM (Pawar & Gawande, 2015). Fenton's reagent makes it possible to perform the extraction of MP at ambient temperature, reducing the potential for exceeding the glass transition temperatures of some plastic materials and their corresponding deformation (Hurley et al., 2018). However, preparing the optimal Fenton's reagent resulting in an efficient removal of the OM was more challenging than first anticipated.

The combination of iron (Fe^{2+}) and hydrogen peroxide (H_2O_2), two main ingredients of Fenton's reagent, generates hydroxyl radicals ($OH^{\cdot}$). The hydroxyl radical serves as an oxidant that can react with Fe^{2+}, H_2O_2, or any OM present (Duesterberg & Waite, 2008). The following reactions take place (Vasquez-Medrano, Prato-Garcia, & Vedrenne, 2018):

$$Fe^{2+} + H_2O_2 \longrightarrow Fe^{3+} + OH^{\bullet} + OH^{-} \tag{3.1}$$

$$Fe^{3+} + H_2O_2 \longrightarrow Fe^{2+} + HO_2^{\cdot} + H^+ \quad (3.2)$$

The formed $OH^{\cdot}$ is a powerful oxidant, which can attack most of the organic molecules and is not highly selective. The hydroxyl radicals attack organic molecules by either abstracting a hydrogen atom or adding a hydrogen atom to the double bonds (Nidheesh, Gandhimathi, & Ramesh, 2013).

The Fenton reaction requires a specific set of conditions to achieve maximal efficiency of the reaction. According to Kušić, Božić, and Koprivanac (2007) and Rodrigues, Caetano, and Durão (2008) the best results are obtained when the Fenton is added at a pH of 3. At a lower pH value, the effectiveness of the Fenton reaction declines because the complexation of Fe^{3+} with H_2O_2 decreases, inhibiting the regeneration of Fe^{2+} (reaction 3.2). At higher pH values the concentration of free Fe^{2+} ions decreases due to the formation of ferrous complexes, thus disabling the formation of OH radicals (reaction 3.1). The pH can be adjusted using NαOH or H_2SO_4 (Kušić et al., 2007; Rodrigues et al., 2008). The optimal reaction temperature is found to be 30°C. Below that temperature, there is a slower H_2O_2 / $FeSO_4$ reaction rate. But above that temperature, there exists a rapid decomposition of H_2O_2, which can no longer contribute to OM removal (S. H. Lin & Lo, 1997). The optimum $FeSO_4$:H_2O_2 molar ratio has been defined as 1:5 by Rodrigues et al. (2008).

To fulfill all previous mentioned conditions, a solution of Fenton's reagent was prepared using 150 ml of H_2O_2 and 278,00 g of $FeSO_4$. This mixture was diluted to a volume of 500 ml (final Fenton solution). To each soil sample, 120 ml of this final Fenton solution was added. The pH of each soil sample, after adding Fenton's reagent, was measured using a digital pH meter. A solution of 1 M NaOH was added to each separate sample to increase the pH from approximately 2,1 to a pH of 3. After adding Fenton's reagent and adjusting the pH to an optimal level, the samples were placed in a warm water bath, base model WNB45 from Lemmert, at 30°C for 1-2 days. When no visible reaction occurred anymore, the samples were placed in an oven at 50°C for 1-2 weeks until completely dry.

Figure 3.8: Warm water bath, basic WNB45 model from Lemmert.

3.4.3 Density separation

Sodium polytungstate (SPT) $H_2Na_6O_{40}W_{12}$ is a medium used for density gradient separation. This nontoxic solid can be mixed with water to form a liquid with a fluid density that can be adjusted from pure water with a density of 1,00 g/cm³ to a saturated solution with a density of 3,10 g/cm³ (Skipp, 1993).

MP density can range from 0,91 g/cm^3 for low-density polyethylene (LDPE), up to 2,20 g/cm^3 for polytetrafluorethylene (PTFE), passing through Polypropylene (PP), Polystyrene (PS) and olyethylene terephthalate (PET) with densities of 0,85; 1,05 and 1,37 g/cm^3, respectively (Borges-Ramírez, Mendoza-Franco, Escalona-Segura, & Rendón-von Osten, 2020).

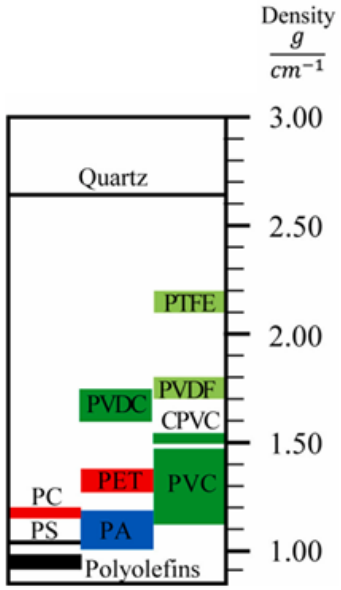

Figure 3.9: Comparison of densities of different plastic materials (CPVC: chlorinated polyvinyl chloride; PA: polyamide; PC: polycarbonate; PET: polyethylene terephthalate; PS: polystyrene; PTFE: polytetrafluoroethylene; PVC: polyvinyl chloride; PVDC: polyvinylidene dichloride; PVDF: polyvinylidene difluoride. Retrieved from Grause et al. (2022).

First an SPT-solution with a density of 1,21 g/cm^3 was used to separate the light-density MP from the soil matrix (all MP particles with a density lower than 1,21 g/cm^3). The samples were put in the Eppendorf Centrifuge 5810R for 20 minutes at 9000 rpm. This resulted in the settling of mineral matter at the bottom because it is denser (2,4 - 2,9 g/cm^3) than the SPT and the light-density MP being present in the liquid SPT-layer (Rühlmann, Körschens, & Graefe, 2006). Afterwards, the supernatant containing the MP was carefully removed using a pipet and filtered over a glass fibre filter with a pore size of 1,2 μm (Ø 47 mm, borosilicate glass, Whatman). MP (and remaining OM) (>1,2 μm) were retained on the filter, while the SPT had passed through. The MP investigated in this research will have a size rang of 2 mm (sieve mesh size) to 1,2 μm.

After the first round of centrifugation and filtration, the same sample was used to repeat the density separation procedure on. There was no option but to use the same tubes, with still some leftover SPT present after the first density separation (density 1,21 g/cm^3) for the second density separation. This leftover SPT could not be removed since the same sample was needed for the second extraction round and removing the SPT is not possible without a possible loss of MP (and even soil). An SPT-solution with a density of 1,80 g/cm^3 was added to the samples. This resulted in the heavy-density MP (all MP particles with a density between 1,21 g/cm^3 and 1,80 g/cm^3) remaining on the filter papers.

The samples originating after the first density separation (1,21 g/cm^3) and the samples after the second density separation (1,21 g/cm^3 and 1,80 g/cm^3) were considered as two independent samples and analyzed separately.

3.4.4 Second attempt for the removal of OM: Fenton's reagent

After filtration it was clear that the OM was not removed properly (see Figure 3.10a). It was decided to repeat the whole extraction procedure again from the beginning, starting with the dispersion of soil aggregates (subsection 3.4.1). This time, the pH wasn't adjusted, no NαOH was added. The adjustment of the pH was an extra step which was never tested during the first extraction trials. Therefore, it was suspected that this might have caused the suboptimal OM degradation. Every other step in the extraction procedure remained the same. Unfortunately, after filtration still some visible OM remained on the filter papers (see Figure 3.10b).

(a) OM remaining after the first attempt to remove OM using Fenton's reagent.

(b) OM remaining after the second attempt to remove OM using Fenton's reagent.

Figure 3.10: Remaining OM after centrifugation and filtration after the first attempt (3.10a) and after the second attempt (3.10b) when using Fenton's reagent.

To confirm whether the OM had indeed been insufficiently removed, the total organic carbon (TOC) content of three random samples from different locations (Kempense Heuvelrug (KH1A), Dourbes (D2A) and Pelt (P1A)) was determined using the MCS Formacs TOC-module for solid samples from Skalar as shown in Figure 3.11. This was done for untreated soil, soil after the first attempt for OM removal (Fenton + NαOH), and soil after the second attempt for OM removal (Fenton) from the three locations.

Figure 3.11: MCS Formacs TOC-module for solid samples from Skalar.

The total carbon (TC) content is determined by heating the samples to 1100 °C, where the total carbon present in the samples is converted to CO_2 and measured with an infrared detector (NDIR detector). The inorganic carbon (IC) content is determined by acidifying the sample with H_3PO_4 (4%) in an oven at 200 °C where all inorganic carbon (IC) is converted to CO_2 and measured with the same NDIR detector. The TOC-content can be found by subtracting the IC-content from the TC-content. Finally, the OM content can be derived from the TOC-results by using a conventional conversion factor of 1,724. This factor is based on the assumption that SOM contains 58% of carbon (Pribyl, 2010). Soil with the highest TOC-content will therefore also have the highest OM content.

Table 3.2: Total carbon (TC) content for untreated soil, soil after the first attempt to remove OM (Fenton + NaOH) and soil after the second attempt (Fenton). The TC content was measured for three random samples from Kempense Heuvelrug, Dourbes and Pelt.

	TOC-content (%)		
	Untreated soil	Fenton + NaOH	Fenton
Kempense Heuvelrug	2,227	0,451	0,254
Dourbes	5,844	0,714	0,526
Pelt	7,351	1,399	0,277

Table 3.2 shows that the lowest TOC-content, and therefore also the lowest amount of OM, was found in samples after the second attempt, where the pH was not adjusted. This confirmed earlier assumptions made that adjusting the pH using NαOH results in suboptimal OM degradation. However, even when not making any adjustment to the pH, a low percentage of OM was still found in all samples.

Due to limited time and a limited amount of soil from all the different sampling locations, it was decided to not restart the whole process, but to remove the remaining OM on the filter papers using H_2O_2.

3.4.5 Final removal of the OM using H_2O_2

After density separation and filtration the filters, that contained MP and remaining OM, were carefully rinsed off with demineralized water and this water was collected in metal cups. The

metal cups were then placed in an oven to dry for about 24 hours at 50°C. Afterwards, 33 ml of H_2O_2 (30%) was added to each cup. This mixture was collected in small glass bottles. The bottles were then placed in a warm bath, model WNB45 from Lemmert, at 70°C for 24 hours to speed up the breakdown of OM by H_2O_2. Afterwards, the content of each bottle was filtered over a glass fibre filter. Each bottle was rinsed with demineralized water to remove remaining MP and all water was also passed through the filter.

The end result was two filter papers for each replication from each sampling location and each depth (0-5 cm and 5-20 cm), one containing low-density MP and one containing high-density MP. Finally, the filter papers were dried in the oven at 50°C for about 24 hours, after which they were ready to be taken to the FTIR for further analysis.

Figure 3.12: Filter papers at the end of the extraction procedure.

A unique code was given to each sample, shown in Figure 3.13. This code will be used further on when referring to a specific sample.

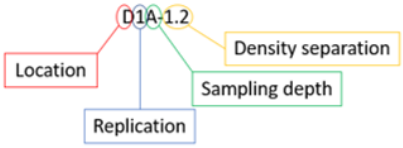

Figure 3.13: Example of the sample code for a sample taken at Dourbes.

3.4.6 Identification

The Attenuated Total Reflectance (ATR) FTIR technique was used in transmittance mode to determine the MP present in the samples. In this technique, a sample is placed in contact with a crystal with a high refractive index. The sample is then irradiated with infrared radiation, and the light that is reflected back from the crystal is analyzed. In transmittance mode, the IR beam is passed through the sample, and the amount of light that passes through the sample is measured (Grdadolnik, 2002). The IR spectra graphs and data were obtained through FTIR (Vertex 70 Bruker) and OPUS (Bruker) software version 7. The version was licensed to VERTEX 70/80 SYSTEM Universiteit Gent. The MP present on the filters were

thoroughly scraped off in order for them to end up in the sample compartment of the FTIR spectrometer. Before measuring the samples, 20 background scans were pooled followed by averaging 10 sample scans with a spectral resolution of 1 cm^{-1} in a wavenumber range from 4000 cm^{-1} to 400 cm^{-1} to produce the final spectrum. Between each measurement the equipment was cleaned with ethanol to prevent contamination.

To analyze the data generated by the FTIR spectrometer, the Open Specy software was used. This is a free available spectral matching tool which allows users to upload FTIR or Raman spectra, and to process, compare and identify them using spectra from an onboard reference library using correlation-based matching criteria (Cowger et al., 2021). The FTIR library consists of 325 spectra from Primpke, Wirth, Lorenz, and Gerdts (2018), 272 spectra from Chabuka and Kalivas (2020) and 39 spectra from Thermo Fisher Scientific (2023). The matching procedure consists of a Pearson correlation (r) between the reference spectra from the library and the uploaded or processed spectrum (Cowger et al., 2021). Pearson's r is used directly as the hit quality index for ranking matches. The software shows the 100 highest matches. Top matches need to be above a Pearson correlation coefficient of 0,60. If not, they should be suspected to be a result of incorrect processing, poor quality spectra, or of a material type not currently in the reference library (Cowger et al., 2021). More information about the use of Open Specy can be found in Appendix A.

After looking at the results from Open Specy, it was decided to also perform a manual peak analysis of the same FTIR spectra, obtained through FTIR (Vertex 70 Bruker) and OPUS (Bruker) software. The spectra were uploaded and processed with the Origin LabPro 2021 software. Because of limited time, a selection was made for the spectra to be analyzed. It was decided to look at spectra from the first replication from each location separated at a density of 1,21 g/cm^3 for both soil from the top (A) and bottom layer (B).

Given the uncertainties and challenges that occurred when identifying FTIR spectra, it was also tried to revert to Raman spectroscopy for the identification of individual MP. First particles, believed to be MP, were searched for and visualized using the Keyence Digital Microscope VHX-500F series (Figure 3.14). An indication of the location of these particles was made on the corresponding filter paper using a marker, so that they could be easily retraced during the Raman procedure.

Figure 3.14: Keyence Digital Microscope VHX-500F series.

The Raman setup consisted of a WITec alpha 300 microscope that can operate in optical mode and Raman mode. Analysis of samples always started with optical microscopy. When one of the previous indicated particles was found, the switch to Raman mode was made. The objective used was the Nikon Plan fluor 10x/0.30 objective. In Raman mode, the sample was excited by a laser diode (785 nm, Toptica XTRA II) and Raman signals were transferred by a multimode fibre (diameter 200 μm) and detected by a spectrometer (UHTS 300) equipped with a -70°C cooled CCD camera (ANDOR iDus 401 BR-DD). This system was connected to a computer and operated using Control FIVE software. Single spectra were produced by focusing on a very small area around the centre of the laser position. Afterwards, spectra and pictures were analysed, again using Project FIVE software.

RESULTS AND DISCUSSION

4.1 Methodological challenges with the use of Fenton's reagent for OM removal

Table 3.2 clearly shows that using Fenton's reagent for the removal of OM was never completely efficient. During the first attempt, the adjustment of the pH using NαOH, resulted in an unexpected suboptimal OM degradation. According to Kušić et al. (2007) and Rodrigues et al. (2008) the Fenton reaction occurs optimally when Fenton is added at a pH of 3. In wastewater treatment NαOH or H_2SO_4 is added to the wastewater to bring it to an optimal pH, after which the Fenton solution is added to the wastewater (Kušić et al., 2007; Rodrigues et al., 2008). Soil pH is controlled by many variables such as the leaching of basic cations, the dissolution of CO_2 in soil water producing carbonic acid, inputs from acid rain and N uptake by plants, making pH adjustments more complex (Neina, 2019). It was decided to add NαOH directly after adding the Fenton solution to the soil samples. The following reactions can help in understanding why adding NαOH directly to Fenton's reagent can inhibit the breakdown of OM (Ogata, Nakamura, & Kawasaki, 2018).

The hydroxide ion can react with H_2O_2 present in the Fenton solution. The following reaction can occur, resulting in a decomposition of the H_2O_2:

$$H_2O_2 + OH^- \longrightarrow H_2O + HO_2^- \tag{4.1}$$

In addition, Fe^{3+} is not reduced in basic conditions, resulting in a precipitation of Fe_2O_3:

$$2\,Fe^{3+} + 6\,OH^- + (n-3)\,H_2O \longrightarrow Fe_2O_3 \cdot nH_2O \tag{4.2}$$

Reaction 4.1 will have a negative influence on both Fenton reactions (reaction 3.1 and reaction 3.2) described in subsection 3.4.2. Reaction 4.2 will prevent reaction 3.2 from occurring, by inhibiting the regeneration of Fe^{2+} and stopping the chain reaction. Using NαOH for pH adjustment to require optimal reaction conditions by directly adding it to Fenton's reagent can quench the Fenton reaction (Wink, Nims, Saavedra, Utermahlen Jr, & Ford, 1994).

- **The advantages of using Fenton's reagent**

The most important advantage of working with Fenton's reagent to remove OM is that the solution can be prepared and added at ambient temperature, reducing the potential for exceeding the glass transition temperatures of some plastic materials (Hurley et al., 2018). The glass transition temperatures of polybutylene terephthalate (PBT), PMMA, and PA are 40 °C, 50 °C, and 50–75 °C, respectively. NR and ethylene-vinyl acetate may start melting at temperatures of 30–65 °C (Thomas et al., 2020). This advantage was lost by adding H_2O_2 (30%) to the samples and keeping them in a hot water bath for 1-2 days at 70 °C. Polymer degradation of previous mentioned plastic materials could occur due to the elevated reaction temperature (Thomas et al., 2020). Next to polymer degradation caused by elevated reaction temperature, H_2O_2 oxidation could also damage the polymer structure of PE and PP (Hurley et al., 2018).

Fenton's reagent doesn't affect the particle number, shape and size of MP. Quantification of MP remains possible after treatment with Fenton via manual counting under microscopes or automatic mapping facilitated by FTIR spectroscopy, Raman spectroscopy, or fluorescence dying methods. However this remains a challenging and time-consuming method (J. Lin et al., 2021).

- **The disadvantages of using Fenton's reagent**

Given the complex nature of soils, a suitable and efficient method for standardized MP analysis in the soil matrix has yet to be found. There exist a lot of different published methods for sampling, extraction, purification, and identification/quantification of MP in complex environmental matrices, such as soil samples (Möller et al., 2020). A standard procedure for the removal of OM using Fenton's reagent is still lacking.

As experienced in this thesis and described by other researchers, certain biogenic matter will not be removed when using Fenton's reagent, thus a complementary organic removal step may be necessary (Möller et al., 2020; Sun & Yan, 2007). Here, it was decided to use H_2O_2 to remove remaining OM after treatment with Fenton.

The Fenton reaction requires and generates highly reactive elements, such as hydrogen peroxide, hydroxyl radicals, and other radical species. Their reactivity enables them to oxidize a large number of cellular constituents, making them toxic/dangerous for living organisms (Buyuksonmez, Hess, Crawford, & Watts, 1998). The Fenton solution needs to be prepared carefully while wearing protective clothes and gloves. During the MP extraction procedure in the lab, Fenton caused recalcitrant stains on lab coats, glass work and other lab material that came into contact with the Fenton solution.

4.2 MP analysis

During the identification procedure, starting with the analysis of FTIR data from all the samples using Open Specy, it became clear that it is difficult to identify microplastics of various sizes, shapes and polymer type originating from complex environmental samples, fully and reliably using a single analytical method. Therefore, a series of different techniques was used in an attempt to identify the MP present in the samples and to overcome some challenges that could be avoided by using a different technique.

Visual identification of MP offers an easy, simple and fast method to get a first idea of what is present in the samples. Figure 4.1 contains a few pictures of interesting particles, made with the Keyence Digital Microscope, that are likely to be MP.

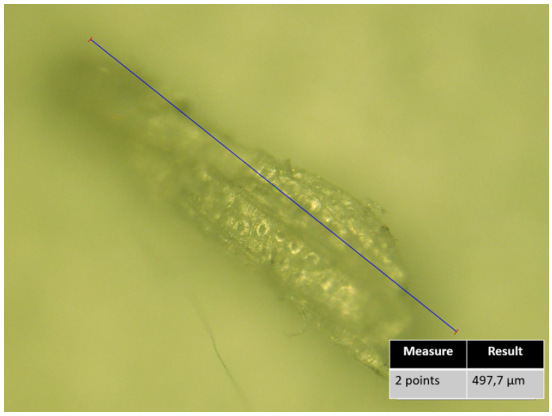

(a) P1A-1.2.

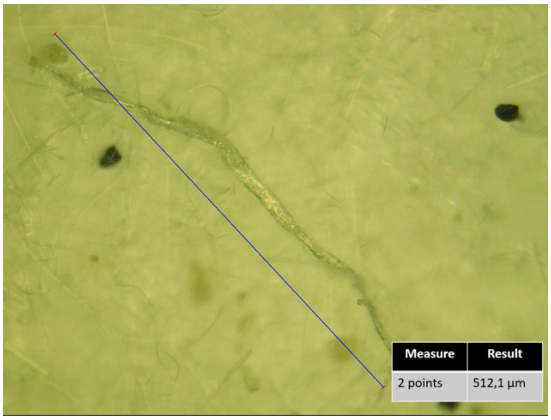

(b) GB1B-1.2.

(c) 1AR1A-1.2 (1).

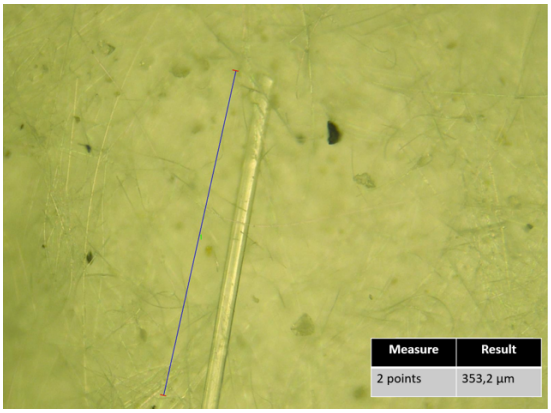

(d) 1AR1A-1.2 (2).

Figure 4.1: Pictures of suspected MP particles taken with the Keyence Digital Microscope.

The pictures taken with the Keyence Digital Microscope don't give any information about the chemical composition of the particles present. A study by Eriksen et al. (2013) described the misidentification of particles initially identified as MP by visual observation to be approximately 20%. Therefore, spectroscopic techniques are necessary to draw an indisputable conclusion about the identity of the particles.

A first attempt for chemical identification was done by identifying MP based on their FTIR spectra. Automated software (section 4.2.1) was used to identify the peaks that occurred in these spectra. A second identification technique, manual peak identification (section 4.2.2), was used in an attempt to overcome the problems that occurred during automated identification. A final identification technique was done using Raman spectroscopy, where the Raman spectrum of individual particles was investigated (section 4.2.3).

The flowchart in figure 4.2 gives a chronological overview of the different techniques that were tested when identifying MP. For each attempt, the disadvantages, who were often tried to overcome in the following technique, and advantages are given. The following sections thoroughly describe all the different attempts tried when identifying MP in accordance with the sequence of steps in the flowchart.

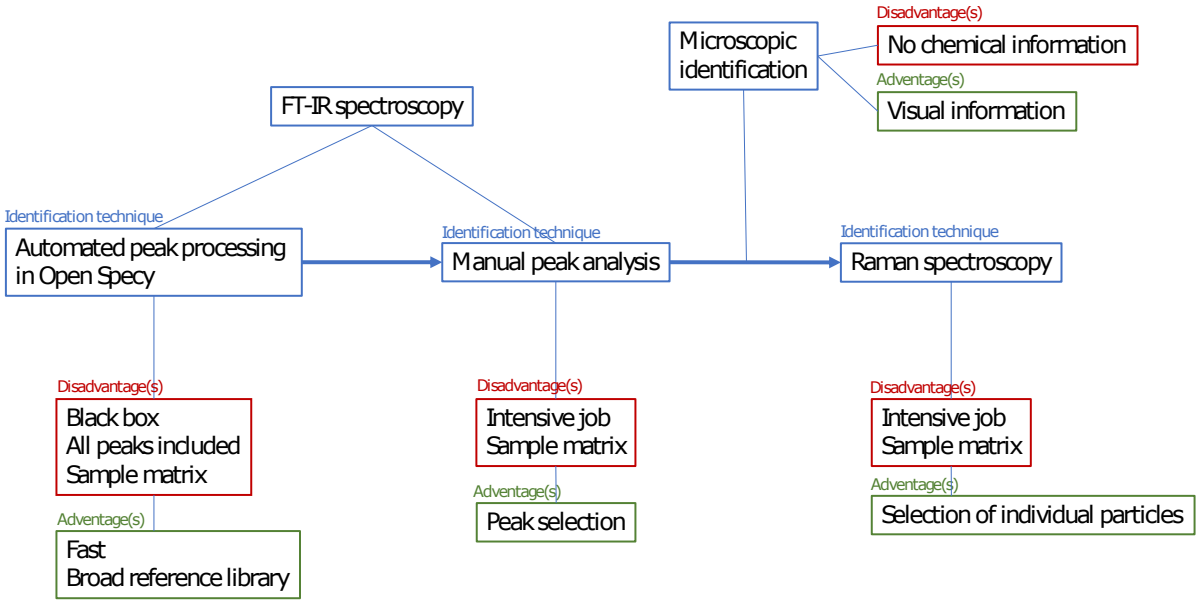

Figure 4.2: Flowchart of the different steps followed during the identification procedure. For each step, the advantages and disadvantages are given.

4.2.1 Open Specy

The results generated with Open Specy for all the samples from each location and each replication can be found in Appendix B.

Open Specy was chosen as an identification tool for MP over manual peak identification because of following reasons:

- The processing of a large number of samples (84) takes less time when using automated software compared to manual peak identification as an alternative. Analysis of environmental microplastics is a high sample throughput task and it is not feasible to evaluate every single FTIR spectrum (Renner, Schmidt, & Schram, 2017).
- Environmental samples contain a possible endless range in different polymer materials. When using a reference spectral library containing a broad range of different polymers, more materials can be identified compared to looking up peak values of a narrow selection of polymers and performing manual peak identification with these values.
- Open Specy allows users to process their uploaded spectra using smoothing and polynomial baseline correction techniques (see appendix A). No additional pre-processing is necessary to analyze spectra.
- New specialized matching techniques that focus on peak regions of the reference spectra are shown to drastically outperform the standard techniques for MP research, such as manual identification (Cowger et al., 2021).

4.2.1.1 Discussing the value of Pearson's r

Only in 11,90 % of all samples, MP were identified with a Pearson correlation above 0,60.

The reference spectra from Primpke et al. (2018) contain spectra of common polymer types as well as natural materials often present in environmental samples, such as natural fibers. The reference spectra of the polymers were generated mostly using polymer particles from polymer manufacturers (72%) (De Frond, Rubinovitz, & Rochman, 2021). No additional information could be found on the spectra in the library originating from Thermo Fisher Scientific (2023). The spectral library from Chabuka and Kalivas (2020) was augmented with additional polymer samples such as cellulose, fibers, films, and colored plastics to avoid misidentification. The effect of physical and photochemical weathering was taken into account for PET and HDPE samples. FTIR spectra of PET and HDPE polymers that were exposed to simulated physical and photochemical weathering were added to the reference library (Chabuka & Kalivas, 2020).

A major challenge to microplastic identification is that weathered MP undergo surface chemical changes which limits spectroscopic matching and thus identification (Phan, Padilla-

Gamiño, & Luscombe, 2022). MP pollution is the result of mismanaged waste from a broad array of items of different colors and shapes with different sources and usage. Plastics undergo degradation and fragmentation, which can destroy the physical integrity of the plastics and alter their chemical properties. Leaching of chemical additives and colonization by microorganisms, creating a biofilm on the particle surface, both impact the quality of FTIR spectra acquired (De Frond et al., 2021). MP weathering in different environments can lead to different IR spectra (Phan et al., 2022). A study by Campanale, Savino, Massarelli, and Uricchio (2023) reflected changes in peaks corresponding to hydroxyl groups (3100 to 3700 cm^{-1}), alkenes or carbon double bonds (1600 and 1680 cm^{-1}) and carbonyl groups (1690 and 1810 cm^{-1}) when comparing artificial and natural weathered plastics to the pristine materials. Moreover, new unique peaks were also observed, almost all in the fingerprint region (1500 to 500 cm^{-1}). These new spectral bands due to chemical changes can overlap with the most characteristic identification ones, complicating MP identification (Fernández-González, Andrade-Garda, López-Mahía, & Muniategui-Lorenzo, 2021).

The low Pearson correlation could be a consequence of (severe) weathering of MP that is not thoroughly taken into account in the reference spectra from the library. Including more spectra of weathered polymers in the spectral library to obtain a reliable identification of MP is critical. The visible appearance of MP, related to the chemical additives used in production, does not significantly affect their spectral output. This may benefit using FTIR analyses over Raman spectroscopy, since bright colors can lead to particle fluorescence and signal overlay from pigments and dyes in Raman spectroscopy (De Frond et al., 2021). But various degrees of environmental degradation do alter the polymer composition and thus alter the chemical fingerprint, making the identification of MP using FTIR spectral libraries more challenging (De Frond et al., 2021; Fernández-González et al., 2021). In addition to the content of the reference libraries used, there are more factors involved in achieving an accurate spectral match using FTIR spectroscopy, for example, measurement parameters, spectral noise, and spectral pre-processing (De Frond et al., 2021).

4.2.1.2 Effect of applying two density separations

During the extraction procedure it was decided to apply two density separations, based on the method for MP extraction from compost followed by Gui et al. (2021) (section 3.4.3). It can be expected to only find MP with a density lower than 1,21 g/cm^3 in the samples after the first density separation (left side of table 4.1). Subsequently, MP with a density between 1,21 g/cm^3 and 1,80 g/cm^3 can only be present in samples resulting from the second density separation (right side of table 4.1).

Table 4.1: Overview of all the plastic polymer types found in the samples and their corresponding density (Omnexus, n.d.; Scientific Polymer Product Inc., n.d.).

Density below 1,21 g/cm^3		Density above 1,21 g/cm^3	
Material	Density	Material	Density
EPDM	0,86	CR	1,23
EPR	0,86	PSU	1,24-1,25
SIS	0,92	PET	1,30-1,40
PP	0,90-0,95	PC	1,30-1,59
PE	0,84-0,97	PVC	1,38
HDPE	0,94-0,97	PDMS	1,40
XPS	0,95-1,05	PTFE	2,10-2,20
ABS	1,02-1,21		
PS	1,04-1,25		
SAN	1,06-1,10		
SAA	1,08		
PA 6	1,12-1,41		
PEG	1,13		
PEO	1,13		
PA 66	1,13-1,15		

When looking at the results in appendix B, it is clear that applying two density separations during the extraction procedure did not result in a corresponding separation of MP by density. MP with a density greater than 1,21 g/cm^3 were found in samples after the first extraction round (density separation at 1,21 g/cm^3). After the second extraction round (density separation at 1,80 g/cm^3), MP with a density below 1,21 g/cm^3 could still be found.

The following explanations could help understand how the MP with a density above 1,21 g/cm^3 could have ended up in samples extracted only with the SPT-solution of 1,21 g/cm^3:

- MP particles can be made up of more than one polymer type. Compositions (copolymers) such as PET-PA, PET-PS and PP-PS have been observed by Nematollahi et al. (2022).
- The parameters chosen during the density separation might have been suboptimal. Phuong, Poirier, Lagarde, Kamari, and Zalouk-Vergnoux (2018) and Monteiro et al. (2022) mention optimal conditions for centrifugation to be 5 minutes at 500-3500 rpm. A higher acceleration is recommended. However, a high speed at 9000 rpm for 20 minutes is not considered in previous research.
- CR, PET, PVC, PC, PDMS and PTFE were found with corresponding r values of respectively 0,34; 0,43; 0,57; 0,30; 0,57 and 0,73. The values for CR, PET and PC are rater low

and the quality of the match with the reference spectra for these materials could be questionable.

The presence of MP with a density below 1,21 g/cm^3 in samples after the second extraction suggests that not all light-density MP were extracted after the first extraction round. The following explanations could help understand how the MP with a density below 1,21 g/cm^3 could have ended up in samples after the second density separation:

- After removing the supernatant containing the MP from the first density separation round, the same tubes with the same soil were used for density separation at 1,80 g/cm^3. Residues from the first attempt were not removed to make sure no MP were lost. These residues could have been a possible source of MP with a density below 1,21 g/cm^3.
- The upward movement of MP could be hindered by the settling of the sand, reducing the recovery at the end of the centrifugation process (Grause et al., 2022). Remaining MP that were suppressed by sand particles during the first centrifugation session, could have been recovered during the second round of centrifugation.

4.2.1.3 MP results for each sampling location

For each location, an overview of the different plastic polymers that were found is given. The Pearson correlation of each polymer corresponds to the highest r from all the samples on the location that contained this polymer.

- **Urban soil: Coupure**

A study by Zhou et al. (2022) indicated that the most common polymer types found in urban soils are PET, PP and ABS. Nematollahi et al. (2022) state that PET and PA are the most common polymer types in urban soils. PET, PP, ABS and PA 6 were found in the samples with a corresponding r of respectively 0,36; 0,65; 0,48 and 0,32.

PP, PS and PVC had a value for r above 0,60; which suggest an indisputable presence of these plastic materials in the soil from Campus Coupure. PS and PVC are one of the most common MP found in soils, regardless their land-use (Leitão, van Schaik, Ferreira, Alexandre, & Geissen, 2023).

Table 4.2: Overview of all the different polymer types found at Campus Coupure and their corresponding highest Pearson correlation. This table is based on the results given in Appendix B.

EPDM	**EPR**	**SIS**	**PP**	**PE**	**HDPE**
0,57	0,47	0,35	0,65	0,42	0,53
XPS	**ABS**	**PS**	**SAN**	**SAA**	**PA 6**
0,58	0,48	0,71	/	0,36	0,32
PA 66	**PEG**	**PEO**	**CR**	**PSU**	**PET**
/	0,40	0,41	/	/	0,36
PC	**PVC**	**PDMS**	**PTFE**		
/	0,63	0,44	/		

- **Pasture field: Gentbrugse Meersen**

MP concentrations are expected to be higher in ecosystems with low to null tree cover, such as savannas, induced grasslands, or in this case pastures, because wind-dispersed particles may find fewer obstacles compared to a forest or tree plantation (Álvarez-Lopeztello, Robles, & del Castillo, 2021). The presence of a landfill, only 2,20 km away (bird's eye view) from the sampling location was noticed. The continuous exposure of plastic garbage to open air in this landfill can cause coarse plastic fragments to break up, which results in the release of MP to the surrounding environment. Atmospheric deposition plays an important role in the distribution of these plastic fragments (Qiu, Song, Zhang, Xie, & He, 2020).

All the polymers in the samples from Gentbrugse Meersen were identified with a Pearson below 0,60.

Table 4.3: Overview of all the different polymer types found at Gentbrugse Meersen and their corresponding highest Pearson correlation. This table is based on the results given in Appendix B.

EPDM	**EPR**	**SIS**	**PP**	**PE**	**HDPE**
0,49	0,42	/	0,55	0,32	0,59
XPS	**ABS**	**PS**	**SAN**	**SAA**	**PA 6**
/	0,39	0,46	/	0,42	0,38
PA 66	**PEG**	**PEO**	**CR**	**PSU**	**PET**
/	0,39	0,42	/	/	0,40
PC	**PVC**	**PDMS**	**PTFE**		
/	0,54	0,55	/		

- **Agricultural field: Ardooie**

Sewage sludge is commonly recycled to agricultural land as a sustainable and renewable source of fertiliser in many European countries. Belgium only re-used 13 % of its total production of sewage sludge in agriculture in 2012. This low percentage is due to legal constraints (Delvigne et al., 2016). Sludge from treatment plants for domestic, urban and/or industrial wastewater can still be used in agriculture, but the application of sewage sludge originating from urban waste water is forbidden in Belgium (Belgische Federale Overheidsdiensten, 2023). PP, PE, PA and PS are the most common polymer types found in sewage sludge (Koyuncuoğlu & Erden, 2021). The highest r values found for these polymers on both locations were 0,57; 0,37; 0,38; 0,31 and 0,63 for PP, PE, PA 6, PA 66 and PS for location 1 and 2 respectively.

The main goal of studying two different sampling locations at Ardooie was to investigate the impact of the proximity of the highway on the polymer types present in the samples from both locations. As mentioned before, TWP mainly consist of NR and the synthetic rubbers styrene-butadiene-rubber (SBR) and butadiene-rubber (BR) (Hüffer et al., 2019). None of these polymers were found at Ardooie. NR was not expected to be found since the H_2O_2 added for removal of OM caused severe polymer degradation (Thomas et al., 2020).

Vehicles contain a high proportion of plastics in general. Mainly PP, PE and PVC are frequently used in the automotive industry (Čabalová et al., 2021). For location 1, furthest from the highway, PP and PVC were found with a corresponding r value of respectively 0,57 and 0,60. At location 2, closest to the highway, PP, PE and PVC were found with r values of 0,57; 0,37 and 0,33.

Table 4.4: Overview of all the different polymer types found at Ardooie, location 1, and their corresponding highest Pearson correlation. This table is based on the results given in Appendix B.

EPDM	**EPR**	**SIS**	**PP**	**PE**	**HDPE**
0,51	0,44	/	0,57	/	0,51
XPS	**ABS**	**PS**	**SAN**	**SAA**	**PA 6**
0,50	/	0,63	0,33	0,44	/
PA 66	**PEG**	**PEO**	**CR**	**PSU**	**PET**
/	0,40	0,41	/	0,32	0,39
PC	**PVC**	**PDMS**	**PTFE**		
/	0,60	0,57	/		

Table 4.5: Overview of all the different polymer types found at Ardooie, location 2, and their corresponding highest Pearson correlation. This table is based on the results given in Appendix B.

EPDM	**EPR**	**SIS**	**PP**	**PE**	**HDPE**
0,50	0,41	/	0,57	0,37	0,45
XPS	**ABS**	**PS**	**SAN**	**SAA**	**PA 6**
/	/	0,33	/	/	0,38
PA 66	**PEG**	**PEO**	**CR**	**PSU**	**PET**
0,31	0,40	0,40	/	/	0,37
PC	**PVC**	**PDMS**	**PTFE**		
/	0,33	0,46	/		

- **Geophysical center: Dourbes**

The location for the establishment of this center for geophysical research was deliberately chosen in a remote area, far away from any electrical and magnetic disturbances, and was inaugurated in 1956 (Koninklijk Meteorologisch Instituut, 2022). From 1950 to 2012, plastics production boomed from 1,7 million tons to nearly 300 million tons, as plastics gradually replaced materials like glass and metal (Gourmelon, 2015). This means the center was established before the use of plastic became a ubiquitous phenomenon. This likely causes MP presence to be the result of external inputs only.

In remote area's, atmospheric deposition can be considered as an important source for MP contamination. Research has shown the transport of MP over distances up to 95 km through air mass trajectories. It is likely for airborne MP, originating in urban environments, to end up in pristine environments through atmospheric deposition (Wright, Ulke, Font, Chan, & Kelly, 2020).

PVC was identified as the only MP with a significant r value (0,61), likely to have ended up there through atmospheric deposition or littering, since the domain is still influenced by the presence of people who work there.

Table 4.6: Overview of all the different polymer types found at Dourbes and their corresponding highest Pearson correlation. This table is based on the results given in Appendix B.

EPDM	EPR	SIS	PP	PE	HDPE
0,52	0,43	/	0,57	/	0,50
XPS	**ABS**	**PS**	**SAN**	**SAA**	**PA 6**
0,41	/	0,57	/	/	0,40
PA 66	**PEG**	**PEO**	**CR**	**PSU**	**PET**
0,34	0,41	0,42	0,53	/	0,37
PC	**PVC**	**PDMS**	**PTFE**		
/	0,61	0,52	/		

- **Nature reserves: Pelt and Kempense Heuvelrug**

In these nature reserves, atmospheric deposition can also be considered as an important source for MP contamination.

Next to atmospheric deposition, hiking and trail running are sources of MP on recreational trails in protected environments (Forster, Wilson, & Tighe, 2023). Both nature reserves, Pelt and Kempense Heuvelrug, are frequently visited by hikers. Since sampling locations were always selected next to hiking trails, a possible influence from these hiking activities could be suspected. The majority of MP found on trail surfaces consist of polyurethane (PU), PET and PS. These MP originate from clothing, footwear, litter, and diffuse sources (Forster et al., 2023). The highest r value for PET and PS was 0,43 and 0,40 at Pelt and 0,43 and 0,66 at Kempense Heuvelrug.

Table 4.7: Overview of all the different polymer types found at Pelt and their corresponding highest Pearson correlation. This table is based on the results given in Appendix B.

EPDM	EPR	SIS	PP	PE	HDPE
0,54	/	/	0,58	/	0,55
XPS	**ABS**	**PS**	**SAN**	**SAA**	**PA 6**
/	/	0,40	/	/	0,32
PA 66	**PEG**	**PEO**	**CR**	**PSU**	**PET**
/	0,41	0,42	0,34	/	0,43
PC	**PVC**	**PDMS**	**PTFE**		
/	0,43	0,51	/		

An important notice has to be made regarding the sampling location in Pelt. At a distance of only 1,5 km away (bird’s eye view), the Ford Lommel Proving ground (Ford LPG) is located.

Operational from 1965, this track covers a distance of 100 kilometres and is used as Ford's most important test track in Europe whole year round with an average of 5 to 10 million km of track tested every year with Ford cars (Ford Motor Company, 2020). It is possible that TWP, derived from cars tested on this track, can end up in the soil of the nearby nature reserve through atmospheric deposition.

Table 4.8: Overview of all the different polymer types found at Kempense Heuvelrug and their corresponding highest Pearson correlation. This table is based on the results given in Appendix B.

EPDM	**EPR**	**SIS**	**PP**	**PE**	**HDPE**
0,57	0,47	/	0,62	/	0,55
XPS	**ABS**	**PS**	**SAN**	**SAA**	**PA 6**
0,52	/	0,66	/	0,42	0,31
PA 66	**PEG**	**PEO**	**CR**	**PSU**	**PET**
0,30	0,38	0,42	0,34	/	0,43
PC	**PVC**	**PDMS**	**PTFE**		
0,30	0,63	0,50	0,73		

PP, PS and PVC are the plastic polymers identified with a significant Pearson correlation at Kempense Heuvelrug (respectively 0,62; 0,66 and 0,63). These three plastic materials are most frequently sampled in environmental samples in Europe (together with PE, PET and PA). These polymer types have a broad application rate, they are used in the automotive industry, furniture, consumer packagings, electrical and electronic equipment and clothing (Kawecki et al., 2018).

4.2.1.4 Limitations of Open Specy and evaluation of the results

The Open Specy software can be considered as a black box for users. The behaviour of the system can only be observed by looking at the input (FTIR spectrum) and the output (Pearson correlation for identified polymers). No threshold value is set for determining when a deviation from the baseline in the spectrum can be considered a peak. Disturbances, such as background noise and interference of the sample matrix, can cause deviation from the baseline and can falsely be identified as a peak caused by a polymer material. Matches can occur between peaks not originating from MP present in the samples and the polymer materials in the reference library.

As mentioned before, FTIR is highly sensitive for water interference. A spectrum can be dominated by water absorption bands in the mid-infrared region due to the intense OH stretching between 3600 and 3100 cm^{-1} (Berthomieu & Hienerwadel, 2009). The software does not exclude peaks caused by water interference from the matching procedure.

The pre-processing of the spectrum occurs automatically (see Appendix A for more information). The baseline correction occurs iterative, based on an 8th polynomial fit to the entire spectrum. It was noticed that for some samples, peaks below the baseline were no longer visible after correction.

The spectra uploaded in Open Specy originate from environmental samples. As a result, the spectra contain a broad range of peaks derived from all the materials present in the samples (MP and sample matrix). Formula A.3 in Appendix A for calculating the Pearson correlation, will compare the peaks from the reference library with all the peaks in the spectrum, also the ones possibly caused by noise or interference of the sample matrix. These peaks will influence the matching procedure based on the Pearson correlation. The broad range of peaks in environmental samples also enhances the possibility that peaks originating from a polymer material present in that sample, are buried by other peaks caused by other polymers or other materials present in the sample matrix and background noise, which complicates the identification procedure (Fan, Huang, Lin, & Li, 2021).

- **Analysis of pure polymer spectra**

When looking at the Open Specy results in appendix B, many matches with polymers from the reference library occurred for values of Pearson's r lower than the threshold of 0,60. This threshold was chosen to exclude any doubt caused by incorrect matching due to wrongly processing or poor quality of the uploaded spectra. When applying this treshold, there is no guarantee that spectra qualities are sufficient to find adequate matches (Renner et al., 2017). In order to check the degree to whether this software is able to identify polymer materials with a significant r some 'pure' polymer materials were measured with the FTIR (Vertex 70 Bruker) and OPUS (Bruker) software. If these 'pure' polymer materials are indicated with significant values for r, this can be a first indication of a correct identification of MP using the Open Specy software and that the values found for Pearson's r can be considered valuable.

The spectra were uploaded in Open Specy to check whether the software was able to correctly identify them.

Table 4.9: Results from the identification of the FTIR spectra originating from 'pure' materials of PVC, HDPE, PET, PMMA and PP using Open Specy. The three highest matches and their corresponding Pearson correlation is given.

Polymer type	Top 3 matches	Pearson's r
PVC	PEO	0,57
	PP	0,57
	PEG	0,56
HDPE	PVC	0,43
	PS	0,39
	PTFE	0,37
PET	HDPE	0,56
	PP	0,56
	EPDM	0,53
PMMA	PVC	0,45
	PC	0,36
	PTFE	0,24
PP	PTFE	0,71
	PVC	0,48
	PC	0,35

As can be seen in table 4.9, none of these 'pure' polymer materials was identified correctly by Open Specy. A first possible explanation can be that the peaks in the spectra from the reference library are insufficient and that the quality of these spectra is poor which makes finding a match difficult. To check whether the spectra from the reference library are suitable for the identification of their corresponding polymer materials, the peaks in the spectra from the reference library were compared with characteristic peak values for polymers found in literature (reference peak values for different polymers are listed in in table 4.10). The FTIR spectrum for PMMA was not found in the reference library, therefore this polymer can be excluded from identification.

Figure 4.3 gives an overview of the spectra from PVC, HDPE, PET and PP that are present in the reference library. The peak values found in literature for these corresponding polymer types, are indicated on the spectra. Peak values from literature were also identified as peaks in the spectra from the reference library. The polymer reference library can therefore be regarded as a correct identification tool and the explanation for the incorrect identification of the 'pure' polymer materials has to be found elsewhere.

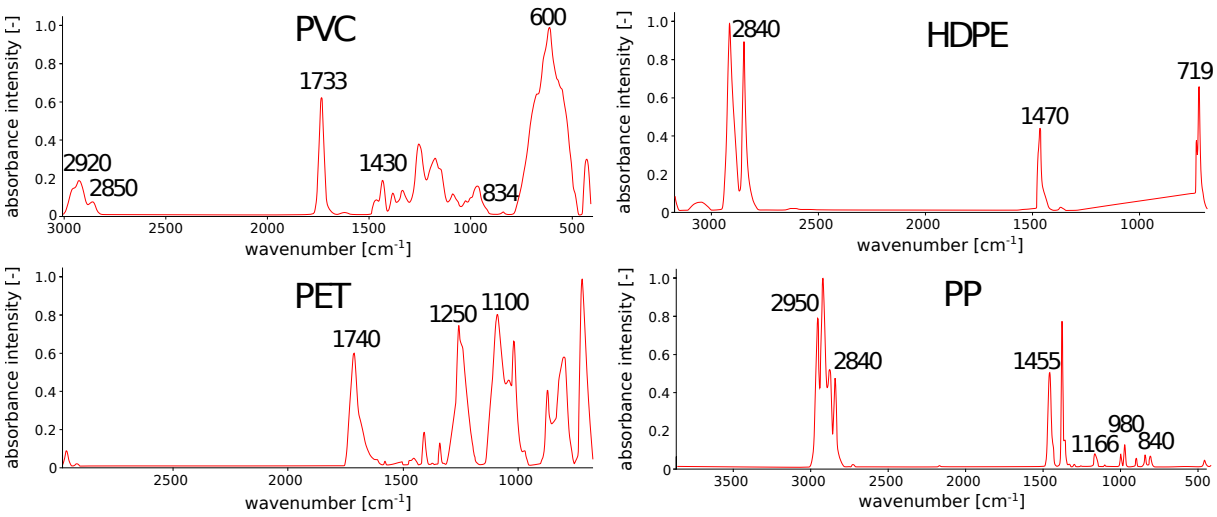

Figure 4.3: FTIR spectra from the reference library in Open Specy for PVC, HDPE, PET and PP. The peak values corresponding with those found in literature are indicated on the spectra (Charles, 2009; European Commission, 2013; Mecozzi et al., 2016).

A possible explanation for these poor matching results can be that the polymers, earlier referred to as 'pure', used for the comparison with the reference library are possibly influenced by processing and additives and can therefore not be considered as pure. The spectrum for PVC was obtained by putting little pieces of a PMD-garbage bag in the sample compartment of the FTIR spectrometer. Little pieces of a plastic PMMA ring, with no further information except for the the material of which it consists, were used to obtain a spectrum for PMMA. The same was done with little pieces of a plastic bag that consisted of HDPE. PP and PET were available as a powdery substance in a glass jar, but no additional information about the origin of these powders was available. Almost all commercial plastics are compounded with additives to improve their processing and end-use performance. Reinforcements such as fibers, fillers and coupling agents are added to improve the strength of polymers. Plasticizers are added to improve the flexibility and softness of polymers. Lastly, colorants and flame retardants are other examples in the long list of additives often used to improve plastic polymer properties (Deanin, 1975). Wagner et al. (2020) mention the presence of unknown additives to be a stumbling block in the FTIR analysis of plastic polymers.

It can also be noted that when comparing the spectra from the 'pure' polymer materials to the spectra in the library, some peaks in the 'pure' polymer spectra could be buried by background noise or were maybe not visible due to insufficient spectral quality. Since the matching procedure of the software is only based on the peaks who are visible in the uploaded spectrum, misidentification is possible. This gives a first indication on how important preprocessing spectral data and correcting for background noise is when identifying MP using automated software.

- **Interference of the sample matrix**

When uploading the results in Open Specy, possible background interference was not taken into account. Environmental samples typically contain a large number of matrix components, which may be extracted with the analyte of interest, in this case MP, and disturb the analysis. A first important element to taken into account when analyzing the spectra, are the filter papers used for the extraction of the MP. When scraping of MP residues from the filter papers, small bits of the filter itself inevitably came with. In order to investigate the influence of the filter papers on the FTIR measurements, the content of three blank filter papers was thoroughly scraped off in the sample compartment of the FTIR spectrometer. Between the measurement of each filter paper, the equipment was cleaned using ethanol and a background scan was performed. The spectra were uploaded in Origin Pro.

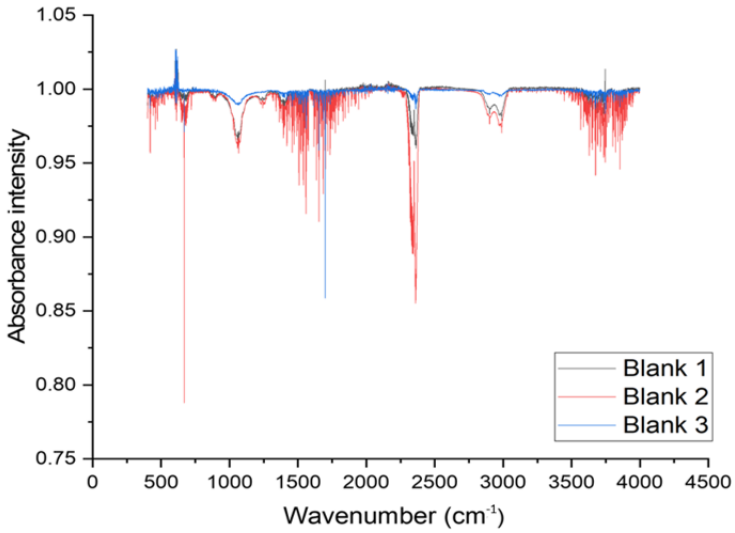

Figure 4.4: Combined plot of the FTIR spectra of three different blank filter papers (Blank 1, Blank 2 and Blank 3).

All of the spectra show a more or less similar pattern, indicating a possible interference of the spectra originating from the filter papers with the spectra originating from the MP. An important notice to be made is the presence of peaks originating from cosmic radiation. These peaks can be recognized as narrow spectral bands (lines) in FTIR or Raman spectra (Brandt, Mattsson, & Hassellöv, 2021). These narrow bands are ignored and not considered as peaks during the further course of this master's thesis.

Blank 1 seemed to be showing the most moderate peak values that were situated between the peak values of Blank 2 and 3. Therefore it was chosen to work with the spectrum from this blank in further research. Peaks were fitted on the FTIR spectrum of blank 1 with the Peak Analyzer (Pro) in Origin Pro. A baseline was subtracted from the spectrum, created by manually indicating baseline anchor points, and the most prominent peaks were indicated. Important peaks were located at 609, 1056, 2350, 2905 and 2980 cm^{-1}.

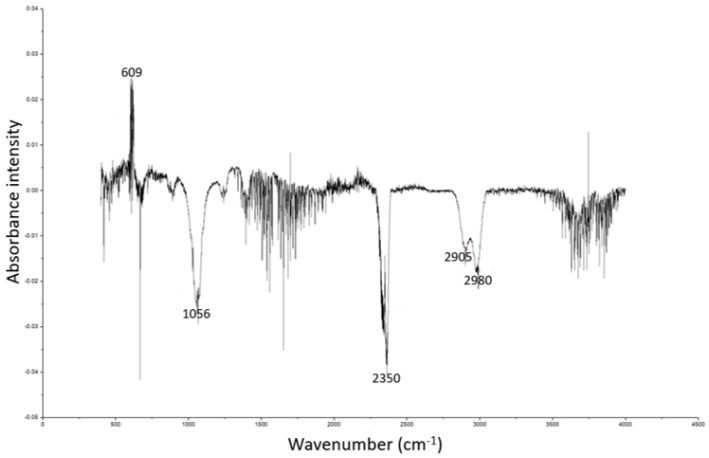

Figure 4.5: Most prominent peaks indicated in the spectrum of Blank 1.

The peaks originating from the blank filter paper can be compared with the peaks from the different polymers in the reference library from Open Specy. An interval of ± 50 cm^{-1} was used to account for peaks who showed a broad peak range in the reference library. The peak value from the filter at 2980 cm^{-1} interfered with the spectra of PP, PSU and PVC. The peak value of the filter paper at 2905 cm^{-1} interfered with almost all polymer spectra, namely PP, PEO, PEG, PET, EPDM, HDPE, PA, EPR, SIS, PE, XPS, ABS, PS, SAA, PA 66 and PTFE. The peak from the filter at 2350 cm^{-1} only interfered with the spectrum of PET. The peak at 1056 interfered with PEO, PEG, PET, PDMS, ABS, PS, SAA, CR, PC and PTFE. Finally, the peak at 609 cm^{-1} interfered with PA, SIS, PA 66 and PVC.

When looking at microscopic images of the filter papers using the Keyence Digital Microscope, some other materials, clearly not MP, were also present (Figure 4.6). This could be some remaining OM that was not completely removed or some mineral matter still present due to insufficient quality of the density separation. The disturbance caused by the supplementary material present on the filter papers is more challenging to look at. For measurements with the FTIR spectrometer, the material present on the filter papers is always entirely scraped of and is not possible to select individual particles. Therefore, it is not possible to measure the FTIR spectrum the unidentified particles.

(a) *(b)*

Figure 4.6: Pictures taken with the Keyence Digital Microscope of unidentified materials on the filter paper of sample CP1B-1.2.

4.2.2 Manual peak analysis

To overcome some challenges that arose when using the automated Open Specy software for MP identification, it was decided to do a manual peak analysis. This way a selection of peaks can be indicated, instead of automatically processing and comparing all peaks with the spectral library. It is possible that peaks originating from background noise, bury other peaks derived from MP present in the samples. Because the software searches for matches based on the comparison of all peaks from the polymer materials in the reference library, some MP may not be identified since not all peaks of a specific polymer type are always visible in the spectrum. To overcome these problems, manual peak identification can be chosen, where pre-processing of the spectra does not happen automatically, and the user can identify peaks of choice for identification (Renner et al., 2017).

To remove the noise caused by the sample matrix, present in all samples, the absorbance intensity values from Blank 1 were subtracted from the absorbance intensity values from the FTIR spectrum of each sample in Origin Pro. No other measures were taken to include the influence of the supplementary materials present on the filters, since no FTIR data was available.

Peaks were fitted with the Peak Analyzer (Pro) in Origin Pro. A baseline was subtracted from each spectrum, created by manually indicating baseline anchor points. Peaks were manually indicated for each spectrum. Finally, a fitting of the peaks was performed using the Levenberg-Marquardt algorithm, in order to create a smooth spectrum, only showing the peaks indicated. The spectra with the identified peaks are shown in Appendix C.

The peaks from the FTIR spectra from the samples were compared with the characteristic peaks of some common polymers found in literature (table 4.10). A more strict interval of ± 10 cm^{-1} was applied this time when comparing the reference peaks from literature to the sample peaks. This was chosen because the reference peaks found in literature originate from sharp, narrow peaks and being more strict when comparing peak values enhances the probability of indicating a correct match.

Table 4.10: Reference peak (cm^{-1}) values of some polymer types found in literature: PS (Fang et al., 2010), PVC, PP (European Commission, 2013), PTFE (Piwowarczyk et al., 2019), EPDM (Santos et al., 2013), PEG (Chieng et al., 2013), PEO (Ratna et al., 2006), PA (Ahlblad et al., 1997), HDPE (Charles, 2009), PET (Mecozzi et al., 2016) and PMMA (Ramesh et al., 2007).

PS	PVC	PP	PTFE	EPDM	PEG	PEO	PA	HDPE	PET	PMMA
700	600	840	642	1380	1060	1116	1405	719	900	1160
1207	834	980	1150	1460	1353	1320	1600	1470	1100	1720
1470	1430	1166	1211	2850	1456	2670	2863	2840	1250	2951
3000	1733	1455		2920	2870	2790	2927	3020	1370	
3450	2850	2840			3417	3000			1740	
	2920	2950								

Table 4.11 gives an overview of the peaks from the samples that corresponded with a peak of a polymer material from literature. A full overview of all peaks identified, including the ones who did not result in a match with a polymer material, can be found in Appendix C. Again, caution should be taken when looking at these results. Spectra qualities, even after correction for interference with the filter paper, were still strongly influenced by other elements present in the sample matrix. To overcome this problem, Renner et al. (2017) suggest to identify and filter the vibrational bands in the FT-IR spectrum who indisputably belong to microplastics and compare only these highly characteristic data sets to reference peak values from literature. Another study by Renner et al. (2019) emphasizes the importance of pre-processing data. Noise removal, baseline correction and normalization are mentioned as important steps needed to be taken before identifying peaks. As mentioned earlier, correcting for all elements from the sample matrix was a challenge task during manual peak analysis. Insufficient correction for background noise and a lax selection of peak values used during manual identification might have led to suboptimal results. It may also be doubted whether identifying plastic materials in samples based on a match with a single peak is reliable enough, and if not, how many peaks should be identified as a match before concluding that the polymer type is present.

When taken into account all of previous mentioned limitations and challenges, it can still be useful to compare the results produced with Open Specy with those from manual peak analysis. When a plastic material is identified during both procedures, chances are higher that it is actually present in the sample, although extra identification and verification steps will still be necessary. The Pearson values of all materials found in each individual sample can be found in Appendix B. For sample CP1A-1.2 and CP1B-1.2, PP was identified with a Pearson of 0,51 and 0,55 respectively. The value of r is to low to be considered a truthful identification of PP, but when relying on manual analysis only, it can be concluded that PP is present in both samples. For sample GB1A-1.2, PP was identified during manual peak comparison, but

in Open Specy the Pearson for PP was 0,53, and thus not significant. PTFE, PS and PEO did not show up during the identification in Open Specy but were identified during manual peak identification. PEG and PP were identified during manual peak comparison in sample GB1B-1.2, but the Pearson for these materials, 0,39 and 0,55, was again not high enough to confirm a conclusive match. PP was identified during manual peak comparison in sample 1AR1A-1.2, but the r value for PP in this sample was not significant (0,57). PP and PS were identified during manual peak analysis of sample 1AR1B-1.2, but did not show up during the identification in Open Specy. PEO was found in this sample during manual identification and with a Pearson value of 0,40. Only PP, PVC and PA all showed up during manual and automated analysis of sample 2AR1A-1.2, but the r values of these materials were not significant. PP was identified with a Pearson correlation of 0,46 in sample 2AR1B-1.2 and showed up during manual peak analysis. For sample D1A-1.2, only PET was identified during both procedures. Again, the r value of PET was to low to be considered as a valuable match. None of the materials that were identified in sample D1B-1.2 showed up in both identification procedures. PP and PEO were identified during manual peak analysis in sample P1A-1.2 and showed up during the analysis in Open Specy with peak values of 0,56 and 0,39 respectively. Only PP was identified during both procedures for sample P1B-1.2, with a Pearson value of 0,53. Sample KH1A-1.2 showed a significant Pearson correlation for PTFE (0,73) but this material was not identified during manual analysis. Materials identified in sample KH1B-1.2 did not show any similarities between the two identification procedures.

When looking at these results, it can be concluded that the matching procedure in Open Specy is more strict. Since only matches with a Pearson above 0,60 can be considered significant, many polymers that are identified during the manual analysis are also identified during the analysis in Open Specy, but with an insignificant Pearson correlation. The reason why some materials show up during analysis in Open Specy but not in manual peak comparison, and vice versa, might be that correction for background interference from the filter paper was only applied during manual analysis, and not during the analysis in Open Specy. As mentioned in section 4.2.1.4, the peaks originating from the filter interfered with almost all the materials present in the Open Specy reference library.

Table 4.11: Overview of the peak values that resulted in a match during manual peak identification and the corresponding polymer materials. For each sample the peak values are shown with the corresponding polymer types below. The left hand side of the table reports on materials identified in the samples of CP1A-1.2, GB1A-1.2, 1AR1A-1.2, 2AR1A-1.2, D1A-1.2, P1A-1.2 and KH1A-1.2. The right hand side of the table contains information about the same samples, but this time the B layer of the soil was investigated.

CP1A-1.2	1161	2940		
	PP PMMA	PP PMMA		
GB1A-1.2	988	1158	2999	
	PP	PP PTFE PMMA	PS PEO	
1AR1A-1.2	1159	2943		
	PP PTFE PMMA	PP PMMA		
2AR1A-1.2	694	1162	2926	
	PS	PP PMMA	PVC EPDM PA	
D1A-1.2	895	1059	1159	2995
	PET	PEG	PP, PTFE, PMMA	PS, PEO
P1A-1.2	982	1172	1310	2949
	PP	PP	PEO	PP PMMA
KH1A-1.2	1162			
	PP PEG PMMA			

CP1B-1.2	1161	2942	
	PP PMMA	PP PMMA	
GB1B-1.2	1059	1159	2940
	PEG	PP PTFE	PP PMMA
1AR1B-1.2	1165	2943	2997
	PP PMMA	PP PMMA	PS PEO
2AR1B-1.2	1161		
	PP PTFE PMMA		
D1B-1.2	1158	1347	2992
	PP PTFE PMMA	PEG	PS PMMA PEO
P1B-1.2	980	1162	2937
	PP	PP PMMA	PA
KHB1B-1.2	975	1155	2790
	PP	PP PTFE PEG PMMA	PEO

4.2.3 Raman spectroscopy

A final attempt was done for the identification of MP with Raman spectroscopy. During FTIR analysis, it was not possible to focus on specific particles. As a result, the spectra always contained a broad range of peaks originating from all the materials present on the filter papers, being MP, but also all the other materials present on the filter paper, such as remaining OM and mineral matter, and the filter paper itself. During Raman, a single particle can be selected and a single spectrum scan can be obtained for this specific particle. Raman is also considered to be a complementary technique when compared to FTIR. This is because peaks originating from highly symmetric, covalent bonds will be more easily identified during Raman compared to FTIR. Vice versa, peaks from strong covalent bonds will show up in the FTIR spectrum but might not be visible in a Raman spectrum (Smith, 2015).

Because of limited time, a selection of four particles, earlier identified with the Keyence Digital Microscope (Figure 4.1), was investigated using Raman spectroscopy.

(a) P1A-12.

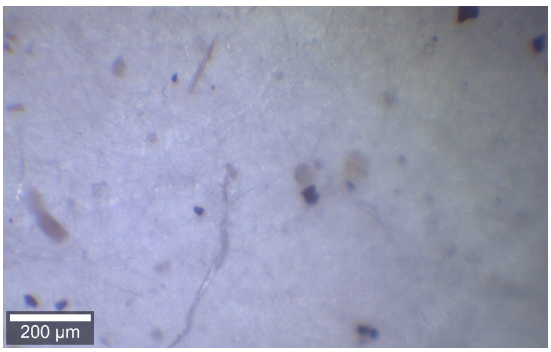

(b) GB1B-12.

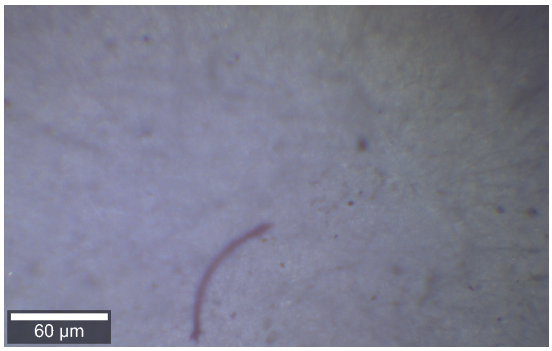

(c) 1AR1A-12 (1).

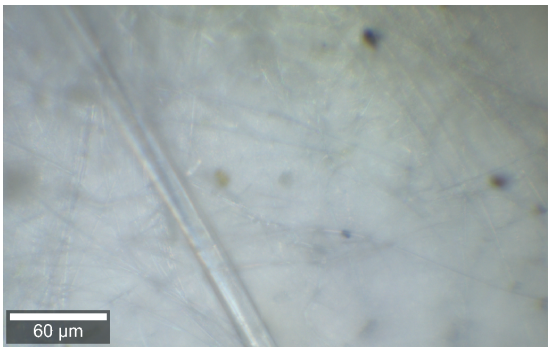

(d) 1AR1A-12 (2).

Figure 4.7: The four particles found with the Keyence Digital Microscope (Figure 4.1) retraced and visualised with the optical mode of the Raman microscope.

The spectra, with indications of the estimated peaks, can be found in appendix D. Peaks were found at 190, 250, 390, 420, 620, 840, 880, 1000, 1790, 1900, 2395, 2885 and 3510 cm^{-1}. When looking at the spectra, some background noise can be noticed, possibly burying other peak values.

Again, the background influence caused by the filter papers was investigated. A 'clear' area, meaning an area where nothing else was present but the filter paper itself, on a filter paper used for extraction (sample KH3A-12) was scanned with the Raman microscope. Comparing with the spectrum of a 'clear' area on a filter that was used during the extraction procedure might be more accurate than the comparison with a blank filter paper, as done in section 4.2.1.4, because the spectrum of the filter paper can be influenced by the extraction procedure.

The peak values on the Raman spectrum of the 'clear' filter area, shown in figure 4.8, exactly corresponded with the peak values earlier found for the four particles from Figure 4.7.

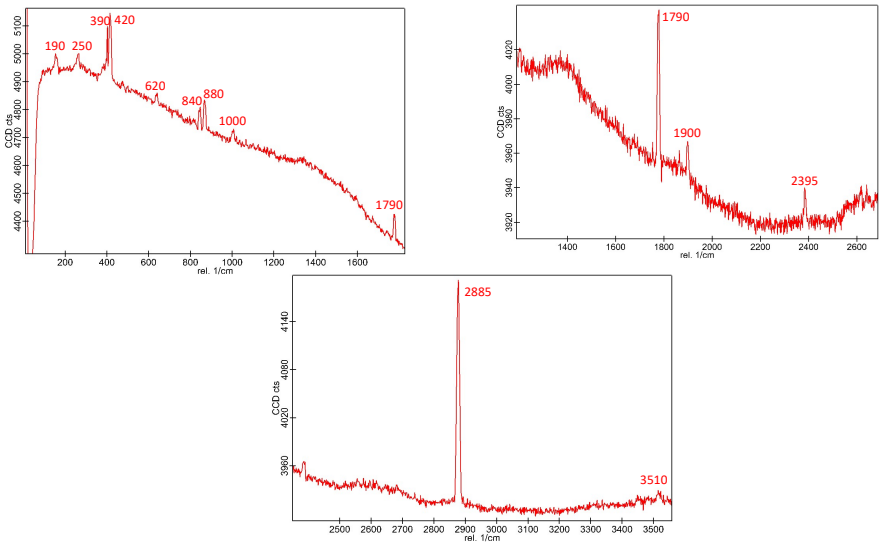

Figure 4.8: Raman spectra with identified peaks for the 'clear' area of a filter paper from sample KH3A-12. The spectrum was divided into three parts, who when combined give an overview of the peaks that occurred over a spectral range of 0 to ± 3500 cm^{-1}.

The filter paper prevents interpretation of the peak values, as all peaks arose due to scattering caused by the filter paper, and not the selected particles. Xu et al. (2019) also mention that in some cases, the background signal can be strong enough to overpower the weak Raman signals being emitted. A possible solution could again be to subtract the spectra originating from the filter paper (figure 4.8) from the spectra originating from the four identified particles (see Appendix D).

During one of the attempts to obtain a Raman scan for the unidentified particle in the sample of P1A-1.2, the laser power was set to maximum value of 40 mW (instead of the normal 2-3 mW). When looking at the particle in optical mode, after focusing the laser on the particle

and performing the single spectrum scan, the part that was focused on was completely burned (Figure 4.9).

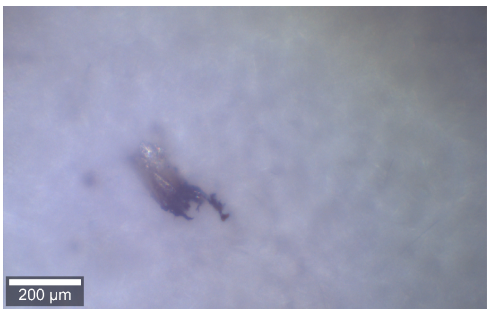

Figure 4.9: Burned particle in sample P1A-1.2 after performing a measurement at full laser power during Raman analysis.

The particle was burned because instead of reflecting (scattering) the incident laser beam, the radiation coming from the laser power was absorbed causing sample degradation by photodecomposition and burning (Nava, Frezzotti, & Leoni, 2021). This gives opportunities towards new thermal based research methods as a possible alternative to investigate the presence of MP in environmental samples and to avoid the background noise caused by the filter paper. In this case, environment samples are first heated and with the increase in temperature, the polymers absorb heat and change gradually from solid state to liquid or gas state, producing endothermic peaks at a specific temperature. The composition and type of microplastics and their additives can be analyzed according to the characteristic thermograms of polymers because polymers differ in their thermal stability (Z. Huang, Hu, & Wang, 2023). A specific example of this technique for MP identification is Thermogravimetric Analysis (TGA). During TGA, the change in mass of a sample is measured as it is heated (or cooled) in a controlled atmosphere. This technique can be used to determine the thermal stability and decomposition kinetics of a material. As the temperature increases, different components of the material may decompose or evaporate, resulting in changes in weight (Majewsky, Bitter, Eiche, & Horn, 2016). Differential Scanning Calorimetry (DSC) measures the heat flow in or out of a sample as it is heated (or cooled), which is related to the changes in the material's energy content. This technique can be used to detect phase transitions, melting and crystallization behavior, and chemical reactions occurring in a sample (Majewsky et al., 2016). TGA and DSC are often combined and referred to as TGA-DSC, where TGA helps identify the thermal stability and decomposition properties of the polymer material, while DSC provides information about its phase transitions and energy changes (Mansa & Zou, 2021).

The combination of TGA and DSC is a possible technique for the identification of MP where an extensive pre-treatment of the environmental samples can be avoided because this technique allows users to focus on a specific particle and to burn it, without incorporating the background (Mansa & Zou, 2021).

CONCLUSION

An increasing trend towards investigating the contamination of the environment with MP has been observed worldwide. Nonetheless, a reliable methodology that would facilitate and automate the extraction and analysis of MP in environmental samples is still lacking. Fenton-based treatment processes received tremendous attention during recent decades as a viable strategy for the removal of OM in soil samples intended for MP research. Despite the immense amount of collected research, no standard procedure exist up until now for the use of Fenton's reagent and insufficient information is available for the effective removal of OM in soil samples. Relying on other methods, such as hydrogen peroxide, that have proven to be effective for OM removal but are less suitable for MP research since they damage the polymer structure of some MP, remains necessary.

Spectroscopic techniques, such as Raman and FTIR, are promising identification tools for MP but are difficult to implement for environmental samples. Spectra are heavily influenced by background noise originating from the sample matrix, making identification of MP challenging and not completely reliable. Applying a combination of several chemical identification techniques and correcting for interference from the environmental sample matrix in combination with thorough spectral processing, will make MP identification more conclusive and robust. Spectral processing is also a crucial factor when applying automated software for MP analysis, as well as the quality and variety of the spectra in the reference database. Results from automated matching procedures can only be valuable if the spectral quality of the spectra to identify is sufficient and if the spectral library is suitable for the identification of MP expected to be found, e.g. weathered or pure polymer materials. Next to FTIR and Raman, promising new techniques are also suggested, such as Thermogravimetric Analysis-Differential scanning calorimetry (TGA-DSC), in the search for finding an optimal identification and quantification tool for MP analysis in soil samples.

The large amount of samples in this study made it difficult to apply different identification techniques on within the time frame of the thesis. Each time, a selection of samples was chosen to apply a different spectroscopic identification technique on, resulting in less conclusive results compared to when all samples could have been analyzed using a range of spectroscopic techniques on all these samples. It can be said, carefully, that MP were present in soil from all locations, but it is difficult to say to what extent they were identified and how reliable the results were. In order to investigate the influence from land use type or proximity to urban activities on the MP present in soil samples, it is necessary to first identify MP through a solid identification procedure. Overcoming such limitations is a major research challenge that must be tackled before further investigation can be done.

BIBLIOGRAPHY

Ahlblad, G., Forsström, D., Stenberg, B., Terselius, B., Reitberger, T., & Svensson, L.-G. (1997). Oxidation profiles of polyamide 6,6 studied by imaging chemiluminescence and FTIR. *Polymer degradation and stability*, *55*(3), 287–293.

Akdogan, Z., & Guven, B. (2019). Microplastics in the environment: A critical review of current understanding and identification of future research needs. *Environmental pollution*, *254*, 113011.

Al-Azzawi, M. S., Kefer, S., Weißer, J., Reichel, J., Schwaller, C., Glas, K., Knoop, O., & Drewes, J. E. (2020). Validation of sample preparation methods for microplastic analysis in wastewater matrices—reproducibility and standardization. *Water*, *12*(9), 2445.

Allen, S., Allen, D., Phoenix, V. R., Le Roux, G., Durántez Jiménez, P., Simonneau, A., Binet, S., & Galop, D. (2019). Atmospheric transport and deposition of microplastics in a remote mountain catchment. *Nature Geoscience*, *12*(5), 339–344.

Álvarez-Lopeztello, J., Robles, C., & del Castillo, R. F. (2021). Microplastic pollution in neotropical rainforest, savanna, pine plantations, and pasture soils in lowland areas of Oaxaca, Mexico: Preliminary results. *Ecological Indicators*, *121*, 107084.

Ambrosini, R., Azzoni, R. S., Pittino, F., Diolaiuti, G., Franzetti, A., & Parolini, M. (2019). First evidence of microplastic contamination in the supraglacial debris of an alpine glacier. *Environmental pollution*, *253*, 297–301.

Araujo, C. F., Nolasco, M. M., Ribeiro, A. M., & Ribeiro-Claro, P. J. (2018). Identification of microplastics using Raman spectroscopy: Latest developments and future prospects. *Water research*, *142*, 426–440.

Belgische Federale Overheidsdiensten. (2023). *Meststoffen.* Retrieved on 5 May 2023, from `https://www.belgium.be/nl/leefmilieu/gereglementeerde_stoffen/meststoffen`.

Berthomieu, C., & Hienerwadel, R. (2009). Fourier transform infrared (FTIR) spectroscopy. *Photosynthesis research*, *101*(2), 157–170.

Bläsing, M., & Amelung, W. (2018). Plastics in soil: Analytical methods and possible sources. *Science of the total environment*, *612*, 422–435.

Borges-Ramírez, M. M., Mendoza-Franco, E. F., Escalona-Segura, G., & Rendón-von Osten, J. (2020). Plastic density as a key factor in the presence of microplastic in the gastrointestinal tract of commercial fishes from Campeche Bay, Mexico. *Environmental Pollution*, *267*, 115659.

Brandt, J., Mattsson, K., & Hassellöv, M. (2021). Deep Learning for Reconstructing Low-Quality FTIR and Raman Spectra- A Case Study in Microplastic Analyses. *Analytical chemistry*, *93*(49), 16360–16368.

Bruinsma, J. (2017). *World agriculture: Towards 2015/2030: an FAO Perspective*. Routledge.

Bumbrah, G. S., & Sharma, R. M. (2016). Raman spectroscopy–basic principle, instrumentation and selected applications for the characterization of drugs of abuse. *Egyptian Journal of Forensic Sciences*, *6*(3), 209–215.

Buyuksonmez, F., Hess, T. F., Crawford, R. L., & Watts, R. J. (1998). Toxic effects of modified Fenton reactions on Xanthobacter flavus FB71. *Applied and Environmental Microbiology*, *64*(10), 3759–3764.

Čabalová, I., Ház, A., Krilek, J., Bubeníková, T., Melicherčík, J., & Kuvik, T. (2021). Recycling of wastes plastics and tires from automotive industry. *Polymers*, *13*(13), 2210.

Cai, L., Wang, J., Peng, J., Tan, Z., Zhan, Z., Tan, X., & Chen, Q. (2017). Characteristic of microplastics in the atmospheric fallout from Dongguan city, China: Preliminary research and first evidence. *Environmental Science and Pollution Research*, *24*(32), 24928–24935.

Campanale, C., Savino, I., Massarelli, C., & Uricchio, V. F. (2023). Fourier Transform Infrared Spectroscopy to Assess the Degree of Alteration of Artificially Aged and Environmentally Weathered Microplastics. *Polymers*, *15*(4), 911.

Chabuka, B. K., & Kalivas, J. H. (2020). Application of a hybrid fusion classification process for identification of microplastics based on Fourier transform infrared spectroscopy. *Applied Spectroscopy*, *74*(9), 1167–1183.

Chae, Y., & An, Y.-J. (2018). Current research trends on plastic pollution and ecological impacts on the soil ecosystem: A review. *Environmental pollution*, *240*, 387–395.

Charles, J. (2009). Qualitative analysis of high density polyethylene using FTIR spectroscopy. *Asian Journal of Chemistry*, *21*(6), 4477.

Chieng, B. W., Ibrahim, N. A., Wan Yunus, W. M. Z., & Hussein, M. Z. (2013). Poly (lactic acid)/poly (ethylene glycol) polymer nanocomposites: Effects of graphene nanoplatelets. *Polymers*, *6*(1), 93–104.

Chilingar, G. V. (1952). Study of the dispersing agents. *Journal of Sedimentary Research*, *22*(4), 229–233.

Corradini, F., Casado, F., Leiva, V., Huerta-Lwanga, E., & Geissen, V. (2021). Microplastics occurrence and frequency in soils under different land uses on a regional scale. *Science of the Total Environment*, *752*, 141917.

Courtene-Jones, W., Quinn, B., Murphy, F., Gary, S. F., & Narayanaswamy, B. E. (2017). Optimisation of enzymatic digestion and validation of specimen preservation methods for the analysis of ingested microplastics. *Analytical Methods*, *9*(9), 1437–1445.

Cowger, W., Steinmetz, Z., Gray, A., Munno, K., Lynch, J., Hapich, H., Primpke, S., De Frond, H., Rochman, C., & Herodotou, O. (2021). Microplastic spectral classification needs an open source community: Open specy to the rescue! *Analytical Chemistry*, *93*(21), 7543–7548.

Deanin, R. D. (1975). Additives in plastics. *Environmental Health Perspectives*, *11*, 35–39.

De Frond, H., Rubinovitz, R., & Rochman, C. M. (2021). μATR-FTIR Spectral Libraries of Plastic

Particles (FLOPP and FLOPP-e) for the Analysis of Microplastics. *Analytical Chemistry*, *93*(48), 15878–15885.

Delvigne, F., Destain, J., Maesen, P., Meers, E., Michels, E., Tarayre, C., & Tarayre, N. (2016). Inventory of wastes produced in Belgium, Germany, France, the Netherlands and the United Kingdom.

Dris, R., Gasperi, J., Rocher, V., Saad, M., Renault, N., & Tassin, B. (2015). Microplastic contamination in an urban area: A case study in Greater Paris. *Environmental Chemistry*, *12*(5), 592–599.

Du, H., Xie, Y., & Wang, J. (2021). Microplastic degradation methods and corresponding degradation mechanism: Research status and future perspectives. *Journal of Hazardous Materials*, *418*, 126377.

Duesterberg, S. E. M., Christopher K., & Waite, T. D. (2008). pH effects on iron-catalyzed oxidation using Fenton's reagent. *Environmental science & technology*, *44*(22), 8522–5827.

Duis, K., & Coors, A. (2016). Microplastics in the aquatic and terrestrial environment: Sources (with a specific focus on personal care products), fate and effects. *Environmental Sciences Europe*, *28*(1), 1–25.

Dziuba, B., Babuchowski, A., Nałęcz, D., & Niklewicz, M. (2007). Identification of lactic acid bacteria using FTIR spectroscopy and cluster analysis. *International dairy journal*, *17*(3), 183–189.

Edinburgh Instruments. (2022). *What is Raman Spectroscopy?* Retrieved on 29 November 2022, from `https://www.edinst.com/blog/what-is-raman-spectroscopy/`.

Eriksen, M., Mason, S., Wilson, S., Box, C., Zellers, A., Edwards, W., Farley, H., & Amato, S. (2013). Microplastic pollution in the surface waters of the Laurentian Great Lakes. *Marine pollution bulletin*, *77*(1-2), 177–182.

Estahbanati, S., & Fahrenfeld, N. L. (2016). Influence of wastewater treatment plant discharges on microplastic concentrations in surface water. *Chemosphere*, *162*, 277–284.

European Commission. (2013). *Report of an interlaboratory comparison from the European Reference Laboratory for Food Contact Materials.* Retrieved on 26 April 2023, from `https://publications.jrc.ec.europa.eu`.

European Compost Network. (2022). *Compost and digestate for a circular bioeconomy.* Retrieved on 26 January 2023, from `https://www.compostnetwork.info/wordpress/wp-content/uploads/ECN-rapport-2022.pdf`.

Fan, C., Huang, Y.-Z., Lin, J.-N., & Li, J. (2021). Microplastic constituent identification from admixtures by Fourier-transform infrared (FTIR) spectroscopy: The use of polyethylene terephthalate (PET), polyethylene (PE), polypropylene (PP), polyvinyl chloride (PVC) and nylon (NY) as the model constituents. *Environmental Technology & Innovation*, *23*, 101798.

Fang, J., Xuan, Y., & Li, Q. (2010). Preparation of polystyrene spheres in different particle sizes and assembly of the PS colloidal crystals. *Science China Technological Sciences*, *53*, 3088–3093.

Fernández-González, V., Andrade-Garda, J., López-Mahía, P., & Muniategui-Lorenzo, S. (2021). Impact of weathering on the chemical identification of microplastics from usual packaging polymers in the marine environment. *Analytica Chimica Acta*, *1142*, 179–188.

Ford Motor Company. (2020). *Lommel Proving Ground.* Retrieved on 10 May 2023, from `https://www.fordlpg.com/nl/index.htm`.

Forster, N. A., Wilson, S. C., & Tighe, M. K. (2023). Microplastic pollution on hiking and running trails in Australian protected environments. *Science of The Total Environment*, *874*, 162473.

Gajst, T. (2016). Analysis of plastic residues in commercial compost. *Nov Goric Univ*.

Gionfra, S. (2018). Plastic pollution in soil. *Institute for European Environmental Policy*.

Gourmelon, G. (2015). Global plastic production rises, recycling lags. *Vital Signs*, *22*, 91–95.

Grause, G., Kuniyasu, Y., Chien, M.-F., & Inoue, C. (2022). Separation of microplastic from soil by centrifugation and its application to agricultural soil. *Chemosphere*, *288*, 132654.

Grdadolnik, J. (2002). ATR-FTIR spectroscopy: Its advantage and limitations. *Acta Chimica Slovenica*, *49*(3), 631–642.

Guasch, H., Bernal, S., Bruno, D., Almroth, B. C., Cochero, J., Corcoll, N., Cornejo, D., Gacia, E., Kroll, A., & Lavoie, I. (2022). Interactions between microplastics and benthic biofilms in fluvial ecosystems: Knowledge gaps and future trends. *Freshwater Science*, *41*(3), 442–458.

Gui, J., Sun, Y., Wang, J., Chen, X., Zhang, S., & Wu, D. (2021). Microplastics in composting of rural domestic waste: Abundance, characteristics, and release from the surface of macroplastics. *Environmental Pollution*, *274*, 116553.

Guo, J.-J., Huang, X.-P., Xiang, L., Wang, Y.-Z., Li, Y.-W., Li, H., Cai, Q.-Y., Mo, C.-H., & Wong, M.-H. (2020). Source, migration and toxicology of microplastics in soil. *Environment international*, *137*, 105263.

Han, N., Zhao, Q., Ao, H., Hu, H., & Wu, C. (2022). Horizontal transport of macro-and microplastics on soil surface by rainfall induced surface runoff as affected by vegetations. *Science of The Total Environment*, *831*, 154989.

He, D., Luo, Y., Lu, S., Liu, M., Song, Y., & Lei, L. (2018). Microplastics in soils: Analytical methods, pollution characteristics and ecological risks. *TrAC Trends in Analytical Chemistry*, *109*, 163–172.

Hodkiewicz, J., & Scientific, T. (2010). Characterizing carbon materials with Raman spectroscopy. *Thermo Scientific Application Note*, *51946*.

Hodson, M. E., Duffus-Hodson, C. A., Clark, A., Prendergast-Miller, M. T., & Thorpe, K. L. (2017). Plastic bag derived-microplastics as a vector for metal exposure in terrestrial invertebrates. *Environmental Science & Technology*, *51*(8), 4714–4721.

Huang, J., Chen, H., Zheng, Y., Yang, Y., Zhang, Y., & Gao, B. (2021). Microplastic pollution in soils and groundwater: Characteristics, analytical methods and impacts. *Chemical Engineering Journal*, *425*, 131870.

Huang, J.-C., Shetty, A. S., & Wang, M.-S. (1990). Biodegradable plastics: A review. *Advances in Polymer Technology*, *10*(1), 23–30.

Huang, Y., Liu, Q., Jia, W., Yan, C., & Wang, J. (2020). Agricultural plastic mulching as a source of microplastics in the terrestrial environment. *Environmental Pollution*, *260*, 114096.

Huang, Z., Hu, B., & Wang, H. (2023). Analytical methods for microplastics in the environment: A review. *Environmental Chemistry Letters*, *21*(1), 383–401.

Huerta Lwanga, E., Gertsen, H., Gooren, H., Peters, P., Salánki, T., Van Der Ploeg, M., Besseling, E., Koelmans, A. A., & Geissen, V. (2016). Microplastics in the terrestrial ecosystem: Implications for Lumbricus terrestris (Oligochaeta, Lumbricidae). *Environmental science & technology*, *50*(5), 2685–2691.

Hüffer, T., Wagner, S., Reemtsma, T., & Hofmann, T. (2019). Sorption of organic substances to tire wear materials: Similarities and differences with other types of microplastic. *TrAC Trends in Analytical Chemistry*, *113*, 392–401.

Hurley, R. R., Lusher, A. L., Olsen, M., & Nizzetto, L. (2018). Validation of a method for extracting microplastics from complex, organic-rich, environmental matrices. *Environmental science & technology*, *52*(13), 7409–7417.

Hurley, R. R., & Nizzetto, L. (2018). Fate and occurrence of micro (nano) plastics in soils: Knowledge gaps and possible risks. *Current Opinion in Environmental Science & Health*, *1*, 6–11.

Ingraffia, R., Amato, G., Bagarello, V., Carollo, F. G., Giambalvo, D., Iovino, M., Lehmann, A., Rillig, M. C., & Frenda, A. S. (2022). Polyester microplastic fibers affect soil physical properties and erosion as a function of soil type. *Soil*, *8*(1), 421–435.

Ivleva, N. P., Wiesheu, A. C., & Niessner, R. (2017). Microplastic in aquatic ecosystems. *Angewandte Chemie International Edition*, *56*(7), 1720–1739.

Jin, T., Tang, J., Lyu, H., Wang, L., Gillmore, A. B., & Schaeffer, S. M. (2022). Activities of microplastics (MPs) in agricultural soil: A review of MPs pollution from the perspective of agricultural ecosystems. *Journal of Agricultural and Food Chemistry*, *70*(14), 4182–4201.

Kaiser, M., & Asefaw Berhe, A. (2014). How does sonication affect the mineral and organic constituents of soil aggregates?—A review. *Journal of Plant Nutrition and Soil Science*, *177*(4), 479–495.

Kawecki, D., Scheeder, P. R., & Nowack, B. (2018). Probabilistic material flow analysis of seven commodity plastics in Europe. *Environmental science & technology*, *52*(17), 9874–9888.

Koninklijk Meteorologisch Instituut. (2022). *Geofysisch Centrum te Dourbes.* Retrieved on 23 September 2022, from `http://dourbes.meteo.be/nl/`.

Koyuncuoğlu, P., & Erden, G. (2021). Sampling, pre-treatment, and identification methods of microplastics in sewage sludge and their effects in agricultural soils: A review. *Environmental Monitoring and Assessment*, *193*, 1–28.

Kušić, H., Božić, A. L., & Koprivanac, N. (2007). Fenton type processes for minimization of organic content in coloured wastewaters: Part I: Processes optimization. *Dyes and pigments*, *74*(2), 380–387.

Leifheit, E. F., Kissener, H. L., Faltin, E., Ryo, M., & Rillig, M. C. (2021). Tire abrasion particles negatively affect plant growth even at low concentrations and alter soil biogeochemical cycling. *Soil Ecology Letters*, 1–7.

Leitão, I. A., van Schaik, L., Ferreira, A., Alexandre, N., & Geissen, V. (2023). The spatial distribution of microplastics in topsoils of an urban environment - Coimbra city case-study. *Environmental Research*, *218*, 114961.

Lin, J., Xu, X.-P., Yue, B.-Y., Li, Y., Zhou, Q.-Z., Xu, X.-M., Liu, J.-Z., Wang, Q.-Q., & Wang, J.-H. (2021). A novel thermoanalytical method for quantifying microplastics in marine sediments. *Science of the Total Environment*, *760*, 144316.

Lin, S. H., & Lo, C. C. (1997). Fenton process for treatment of desizing wastewater. *Water research*, *31*(8), 2050–2056.

Liu, E., He, W., & Yan, C. (2014). 'White revolution'to 'white pollution'—agricultural plastic film mulch in China. *Environmental Research Letters*, *9*(9), 091001.

Liu, K., Wu, T., Wang, X., Song, Z., Zong, C., Wei, N., & Li, D. (2019). Consistent transport of terrestrial microplastics to the ocean through atmosphere. *Environmental science & technology*, *53*(18), 10612–10619.

Luo, Z., Zhou, X., Su, Y., Wang, H., Yu, R., Zhou, S., Xu, E. G., & Xing, B. (2021). Environmental occurrence, fate, impact, and potential solution of tire microplastics: Similarities and differences with tire wear particles. *Science of the Total Environment*, *795*, 148902.

Majewsky, M., Bitter, H., Eiche, E., & Horn, H. (2016). Determination of microplastic polyethylene (PE) and polypropylene (PP) in environmental samples using thermal analysis (TGA-DSC). *Science of the Total Environment*, *568*, 507–511.

Mansa, R., & Zou, S. (2021). Thermogravimetric analysis of microplastics: A mini review. *Environmental Advances*, *5*, 100117.

Mateo-Sagasta, J., Medlicott, K., Qadir, M., Raschid-Sally, L., & Drechsel, P. (2013). Proceedings of the un-water project on the safe use of wastewater in agriculture. *AGRIS*.

Mecozzi, M., Pietroletti, M., & Monakhova, Y. B. (2016). FTIR spectroscopy supported by statistical techniques for the structural characterization of plastic debris in the marine environment: Application to monitoring studies. *Marine pollution bulletin*, *106*(1-2), 155–161.

Möller, J. N., Löder, M. G., & Laforsch, C. (2020). Finding microplastics in soils: A review of analytical methods. *Environmental science & technology*, *54*(4), 2078–2090.

Molugaram, K., Rao, G. S., Shah, A., & Davergave, N. (2017). *Statistical techniques for*

transportation engineering. Butterworth-Heinemann.

Monteiro, S. S., Rocha-Santos, T., Prata, J. C., Duarte, A. C., Girão, A. V., Lopes, P., Cristovão, T., & da Costa, J. P. (2022). A straightforward method for microplastic extraction from organic-rich freshwater samples. *Science of The Total Environment*, *815*, 152941.

Nava, V., Frezzotti, M. L., & Leoni, B. (2021). Raman spectroscopy for the analysis of microplastics in aquatic systems. *Applied Spectroscopy*, *75*(11), 1341–1357.

Neina, D. (2019). The role of soil pH in plant nutrition and soil remediation. *Applied and environmental soil science*, *2019*, 1–9.

Nematollahi, M. J., Keshavarzi, B., Mohit, F., Moore, F., & Busquets, R. (2022). Microplastic occurrence in urban and industrial soils of Ahvaz metropolis: A city with a sustained record of air pollution. *Science of The Total Environment*, *819*, 152051.

Nidheesh, P. V., Gandhimathi, R., & Ramesh, S. T. (2013). Degradation of dyes from aqueous solution by Fenton processes: A review. *Environmental Science and Pollution Research*, *20*, 2099–2132.

Nishikida, K., & Coates, J. (2003). *Infrared and Raman analysis of polymers*. CRC Press.

Nizzetto, L., Futter, M., & Langaas, S. (2016). Are agricultural soils dumps for microplastics of urban origin? *Environmental Science & Technology*, *50*(20), 10777–10779.

Ogata, F., Nakamura, T., & Kawasaki, N. (2018). Improvement of the Homogeneous Fenton Reaction for Degradation of Methylene Blue and Acid Orange II. *Chemical and Pharmaceutical Bulletin*, *66*(5), 585–588.

Omnexus. (n.d.). *Density of plastics: Technical properties.* Retrieved on 1 December 2022, from `https://omnexus.specialchem.com/polymer-properties/properties/density`.

Pawar, V., & Gawande, S. (2015). An overview of the fenton process for industrial wastewater. *IOSR Journal of Mechanical and Civil Engineering*, *2*, 127–136.

Perez, C. N., Carré, F., Hoarau-Belkhiri, A., Joris, A., Leonards, P. E., & Lamoree, M. H. (2022). Innovations in analytical methods to assess the occurrence of microplastics in soil. *Journal of Environmental Chemical Engineering*, 107421.

Phan, S., Padilla-Gamiño, J. L., & Luscombe, C. K. (2022). The effect of weathering environments on microplastic chemical identification with Raman and IR spectroscopy: Part I. polyethylene and polypropylene. *Polymer Testing*, *116*, 107752.

Phuong, N. N., Poirier, L., Lagarde, F., Kamari, A., & Zalouk-Vergnoux, A. (2018). Microplastic abundance and characteristics in French Atlantic coastal sediments using a new extraction method. *Environmental Pollution*, *243*, 228–237.

Piwowarczyk, J., Jędrzejewski, R., Moszyński, D., Kwiatkowski, K., Niemczyk, A., & Baranowska, J. (2019). XPS and FTIR studies of polytetrafluoroethylene thin films obtained by physical methods. *Polymers*, *11*(10), 1629.

Prata, J. C. (2018). Airborne microplastics: Consequences to human health? *Environmental pollution*, *234*, 115–126.

Pribyl, D. W. (2010). A critical review of the conventional SOC to SOM conversion factor. *Geoderma*, *156*(3-4), 75–83.

Primpke, S., Wirth, M., Lorenz, C., & Gerdts, G. (2018). Reference database design for the automated analysis of microplastic samples based on Fourier transform infrared (FTIR) spectroscopy. *Analytical and bioanalytical chemistry*, *410*, 5131–5141.

Qiu, R., Song, Y., Zhang, X., Xie, B., & He, D. (2020). Microplastics in urban environments: Sources, pathways, and distribution. *Microplastics in Terrestrial Environments*, 41–61.

Quénard, L., Samouëlian, A., Laroche, B., & Cornu, S. (2011). Lessivage as a major process of soil formation: A revisitation of existing data. *Geoderma*, *167*, 135–147.

Radford, F., Zapata-Restrepo, L. M., Horton, A. A., Hudson, M. D., Shaw, P. J., & Williams, I. D. (2021). Developing a systematic method for extraction of microplastics in soils. *Analytical Methods*, *13*(14), 1695–1705.

Ramesh, S., Leen, K. H., Kumutha, K., & Arof, A. (2007). FTIR studies of PVC/PMMA blend based polymer electrolytes. *Spectrochimica Acta Part A: Molecular and Biomolecular Spectroscopy*, *66*(4-5), 1237–1242.

Ratna, D., Divekar, S., Samui, A., Chakraborty, B., & Banthia, A. (2006). Poly (ethylene oxide)/clay nanocomposite: Thermomechanical properties and morphology. *Polymer*, *47*(11), 4068–4074.

Rehm, R., Zeyer, T., Schmidt, A., & Fiener, P. (2021). Soil erosion as transport pathway of microplastic from agriculture soils to aquatic ecosystems. *Science of The Total Environment*, *795*, 148774.

Renner, G., Nellessen, A., Schwiers, A., Wenzel, M., Schmidt, T. C., & Schram, J. (2019). Data preprocessing & evaluation used in the microplastics identification process: A critical review & practical guide. *TrAC Trends in Analytical Chemistry*, *111*, 229–238.

Renner, G., Schmidt, T. C., & Schram, J. (2017). A new chemometric approach for automatic identification of microplastics from environmental compartments based on FT-IR spectroscopy. *Analytical chemistry*, *89*(22), 12045–12053.

Rezaei, M., Riksen, M. J., Sirjani, E., Sameni, A., & Geissen, V. (2019). Wind erosion as a driver for transport of light density microplastics. *Science of the Total Environment*, *669*, 273–281.

Rillig, M. C. (2012). *Microplastic in terrestrial ecosystems and the soil?* ACS Publications.

Rochman, C. M., Brookson, C., Bikker, J., Djuric, N., Earn, A., Bucci, K., Athey, S., Huntington, A., McIlwraith, H., & Munno, K. e. a. (2019). Rethinking microplastics as a diverse contaminant suite. *Environmental toxicology and chemistry*, *38*(4), 703–711.

Rodrigues, C., Caetano, N., & Durão, H. (2008). Experimental design to optimize degradation of organic compounds in wastewater from semiconductor industry using fenton reagent. In *Iwa world water congress 2008.*

Rodriguez-Seijo, A., Lourenço, J., Rocha-Santos, T., Da Costa, J., Duarte, A., Vala, H., & Pereira, R. (2017). Histopathological and molecular effects of microplastics in Eisenia andrei

Bouché. *Environmental Pollution*, *220*, 495–503.

Rühlmann, J., Körschens, M., & Graefe, J. (2006). A new approach to calculate the particle density of soils considering properties of the soil organic matter and the mineral matrix. *Geoderma*, *130*(3-4), 272–283.

Saito, T. (1989). Determination of styrene-butadiene and isoprene tire tread rubbers in piled particulate matter. *Journal of Analytical and Applied Pyrolysis*, *15*, 227–235.

Santos, R. P. d., Oliveira Junior, M. S. d., Mattos, E. d. C., Diniz, M. F., & Dutra, R. d. C. L. (2013). Study by FT-IR technique and adhesive properties of vulcanized EPDM modified with plasma. *Journal of Aerospace Technology and Management*, *5*, 65–74.

Savitzky, A., & Golay, M. J. (1964). Smoothing and differentiation of data by simplified least squares procedures. *Analytical chemistry*, *36*(8), 1627–1639.

Scarascia-Mugnozza, G., Sica, C., & Russo, G. (2011). Plastic materials in European agriculture: Actual use and perspectives. *Journal of Agricultural Engineering*, *42*(3), 15–28.

Schmitt, J., & Flemming, H.-C. (1998). FTIR-spectroscopy in microbial and material analysis. *International Biodeterioration & Biodegradation*, *41*(1), 1–11.

Scientific Polymer Product Inc. (n.d.). *Density of polymers (by density).* Retrieved on 20 March 2023, from `https://scipoly.com/density-of-polymers-by-density/`.

Scopetani, C., Chelazzi, D., Mikola, J., Leiniö, V., Heikkinen, R., Cincinelli, A., & Pellinen, J. (2020). Olive oil-based method for the extraction, quantification and identification of microplastics in soil and compost samples. *Science of The Total Environment*, *733*, 139338.

Shim, W. J., Hong, S. H., & Eo, S. E. (2017). Identification methods in microplastic analysis: A review. *Analytical methods*, *9*(9), 1384–1391.

Singh, N., Abdullah, M. M., Ma, X., & Sharma, V. K. (2023). Microplastics and nanoplastics in the soil-plant nexus: Sources, uptake, and toxicity. *Critical Reviews in Environmental Science and Technology*, 1–30.

Skipp, I. K., G. & Brownfield. (1993). Improved density gradient separation techniques using sodium polytungstate and a comparison to the use of other heavy liquids. *US Geological Survey*.

Smith, B. (2015). IR Spectral Interpretation Workshop. *Spectroscopy*, *30*(1).

Sommer, F., Dietze, V., Baum, A., Sauer, J., Gilge, S., Maschowski, C., & Gieré, R. e. a. (2018). Tire abrasion as a major source of microplastics in the environment. *Aerosol and air quality research*, *18*(8), 2014–2028.

Sorolla-Rosario, D., Llorca-Porcel, J., Pérez-Martínez, M., Lozano-Castelló, D., & Bueno-López, A. (2023). Microplastics' analysis in water: Easy handling of samples by a new Thermal Extraction Desorption-Gas Chromatography-Mass Spectrometry (TED-GC/MS) methodology. *Talanta*, *253*, 123829.

Staveley, L. A. K. (2016). *The characterization of chemical purity: Organic compounds*. Elsevier.

Steinmetz, Z., Wollmann, C., Schaefer, M., Buchmann, C., David, J., Tröger, J., Muñoz, K., Frör, O., & Schaumann, G. E. (2016). Plastic mulching in agriculture. Trading short-term agronomic benefits for long-term soil degradation? *Science of the total environment*, *550*, 690–705.

Sun, H.-W., & Yan, Q.-S. (2007). Influence of Fenton oxidation on soil organic matter and its sorption and desorption of pyrene. *Journal of hazardous materials*, *144*(1-2), 164–170.

Thermo Fisher Scientific. (2023). *Omnic Specta Software.* Retrieved on 14 March 2023, from https://www.thermofisher.com/order/catalog/product/833-036200#/833-036200.

Thomas, D., Schütze, B., Heinze, W. M., & Steinmetz, Z. (2020). Sample preparation techniques for the analysis of microplastics in soil: A review. *Sustainability*, *12*(21), 9074.

Tirkey, A., & Upadhyay, L. S. B. (2021). Microplastics: An overview on separation, identification and characterization of microplastics. *Marine Pollution Bulletin*, *170*, 112604.

Vandaele, K., & Poesen, J. (1995). Spatial and temporal patterns of soil erosion rates in an agricultural catchment, central Belgium. *Catena*, *25*(1-4), 213–226.

Vandenabeele, P. (2013). *Practical raman spectroscopy: An introduction*. John Wiley & Sons.

Vasquez-Medrano, R., Prato-Garcia, D., & Vedrenne, M. (2018). Ferrioxalate-mediated processes. *Academic Press*, 89–113.

Verschoor, A. (2015). Towards a definition of microplastics: Considerations for the specification of physico-chemical properties.

Vlaamse Overheid. (n.d.). *Databank ondegrond vlaanderen.* Retrieved on 6 December 2022, from https://www.dov.vlaanderen.be/portaal/?module=verkenner.

Wade, L. G., & Simek, J. W. (2023). *Organic Chemistry* (10th ed.). Pearson.

Wagner, F., Peeters, J. R., Ramon, H., De Keyzer, J., Duflou, J. R., & Dewulf, W. (2020). Quality assessment of mixed plastic flakes from Waste Electrical and Electronic Equipment (WEEE) by spectroscopic techniques. *Resources, Conservation and Recycling*, *158*, 104801.

Wan, Y., Wu, C., Xue, Q., & Hui, X. (2019). Effects of plastic contamination on water evaporation and desiccation cracking in soil. *Science of the Total Environment*, *654*, 576–582.

Weithmann, N., Möller, J. N., Löder, M. G., Piehl, S., Laforsch, C., & Freitag, R. (2018). Organic fertilizer as a vehicle for the entry of microplastic into the environment. *Science advances*, *4*(4), 8060.

WHO, U. (2006). *Guidelines for the safe use of wastewater, excreta and greywater* (Vol. 2). WHO Geneva.

Wink, D. A., Nims, R. W., Saavedra, J. E., Utermahlen Jr, W. E., & Ford, P. C. (1994). The Fenton oxidation mechanism: Reactivities of biologically relevant substrates with two oxidizing intermediates differ from those predicted for the hydroxyl radical. *Proceedings*

of the National Academy of Sciences, *91*(14), 6604–6608.

Wright, S. L., Thompson, R. C., & Galloway, T. S. (2013). The physical impacts of microplastics on marine organisms: A review. *Environmental pollution*, *178*, 483–492.

Wright, S. L., Ulke, J., Font, A., Chan, K. L. A., & Kelly, F. J. (2020). Atmospheric microplastic deposition in an urban environment and an evaluation of transport. *Environment international*, *136*, 105411.

Xu, J.-L., Thomas, K. V., Luo, Z., & Gowen, A. A. (2019). FTIR and Raman imaging for microplastics analysis: State of the art, challenges and prospects. *TrAC Trends in Analytical Chemistry*, *119*, 115629.

Yee, M. S.-L., Hii, L.-W., Looi, C. K., Lim, W.-M., Wong, S.-F., Kok, Y.-Y., Tan, B.-K., Wong, C.-Y., & Leong, C.-O. (2021). Impact of microplastics and nanoplastics on human health. *Nanomaterials*, *11*(2), 496.

Yu, S., Zhu, Y.-g., & Li, X.-d. e. a. (2012). Trace metal contamination in urban soils of China. *Science of the total environment*, *421*, 17–30.

Zhang, K., Hamidian, A. H., Tubić, A., Zhang, Y., Fang, J. K., Wu, C., & Lam, P. K. (2021). Understanding plastic degradation and microplastic formation in the environment: A review. *Environmental Pollution*, *274*, 116554.

Zhang, Y., Gao, T., Kang, S., & Sillanpää, M. (2019). Importance of atmospheric transport for microplastics deposited in remote areas. *Environmental Pollution*, *254*, 112953.

Zhang, Y., Kang, S., Allen, S., Allen, D., Gao, T., & Sillanpää, M. (2020). Atmospheric microplastics: A review on current status and perspectives. *Earth-Science Reviews*, *203*, 103118.

Zhao, J., Lui, H., McLean, D. I., & Zeng, H. (2007). Automated autofluorescence background subtraction algorithm for biomedical Raman spectroscopy. *Applied spectroscopy*, *61*(11), 1225–1232.

Zhou, Y., Wang, J., Zou, M., Jia, Z., Zhou, S., & Li, Y. (2020). Microplastics in soils: A review of methods, occurrence, fate, transport, ecological and environmental risks. *Science of the Total Environment*, *748*, 141368.

Zhou, Y., Wang, J., Zou, M., Yin, Q., Qiu, Y., Li, C., Ye, B., Guo, T., Jia, Z., & Li, Y. (2022). Microplastics in urban soils of Nanjing in eastern China: Occurrence, relationships, and sources. *Chemosphere*, *303*, 134999.

Zhu, F., Zhu, C., Wang, C., & Gu, C. (2019). Occurrence and ecological impacts of microplastics in soil systems: A review. *Bulletin of environmental contamination and toxicology*, *102*(6), 741–749.

Zubris, K. A. V., & Richards, B. K. (2005). Synthetic fibers as an indicator of land application of sludge. *Environmental pollution*, *138*(2), 201–211.

Appendix A

USE OF THE OPEN SPECY SOFTWARE

A.1 Uploading and processing spectra

For each sample, the spectrum generated by the FTIR and OPUS software was uploaded in Open Specy as a .CSV file. It was indicated that transmittance FTIR was used to generate the spectra. This resulted in a display of the uploaded spectrum (shown in figure A.1).

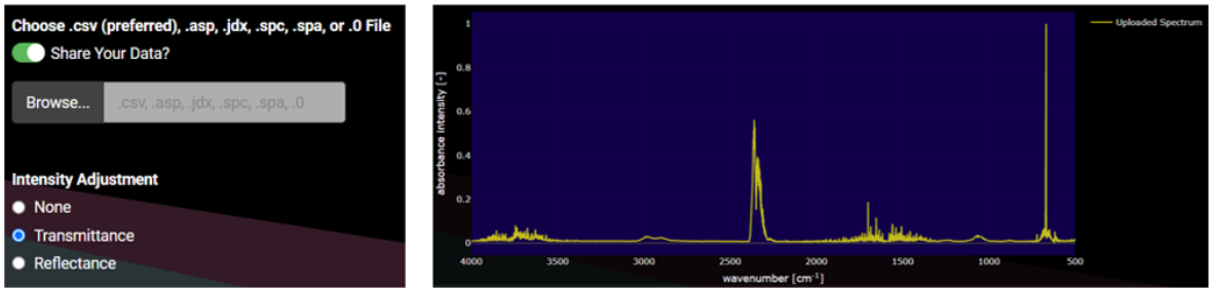

Figure A.1: Uploading spectra in Open Specy.

The uploaded spectrum was processed using smoothing according to the Savitzky and Golay (1964) filter, based on the least squares criterion. The method of least squares assumes that the best fit is the curve that has the minimal sum of deviations, i.e. least square error, from the given set of data. Suppose that the data points are (x_1, y_1), (x_2, y_2), . . . , (x_n, y_n). Where x refers to the wavenumber (cm^{-1}) and y refers to the absorbance intensity. According to the method of least squares, the best fitting curve has the property that following equation is minimum (Molugaram, Rao, Shah, & Davergave, 2017):

$$\sum_{1}^{n} e_i^2 = \sum_{1}^{n} ((y_i - f(x_i))^2 \tag{A.1}$$

Where f(x) is the fitting curve, a third order polynomial, and e_i is the deviation error from each data point given by:

$$e_n = y_n - f(x_n) \tag{A.2}$$

Baseline correction was applied iterative with an eight-order multi-polynomial fitting algorithm from Zhao, Lui, McLean, and Zeng (2007). Lastly, a spectral range selection was also

applied to remove areas of the spectrum where no peaks occurred to improve matching. This resulted in a processed spectrum as shown in figure A.2.

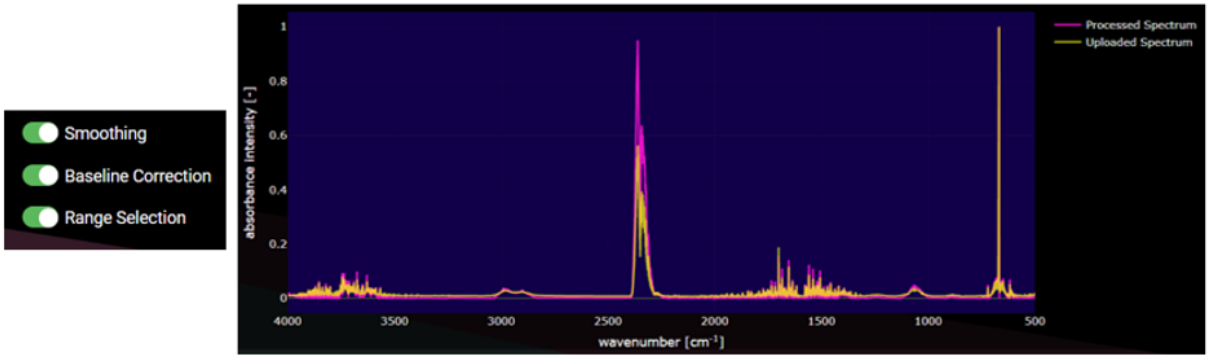

Figure A.2: Processing of the uploaded spectrum.

The processed spectra was used to identify the materials present in the samples. It was indicated that FTIR spectra should be searched for in the reference library and that they needed to be compared with the processed spectrum. Only the peaks were taken into account when comparing the processed spectrum with the reference spectra from the library, since this resulted in the highest Pearson correlation. On figure A.3 the match between the processed spectrum and the spectrum of polypropylene from the reference library is shown.

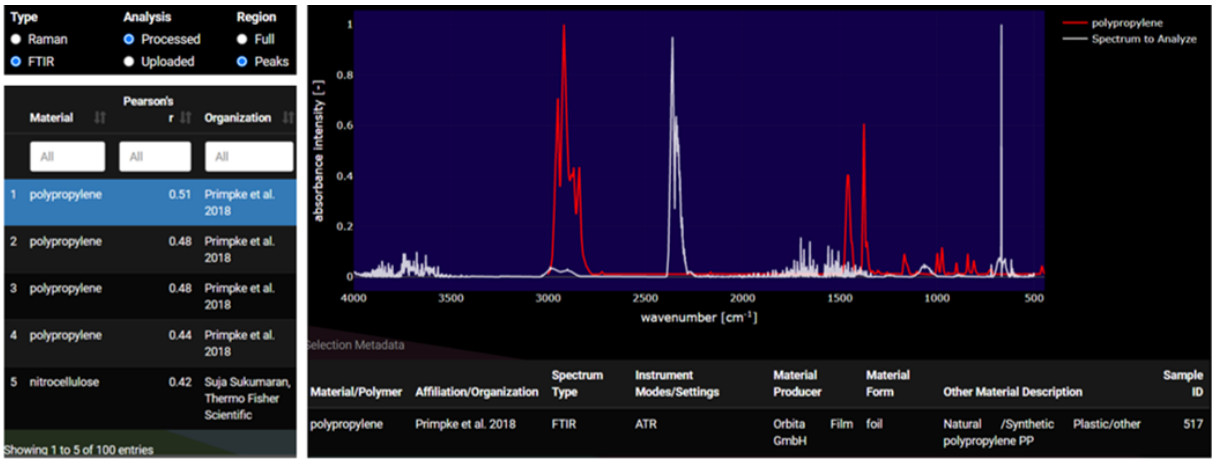

Figure A.3: Matching materials with the processed spectrum.

A.2 Calculating the Pearson correlation coefficient

The matching procedure in Open Specy consists of a Pearson correlation between the spectra from the reference library (reference spectra) and the uploaded spectrum. The Pearson correlation coefficient for the comparison of FTIR spectra can be calculated according to the following formula (Dziuba, Babuchowski, Nałęcz, & Niklewicz, 2007):

$$r_{y_1y_2} = \frac{\sum_{i=1}^{n}(y_{1i} - \overline{y}_1)((y_{2i} - \overline{y}_2)}{\sqrt{\sum_{i=1}^{n}(y_{1i} - \overline{y}_1)^2}\sqrt{\sum_{i=1}^{n}(y_{2i} - \overline{y}_2)^2}} \tag{A.3}$$

Where y_1 and y_2 are values of absorbance at a given wavelength (i) of the two FTIR spectra to be compared (the reference spectra from the library and the uploaded spectrum); n refers to the number of data points; and $\overline{y}_1$ and $\overline{y}_2$ mean values of absorbance calculated for y_1 and y_2.

Appendix B

IDENTIFIED MATERIALS USING OPEN SPECY

This appendix contains all the results generated with Open Specy. For each location, 6 tables are given containing the polymer materials present in the samples from that location and their corresponding Pearson correlation coefficient. The left side of the table contains information about the density separation performed at 1,21 g/cm^3, the right side of the table reports the materials found after the density separation at 1,80 g/cm^3. It was decided to only report matches upward of a Pearson correlation coefficient of 0,30 for each sample. The reference database contained multiple spectra of the same material (e.g. multiple matches with different spectra from the same polymer type present in the database). It was decided to only report the match with the highest correlation coefficient and to only report matches with polymers and not with other substances.

B.1 Campus Coupure

Table B.1: CP1A.

Density 1,21 g/cm^3		Density 1,80 g/cm^3	
Material	Pearson's r	Material	Pearson's r
PP	0,51	PP	0,55
PEO	0,38	PEO	0,42
PEG	0,37	EPDM	0,39
PET	0,36	PEG	0,38
EPDM	0,33	PDMS	0,36
HDPE	0,32	PET	0,35
PDMS	0,31	HDPE	0,35
PA 6	0,30		

Table B.2: CP1B.

Density 1,21 g/cm^3		Density 1,80 g/cm^3	
Material	Pearson's r	Material	Pearson's r
PP	0,55	PP	0,49
EPDM	0,41	PET	0,36
PEO	0,39	PEO	0,35
PDMS	0,38	PEG	0,34
HDPE	0,38	PA 6	0,32
PEG	0,37		
PET	0,36		

Table B.3: CP2A.

Density 1,21 g/cm^3		Density 1,80 g/cm^3	
Material	Pearson's r	Material	Pearson's r
PP	0,59	PS	0,71
EPDM	0,54	PVC	0,63
HDPE	0,53	XPS	0,58
EPR	0,46	PET	0,35
PDMS	0,44	HDPE	0,33
PEO	0,38	PSU	0,33

Table B.4: CP2B.

Density 1,21 g/cm^3		Density 1,80 g/cm^3	
Material	Pearson's r	Material	Pearson's r
PP	0,55	PP	0,57
EPDM	0,40	EPDM	0,54
PEO	0,40	HDPE	0,46
PEG	0,39	EPR	0,42
HDPE	0,39	PE	0,42
PDMS	0,37	PDMS	0,41
PET	0,36	PEO	0,36
PE	0,34	PEG	0,35
EPR	0,30	PET	0,34
		SAA	0,32

Table B.5: CP3A.

Density 1,21 g/cm^3		Density 1,80 g/cm^3	
Material	Pearson's r	Material	Pearson's r
PP	0,65	PP	0,52
EPDM	0,44	EPDM	0,49
PEO	0,41	HDPE	0,44
PEG	0,40	PDMS	0,44
PDMS	0,40	PE	0,36
HDPE	0,40	SAA	0,36
PE	0,36	PEO	0,34
PET	0,36	PET	0,33
EPR	0,34	SIS	0,33

Table B.6: CP3B.

Density 1,21 g/cm^3		Density 1,80 g/cm^3	
Material	Pearson's r	Material	Pearson's r
PP	0,61	PP	0,53
EPDM	0,57	EPDM	0,51
PDMS	0,49	PDMS	0,39
ABS	0,48	EPR	0,35
EPR	0,47	SAA	0,35
		SIS	0,35
		PET	0,31

B.2 Gentbrugse Meersen

Table B.7: GB1A.

Density 1,21 g/cm^3		Density 1,80 g/cm^3	
Material	Pearson's r	Material	Pearson's r
HDPE	0,59	PP	0,41
PDMS	0,55	PET	0,40
PP	0,53	PEO	0,34
EPDM	0,49	PEG	0,31
EPR	0,42		
ABS	0,39		

Table B.8: GB1B.

Density 1,21 g/cm^3		Density 1,80 g/cm^3	
Material	Pearson's r	Material	Pearson's r
PP	0,55	PP	0,48
PDMS	0,48	SAA	0,42
EPDM	0,47	PS	0,41
HDPE	0,45	PET	0,36
EPR	0,42	PVC	0,34
PEO	0,41	EPDM	0,30
PEG	0,39		
PET	0,34		

Table B.9: GB2A.

Density 1,21 g/cm^3		Density 1,80 g/cm^3	
Material	Pearson's r	Material	Pearson's r
PVC	0,46	PVC	0,48
PS	0,46	PS	0,42
PET	0,35	PA 6	0,38
		PET	0,35
		SAA	0,32

Table B.10: GB2B.

Density 1,21 g/cm^3		Density 1,80 g/cm^3	
Material	Pearson's r	Material	Pearson's r
PDMS	0,43	PVC	0,53
PP	0,43	PS	0,32
PVC	0,33	PET	0,31
HDPE	0,30		

Table B.11: GB3A.

Density 1,21 g/cm^3		Density 1,80 g/cm^3	
Material	Pearson's r	Material	Pearson's r
PDMS	0,47	PA 6	0,38
HDPE	0,46	PS	0,36
PP	0,44	PET	0,35
PEO	0,42	PVC	0,34
PEG	0,39		
PET	0,39		
PE	0,32		

Table B.12: GB3B.

Density 1,21 g/cm^3		Density 1,80 g/cm^3	
Material	Pearson's r	Material	Pearson's r
PVC	0,48	PVC	0,54
PS	0,34	PS	0,34
		PET	0,34

B.3 Agricultural field, Ardooie

B.3.1 Ardooie location 1

Table B.13: 1AR1A.

Density 1,21 g/cm^3		Density 1,80 g/cm^3	
Material	Pearson's r	Material	Pearson's r
PP	0,57	PP	0,56
HDPE	0,51	EPDM	0,49
EPDM	0,51	PDMS	0,47
PDMS	0,47	EPR	0,42
EPR	0,44	PEO	0,41
PEO	0,40	PEG	0,39
PEG	0,38		

Table B.14: 1AR1B.

Density 1,21 g/cm^3		Density 1,80 g/cm^3	
Material	Pearson's r	Material	Pearson's r
PDMS	0,57	PP	0,57
PVC	0,42	EPDM	0,51
PEO	0,40	HDPE	0,51
PEG	0,39	PDMS	0,47
PET	0,37	EPR	0,44
		PEO	0,41
		PEG	0,40

Table B.15: 1AR2A.

Density 1,21 g/cm^3		Density 1,80 g/cm^3	
Material	Pearson's r	Material	Pearson's r
PVC	0,57	PS	0,63
PS	0,48	PVC	0,60
XPS	0,43	XPS	0,50
PET	0,30	PET	0,39
		PSU	0,32
		HDPE	0,31

Table B.16: 1AR2B.

Density 1,21 g/cm^3		Density 1,80 g/cm^3	
Material	Pearson's r	Material	Pearson's r
PP	0,43	PP	0,49
PDMS	0,42	PS	0,48
SAA	0,40	PVC	0,46
PS	0,39	SAA	0,44
PET	0,37	PET	0,36
PVC	0,3	XPS	0,34
		SAN	0,33

Table B.17: 1AR3A.

Density 1,21 g/cm^3		Density 1,80 g/cm^3	
Material	Pearson's r	Material	Pearson's r
PP	0,57	PP	0,55
HDPE	0,51	EPDM	0,46
EPDM	0,51	PDMS	0,46
PDMS	0,48	EPR	0,41
EPR	0,44	PEO	0,41
PEO	0,41		
PEG	0,40		

Table B.18: 1AR3B.

Density 1,21 g/cm^3		Density 1,80 g/cm^3	
Material	Pearson's r	Material	Pearson's r
PP	0,56	PS	0,62
EPDM	0,46	PVC	0,60
PDMS	0,45	XPS	0,49
HDPE	0,42	PP	0,42
EPR	0,40	HDPE	0,34
PEG	0,38	PET	0,33
PET	0,35		

B.3.2 Ardooie location 2

Table B.19: 2AR1A.

Density 1,21 g/cm^3		Density 1,80 g/cm^3	
Material	Pearson's r	Material	Pearson's r
PP	0,52	PP	0,56
PEO	0,38	EPDM	0,45
PEG	0,37	PDMS	0,43
PET	0,37	PEO	0,40
EPDM	0,34	EPR	0,39
HDPE	0,33	PET	0,36
PDMS	0,32		
PA 6	0,30		
PE	0,30		

Table B.20: 2AR1B.

Density 1,21 g/cm^3		Density 1,80 g/cm^3	
Material	Pearson's r	Material	Pearson's r
PP	0,46	PP	0,55
PET	0,36	EPDM	0,50
PEO	0,33	PDMS	0,46
PA 6	0,33	HDPE	0,45
PEG	0,31	EPR	0,41
		PEO	0,40
		PE	0,36

Table B.21: 2AR2A.

Density 1,21 g/cm^3		Density 1,80 g/cm^3	
Material	Pearson's r	Material	Pearson's r
PP	0,55	PP	0,42
EPDM	0,41	PET	0,36
PEO	0,40	PEO	0,35
HDPE	0,40	PEG	0,34
PEG	0,39	PA 6	0,34
PDMS	0,38		
PE	0,35		
EPR	0,32		

Table B.22: 2AR2B.

Density 1,21 g/cm^3		Density 1,80 g/cm^3	
Material	Pearson's r	Material	Pearson's r
PP	0,57	PET	0,37
EPDM	0,45	PVC	0,33
HDPE	0,44		
PDMS	0,41		
PEO	0,40		
PEG	0,40		
PE	0,37		
EPR	0,36		
PET	0,36		

Table B.23: 2AR3A.

Density 1,21 g/cm^3		Density 1,80 g/cm^3	
Material	Pearson's r	Material	Pearson's r
PA 6	0,38	PP	0,50
PET	0,36	PEO	0,38
PA 66	0,31	PEG	0,37
		PET	0,36
		PDMS	0,32
		PA 6	0,31
		EPDM	0,31

Table B.24: 2AR3B.

Density 1,21 g/cm^3		Density 1,80 g/cm^3	
Material	Pearson's r	Material	Pearson's r
PP	0,43	PP	0,52
PET	0,35	PEO	0,40
PA 6	0,34	PDMS	0,36
PS	0,33	PET	0,35
PEO	0,31	EPDM	0,35
PEG	0,30	HDPE	0,31
		PE	0,30

B.4 Geophysical center at Dourbes

Table B.25: D1A.

Density 1,21 g/cm^3		Density 1,80 g/cm^3	
Material	Pearson's r	Material	Pearson's r
PA 6	0,40	PP	0,57
PET	0,37	EPDM	0,52
PS	0,35	HDPE	0,50
PA 66	0,34	PDMS	0,48
		EPR	0,43
		PEO	0,42
		PEG	0,41

Table B.26: D1B.

Density 1,21 g/cm^3		Density 1,80 g/cm^3	
Material	Pearson's r	Material	Pearson's r
PVC	0,52	PP	0,56
PET	0,34	EPDM	0,47
PS	0,30	HDPE	0,46
		PDMS	0,45
		EPR	0,41
		PEO	0,40
		PEG	0,38
		PET	0,35

Table B.27: D2A.

Density 1,21 g/cm^3		Density 1,80 g/cm^3	
Material	Pearson's r	Material	Pearson's r
PP	0,53	PDMS	0,52
EPDM	0,46	PP	0,50
PDMS	0,44	HDPE	0,45
HDPE	0,44	EPDM	0,43
EPR	0,40	PEO	0,42
PEO	0,38	EPR	0,40
PEG	0,30	PEG	0,39
PET	0,33	PET	0,35
PVC	0,30		

Table B.28: D2B.

Density 1,21 g/cm^3		Density 1,80 g/cm^3	
Material	Pearson's r	Material	Pearson's r
PP	0,56	PP	0,53
HDPE	0,47	PDMS	0,44
EPDM	0,47	EPDM	0,44
PDMS	0,44	HDPE	0,42
EPR	0,38	PEO	0,40
PEG	0,36	PEG	0,38
PET	0,34	PET	0,35

Table B.29: D3A.

Density 1,21 g/cm^3		Density 1,80 g/cm^3	
Material	Pearson's r	Material	Pearson's r
PS	0,51	PVC	0,61
PVC	0,49	PS	0,57
XPS	0,41	XPS	0,35

Table B.30: D3B.

Density 1,21 g/cm^3		Density 1,80 g/cm^3	
Material	Pearson's r	Material	Pearson's r
PA 6	0,39	PP	0,55
PVC	0,38	EPDM	0,46
PET	0,37	HDPE	0,45
PA 66	0,31	PDMS	0,45
		PEO	0,41
		EPR	0,40
		PEG	0,39
		PET	0,35

B.5 Bosland-site (Pelt)

Table B.31: P1A.

Density 1,21 g/cm^3		Density 1,80 g/cm^3	
Material	Pearson's r	Material	Pearson's r
PP	0,56	PP	0,54
EPDM	0,43	EPDM	0,40
HDPE	0,40	PEO	0,38
PDMS	0,40	PEG	0,37
PEO	0,39	PET	0,36
PEG	0,38	PDMS	0,36
PET	0,35		

Table B.32: P1B.

Density 1,21 g/cm^3		Density 1,80 g/cm^3	
Material	Pearson’s r	Material	Pearson’s r
PP	0,53	PP	0,52
PEO	0,39	PEO	0,42
PEG	0,38	PEG	0,40
PET	0,36	PET	0,36
EPDM	0,36	EPDM	0,36
HDPE	0,33	PDMS	0,34
PDMS	0,33		

Table B.33: P2A.

Density 1,21 g/cm^3		Density 1,80 g/cm^3	
Material	Pearson’s r	Material	Pearson’s r
PP	0,52	PP	0,55
PEO	0,39	EPDM	0,40
PEG	0,38	PEO	0,39
PET	0,36	PEG	0,38
EPDM	0,35	HDPE	0,37
		PDMS	0,36

Table B.34: P2B.

Density 1,21 g/cm^3		Density 1,80 g/cm^3	
Material	Pearson’s r	Material	Pearson’s r
PP	0,50	PVC	0,43
PEO	0,38	PS	0,40
PEG	0,37	PET	0,35
PET	0,36	PA 6	0,32
PA 6	0,31		

Table B.35: P3A.

Density 1,21 g/cm^3		Density 1,80 g/cm^3	
Material	Pearson's r	Material	Pearson's r
PP	0,58	PVC	0,41
HDPE	0,55	PET	0,40
EPDM	0,54	PA 6	0,32
PDMS	0,51		
PEO	0,42		
PEG	0,41		

Table B.36: P3B.

Density 1,21 g/cm^3		Density 1,80 g/cm^3	
Material	Pearson's r	Material	Pearson's r
PP	0,51	PP	0,53
PEO	0,38	PEO	0,39
PEG	0,37	PEG	0,38
PET	0,36	EPDM	0,37
EPDM	0,32	PET	0,36
HDPE	0,31	HDPE	0,35

B.6 Kempense heuvelrug

Table B.37: KH1A.

Density 1,21 g/cm^3		Density 1,80 g/cm^3	
Material	Pearson's r	Material	Pearson's r
PTFE	0,73	PTFE	0,67
PET	0,43	PET	0,43
CR	0,34	PA 6	0,31
PC	0,30	PA 66	0,30

Table B.38: KH1B.

Density 1,21 g/cm^3		Density 1,80 g/cm^3	
Material	Pearson's r	Material	Pearson's r
PVC	0,43	PS	0,51
PET	0,39	PVC	0,51
PS	0,31	PET	0,30

Table B.39: KH2A.

Density 1,21 g/cm^3		Density 1,80 g/cm^3	
Material	Pearson's r	Material	Pearson's r
PP	0,59	PP	0,59
HDPE	0,55	HDPE	0,55
EPDM	0,54	EPDM	0,55
PDMS	0,49	PDMS	0,50
EPR	0,46	EPR	0,47
PEO	0,42		

Table B.40: KH2B.

Density 1,21 g/cm^3		Density 1,80 g/cm^3	
Material	Pearson's r	Material	Pearson's r
PP	0,56	PP	0,53
EPDM	0,48	PDMS	0,45
HDPE	0,47	EPDM	0,45
PDMS	0,46	PEO	0,40
EPR	0,42	PEG	0,38
PEO	0,40	PET	0,35
PEG	0,38		
PET	0,34		

Table B.41: KH3A.

Density 1,21 g/cm^3		Density 1,80 g/cm^3	
Material	Pearson's r	Material	Pearson's r
PP	0,62	PVC	0,44
EPDM	0,57	PS	0,39
HDPE	0,55	PET	0,34
PDMS	0,49	PP	0,30
EPR	0,47		

Table B.42: KH3B.

Density 1,21 g/cm^3		Density 1,80 g/cm^3	
Material	Pearson's r	Material	Pearson's r
PP	0,48	PS	0,66
SAA	0,42	PVC	0,63
PS	0,39	XPS	0,52
PET	0,36	SAA	0,37
PDMS	0,36	PET	0,33
EPDM	0,35	SAN	0,32
PVC	0,33		
HDPE	0,30		

Appendix C

MANUAL PEAK IDENTIFICATION

This Appendix contains the results from the manual peak analysis. For each location, the FTIR graphs are shown from the first replication and density separation at 1,21 g/cm^3 for both soil from the A and B layer. The left FTIR spectra shows the peaks that were manually indicated on the spectrum, after baseline correction. The FTIR spectra on the right show the peaks after performing non-linear fitting of the peaks and the baseline using the Levenberg-Marquardt algorithm.

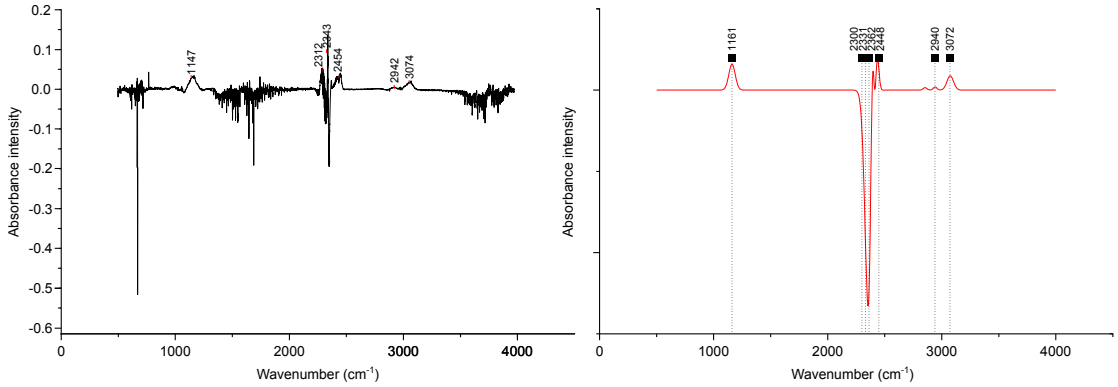

Figure C.1: CP1A-1.2.

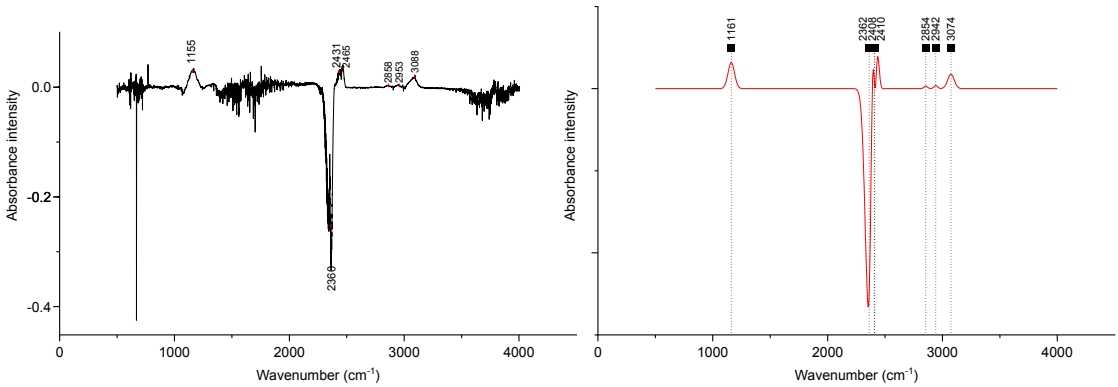

Figure C.2: CP1B-1.2.

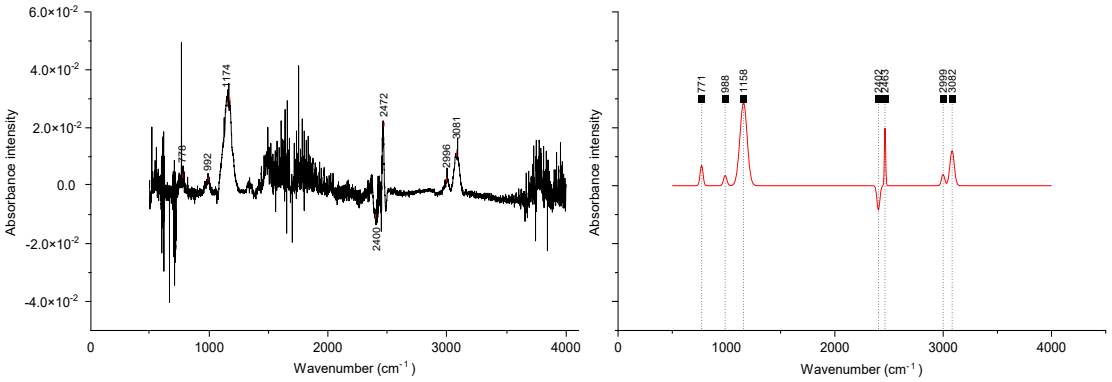

Figure C.3: GB1A-1.2.

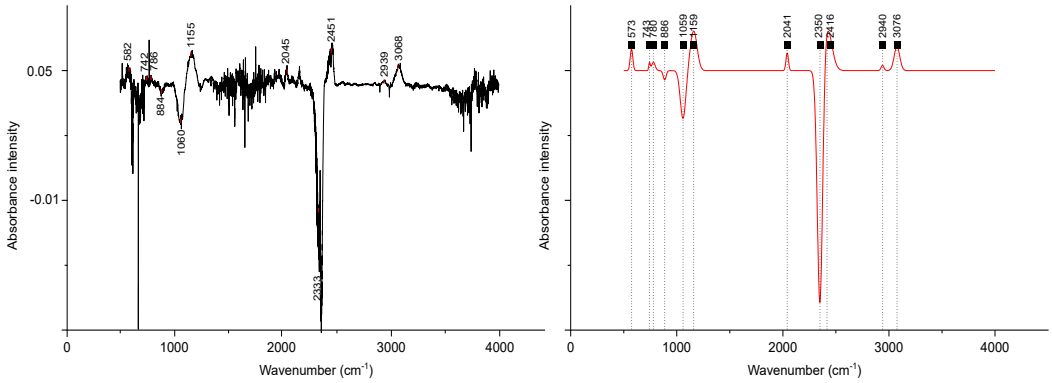

Figure C.4: GB1B-1.2.

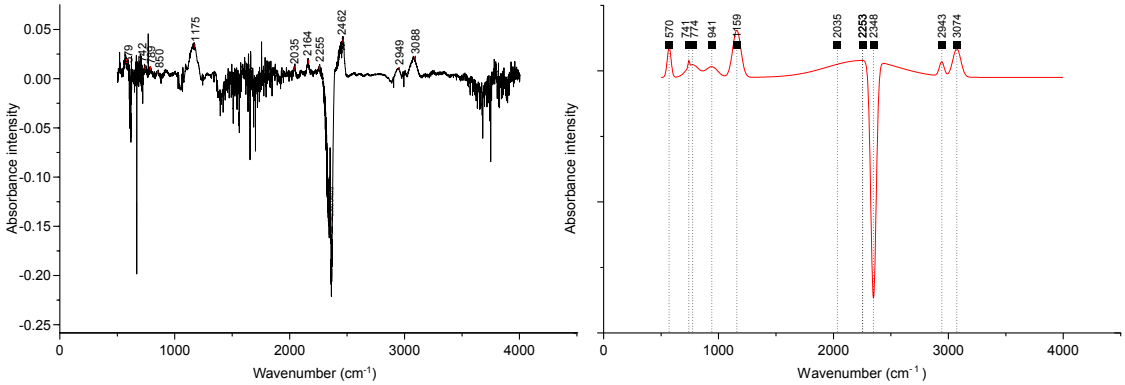

Figure C.5: 1AR1A-1.2.

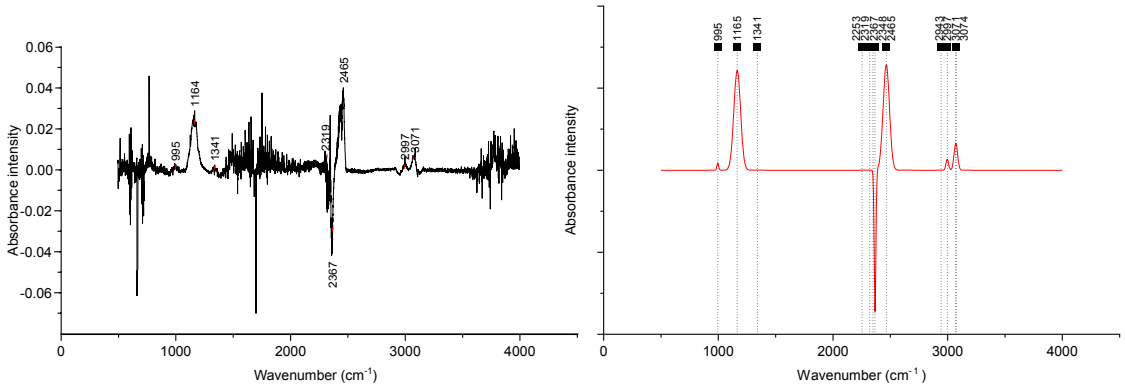

Figure C.6: 1AR1B-1.2.

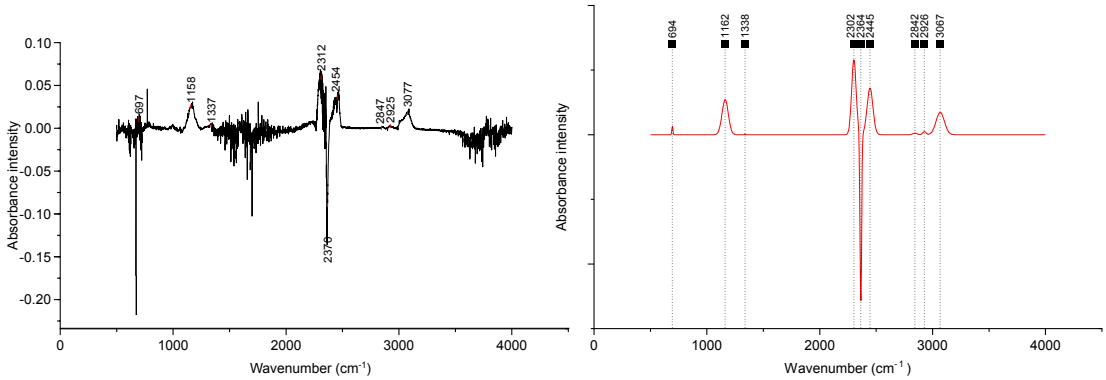

Figure C.7: 2AR1A-1.2.

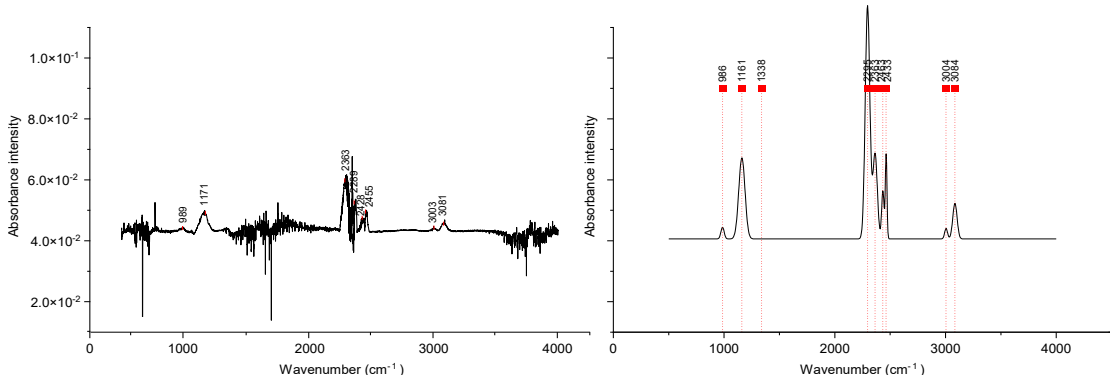

Figure C.8: 2AR1B-1.2.

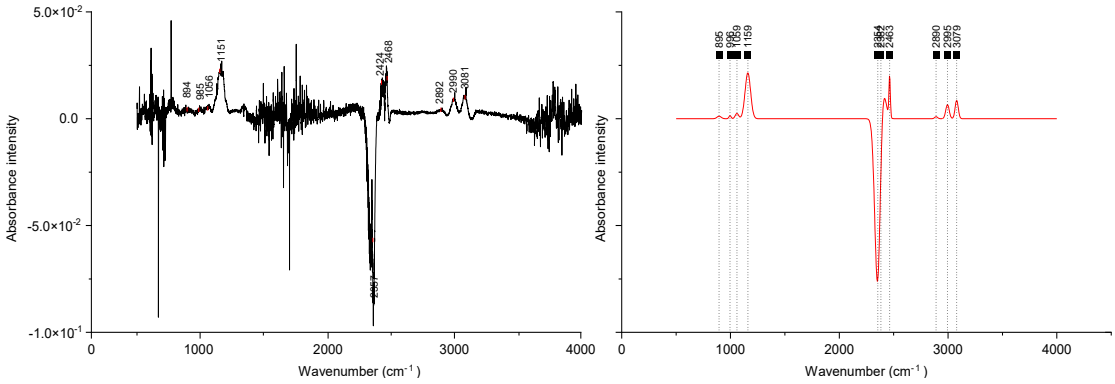

Figure C.9: D1A-1.2.

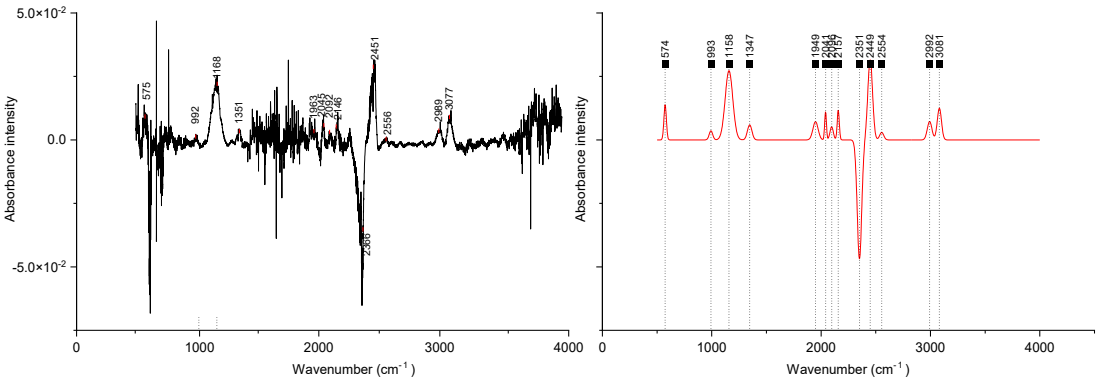

Figure C.10: D1B-1.2.

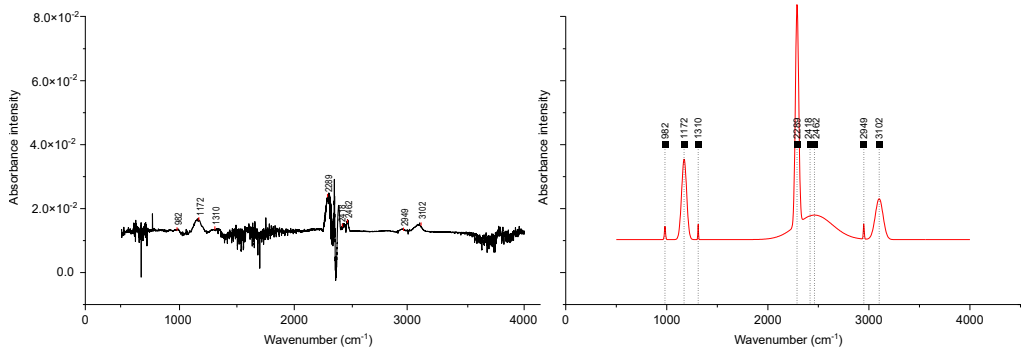

Figure C.11: P1A-1.2.

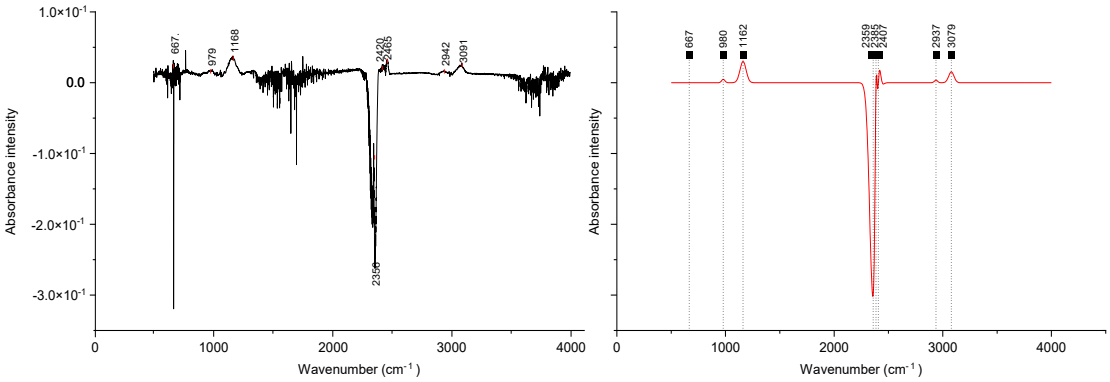

Figure C.12: P1B-1.2.

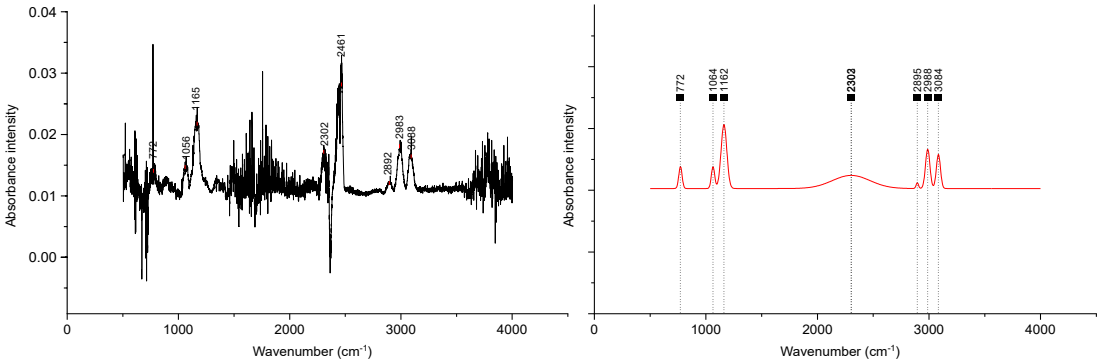

Figure C.13: KH1A-1.2.

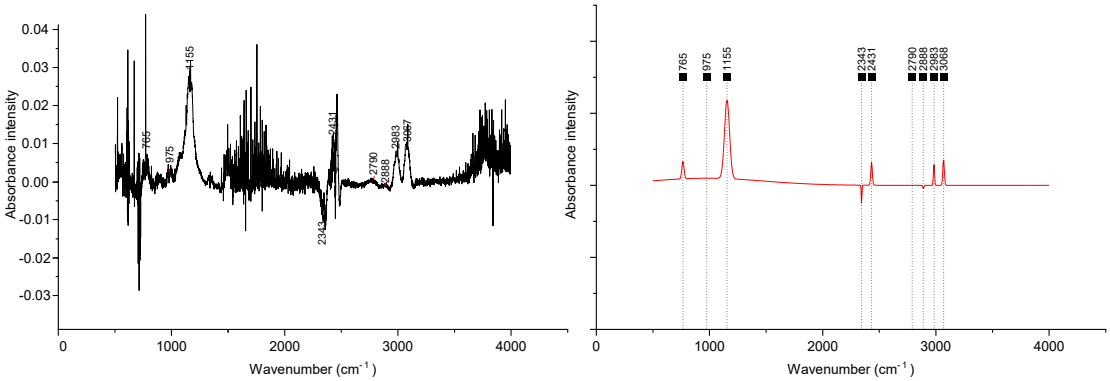

Figure C.14: KH1B-1.2.

Appendix D

PEAK IDENTIFICATION OF THE RAMAN SPECTRA

This section gives an overview of the spectra derived from the scans done with Raman spectroscopy for the four identified particles in figure 4.7. Each spectrum was divided into three parts, when combined they give an overview of the peaks that occurred over a spectral range of 0 to ± 3500 cm^{-1}. The value of the peaks was estimated as accurately as possible, based on the values on the x-axis.

- **Sample P1A-1.2**

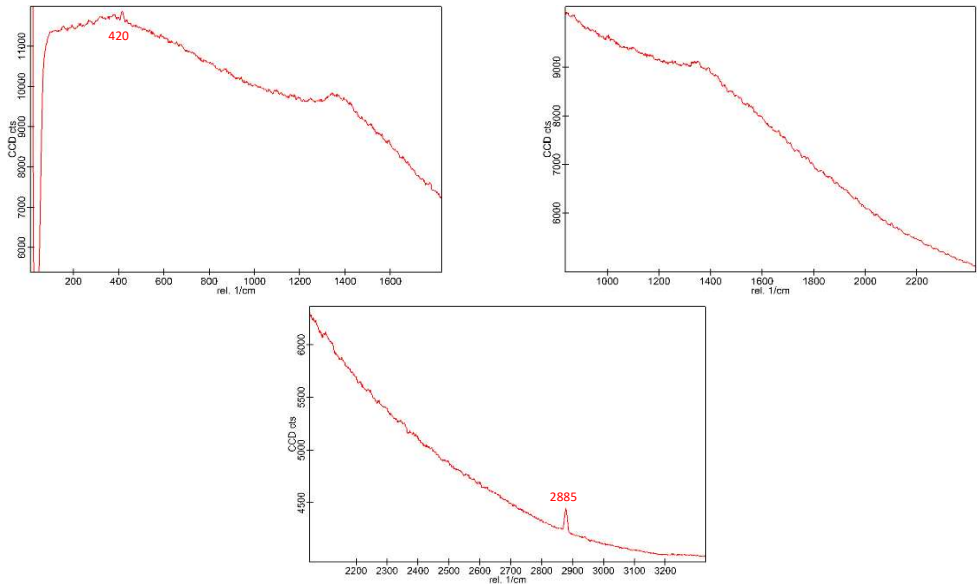

Figure D.1: Raman spectra with identified peaks for the selected particle of sample P1A-1.2.

- **Sample GB1B-1.2**

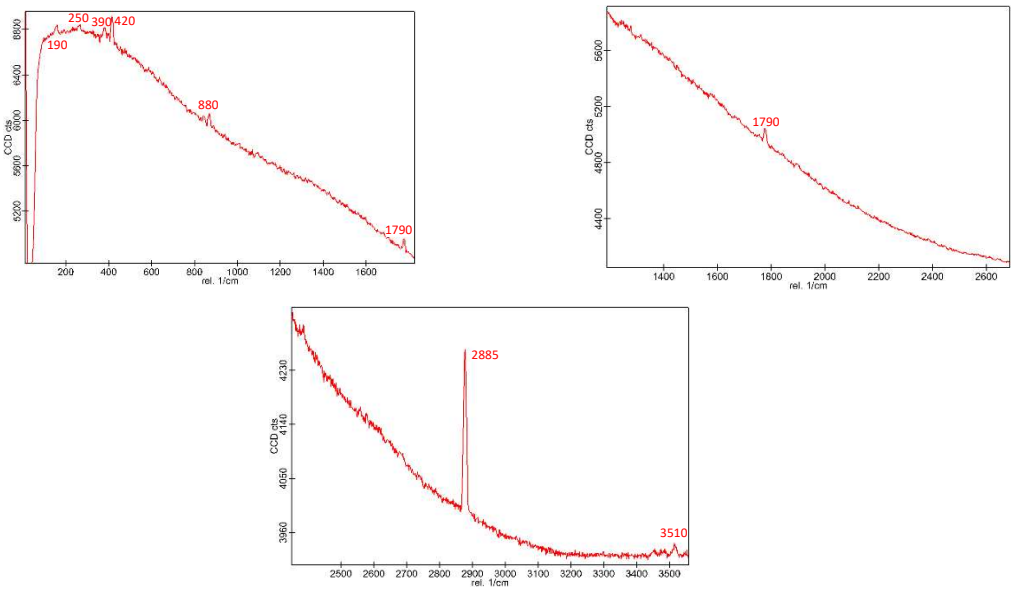

Figure D.2: Raman spectra with identified peaks for the selected particle of sample GB1B-1.2.

- **Sample 1AR1A-1.2 (1) and 1AR1A-1.2 (2)**

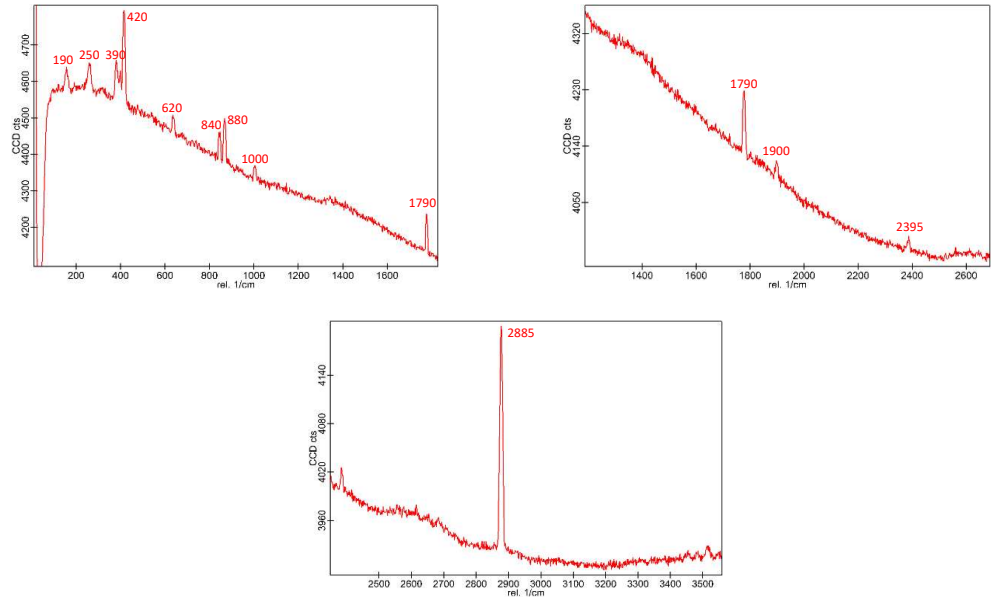

Figure D.3: Raman spectra with identified peaks for the selected particle of sample 1AR1A-1.2 (1).

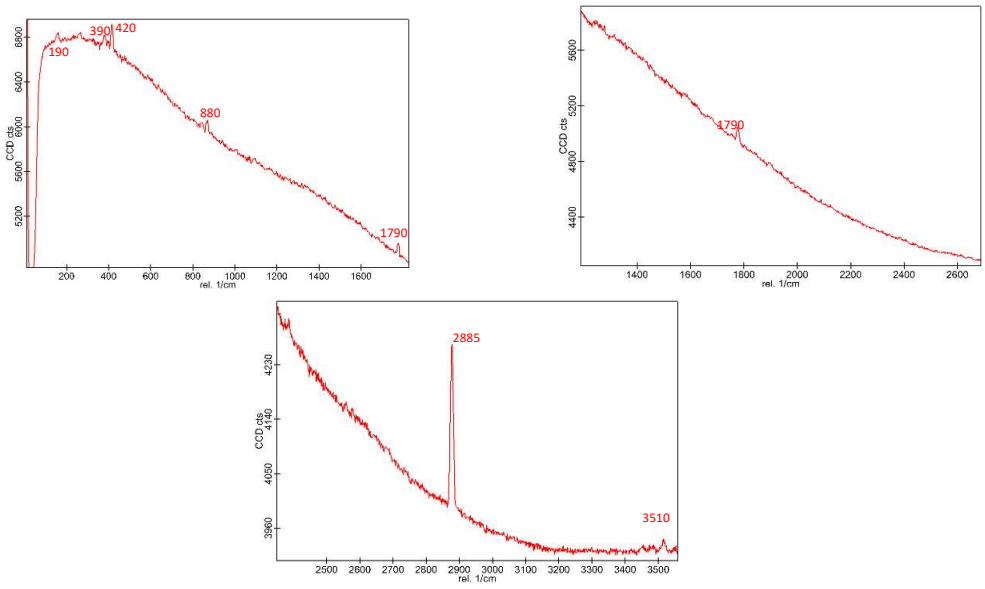

Figure D.4: Raman spectra with identified peaks for the selected particle of sample 1AR1A-1.2 (2).